GDAŃSK UNIVERSITY OF TECHNOLOGY

The author of the doctoral dissertation: Jolanta Kulesza MEng

Scientific discipline: Chemical Sciences

DOCTORAL DISSERTATION

Title of doctoral dissertation:

Comparison of 2D and 3D culture models in the studies of the biological response induced by unsymmetrical bisacridines in cancer cells.

Title of doctoral dissertation (in Polish):

Porównanie modeli hodowli 2D i 3D w badaniach odpowiedzi biologicznej indukowanej przez niesymetryczne bisakrydyny w komórkach nowotworowych.

Supervisor *signature*
Ewa Augustin PhD, DSc, Assoc. Prof.

Gdańsk, year 2023

GDAŃSK UNIVERSITY OF TECHNOLOGY

STATEMENT

The author of the doctoral dissertation: Jolanta Kulesza MEng

I, the undersigned, declare that I am aware that in accordance with the provisions of Art. 27 (1) and (2) of the Act of 4th February 1994 on Copyright and Related Rights (Journal of Laws of 2021, item 1062), the university may use my doctoral dissertation entitled: "Comparison of 2D and 3D culture models in the studies of the biological response induced by unsymmetrical bisacridines in cancer cells." for scientific or didactic purposes.[1]

Gdańsk,..... .....

signature of the PhD student

Aware of criminal liability for violations of the Act of 4th February 1994 on Copyright and Related Rights and disciplinary actions set out in the Law on Higher Education and Science(Journal of Laws 2021, item 478), as well as civil liability, I declare, that the submitted doctoral dissertation is my own work.

I declare, that the submitted doctoral dissertation is my own work performed under and in cooperation with the supervision of Ewa Augustin PhD, DSc, Assoc. Prof.

This submitted doctoral dissertation has never before been the basis of an official procedure associated with the awarding of a PhD degree.

All the information contained in the above thesis which is derived from written and electronic sources is documented in a list of relevant literature in accordance with Art. 34 of the Copyright and Related Rights Act.

I confirm that this doctoral dissertation is identical to the attached electronic version.

Gdańsk,..... ….....

signature of the PhD student

I, the undersigned, agree to include an electronic version of the above doctoral dissertation in the open, institutional, digital repository of Gdańsk University of Technology.

Gdańsk,..... .....

signature of the PhD student

[1] Art 27. 1. Educational institutions and entities referred to in art. 7 sec. 1 points 1, 2 and 4–8 of the Act of 20 July 2018 – Law on Higher Education and Science, may use the disseminated works in the original and in translation for the purposes of illustrating the content provided for didactic purposes or in order to conduct research activities, and to reproduce for this purpose disseminated minor works or fragments of larger works.

2. If the works are made available to the public in such a way that everyone can have access to them at the place and time selected by them, as referred to in para. 1, is allowed only for a limited group of people learning, teaching or conducting research, identified by the entities listed in paragraph 1.

GDAŃSK UNIVERSITY OF TECHNOLOGY

DESCRIPTION OF DOCTORAL DISSERTATION

The Author of the doctoral dissertation: Jolanta Kulesza MEng

Title of doctoral dissertation: Comparison of 2D and 3D culture models in the studies of the biological response induced by unsymmetrical bisacridines in cancer cells.

Title of doctoral dissertation in Polish: Porównanie modeli hodowli 2D i 3D w badaniach odpowiedzi biologicznej indukowanej przez niesymetryczne bisakrydyny w komórkach nowotworowych.

Language of doctoral dissertation: English

Supervisor: Ewa Augustin PhD, DSc, Assoc. Prof.

Date of doctoral defense:

Keywords of doctoral dissertation in Polish: niesymetryczne bisakrydyny, hodowle komórkowe 2D i 3D, wielokomórkowe sferoidy nowotworowe, rak płuc i okrężnicy, odpowiedź komórkowa, apoptoza, nowotworowe komórki macierzyste

Keywords of doctoral dissertation in English: unsymmetrical bisacridines, 2D and 3D cell cultures, multicellular tumor spheroids, lung and colon cancer, cellular response, apoptosis, cancer stem cells

Summary of doctoral dissertation in Polish:

Wielokomórkowe sferoidy nowotworowe są dobrym narzędziem do testowania nowych leków przeciwnowotworowych, w tym tych, działających na nowotworowe komórki macierzyste (NKM), odpowiedzialne za progresję raka, przerzuty i nawroty. Stąd, po wstępnej ocenie wpływu przeciwnowotworowych niesymetrycznych bisakrydyn (UAs) na komórki raka płuc i okrężnicy przy użyciu tradycyjnych kultur jednowarstwowych, rozszerzyłam swoje badania o model sferyczny, co pozwoliło na ustalenie odpowiedzi komórkowej indukowanej przez UAs w komórkach nowotworowych, z dodatkowym uwzględnieniem populacji NKM. Wykazałam, że UAs wpływają na żywotność badanych komórek, a także na ich potencjał sferogenny w 2D i 3D. Udowodniłam również, że najbardziej obiecujące UAs (C-2045 i C-2053) indukowały apoptozę w sferoidach raka okrężnicy HCT116 i płuc A549, w stopniu zbliżonym lub nawet wyższym niż w hodowlach 2D. Zidentyfikowałam także populację komórek o cechach NKM w hodowlach 2D i 3D badanych linii komórkowych poprzez oznaczenie poziomów markerów CD166, CD133, CD44 i EpCAM i wykazałam, że wybrane UAs wpływają na komórki NKM-podobne w obu liniach komórkowych, w A549 wyraźniej w 3D niż 2D. W rezultacie udowodniłam, że UAs wykazują wysokie właściwości przeciwnowotworowe zarówno w warunkach 2D, jak i 3D, oraz wpływają na komórki o cechach NKM, co czyni je obiecującymi kandydatami do przyszłych zastosowań terapeutycznych.

Summary of doctoral dissertation in English:

Multicellular tumor spheroids are a good tool for testing new anticancer drugs, including those that may target cancer stem cells (CSCs), responsible for cancer progression, metastasis, and recurrence. Therefore, following the initial evaluation of the impact of antitumor unsymmetrical bisacridines (UAs) on lung and colon cancer cells using traditional monolayer cultures, I extended my investigations and applied the spherical model. This approach aimed to uncover the cellular

response induced by UAs in these cancer cells, with an additional focus on the CSC-like population. In my research, I showed that UAs affected the viability of the studied cells, as well as their spherogenic potential in 2D and 3D. Furthermore, I proved that the most promising UAs (C-2045 and C-2053) induced apoptosis in HCT116 colon and A549 lung cancer spheroids, to a similar, or even higher extent than in monolayer. Finally, I identified the population of CSC-like cells in 2D and 3D cultures of the studied cell lines by determining the levels of CD166, CD133, CD44, and EpCAM markers and I showed that selected UAs affected the CSC-like population in both cell lines, in A549 more profoundly in 3D than 2D. Thus, I have proven that UAs exhibit high antitumor properties in both 2D and 3D conditions and affect the CSC-like population, which makes them promising candidates for future therapeutic applications.

Michałowi, który niezmiennie jest moim największym oparciem
i bez którego nie dałabym rady.

Najukochańszym rodzicom, w podziękowaniu za to, kim jestem
i za wszystko, co im zawdzięczam.

Dziadkom, bo wiem, że byliby ze mnie bardzo dumni.

Ta praca nie mogłaby powstać bez pomocy i wsparcia wielu osób, które mam ogromne szczęście mieć w swoim życiu i którym zawdzięczam wszystko to, co mam.

Pragnę więc serdecznie podziękować:

Mojej Pani Promotor, Profesor Ewie Augustin, za ukształtowanie mojej kariery naukowej, za ogrom wsparcia i wyrozumiałości, za przekazaną wiedzę i niekończącą się wiarę we mnie, szczególnie w tych trudnych momentach, w których sama w siebie wątpiłam.

Pani Profesor Zofii Mazerskiej, za liczne dyskusje naukowe i nie tylko, za okazane ciepło, życzliwość i zaufanie.

Monice Pawłowskiej, za nieopisaną pomoc w laboratorium i poza nim, za piękną przyjaźń i zrozumienie w kwestiach związanych zarówno z doktoratem, jak i pozostałych.

Agnieszce Kurdyn, za rzeczowe uwagi podczas badań, za spędzony wspólnie czas, poczucie humoru i długie rozmowy, nie tylko naukowe.

Pani Doktor Agnieszce Potędze, Michałowi Kosno i pozostałym członkom zespołu, za pomoc, serdeczność i miłą atmosferę pracy.

Moim wspaniałym rodzicom, za wychowanie i przekazane wartości, za pewność, że zawsze mogę na nich polegać, za miłość i troskę oraz za to, że od dziecka inwestowali w mój rozwój i edukację, cieszyli się z każdego sukcesu i wspierali w trudnych chwilach, nieustannie podkreślając, że uczę się dla siebie.

Najukochańszemu rodzeństwu i całej mojej rodzinie, za to, że zawsze są przy mnie, za wsparcie emocjonalne i nieustającą wiarę w moje możliwości oraz motywację w chwilach zwątpienia, która pomogła mi dążyć do celu.

Moim fantastycznym przyjaciołom, za mnóstwo wsparcia, za to, że byli przy mnie przez te lata i że dzięki nim czas spędzony zarówno na Uczelni, jak i poza nią był wspaniały, co dawało mi siłę kontynuować naukę w najtrudniejszych momentach.

Michałowi, za to, że zawsze mogę na niego liczyć, że nieustannie wspiera mnie we wszystkim co robię i jest obok nawet w tych absolutnie najgorszych chwilach, za jego nieocenioną cierpliwość, wyrozumiałość i miłość, które trzymały mnie w całości i pozwalały iść dalej.

These studies were supported by the National Science Center, Poland,
Grants No. UMO-2016/23/B/NZ7/03324 and UMO-2019/33/B/NZ7/02534.

TABLE OF CONTENTS

ABBREVIATIONS

7-AAD	–	7-aminoactinomycin D
ABC	–	ATP-binding cassette
ALDH	–	aldehyde dehydrogenase
bFGF	–	basic fibroblast growth factor
CAFs	–	cancer-associated fibroblasts
CSCs	–	cancer stem cells
DMSO	–	dimethyl sulfoxide
ECM	–	extracellular matrix
EGF	–	epidermal growth factor
EMT	–	epithelial-mesenchymal transition
ETP	–	etoposide
F12K	–	Kaighn's Modification of Ham's F-12 Medium
FBS	–	fetal bovine serum
GBM	–	glioblastoma multiforme
HGF	–	hepatocyte growth factor
HIF	–	hypoxia-inducible family factors
IR	–	irinotecan
MCTS	–	multicellular tumor spheroids
MDR1	–	multidrug resistance gene 1
MEM	–	Minimum Essential Medium Eagle
MTT	–	3-(4,5-dimethylthiazol-2-yl)-2,5-diphenyltetrazolium bromide
NGF	–	nerve growth factor
OMS	–	organotypic spheroids / organotypic multicellular spheroids
PARP	–	poly(APD-ribose) polymerase
PHEMA	–	2-hydroxyethyl polymethacrylate
ROS	–	reactive oxygen species
RPMI	–	RPMI 1640 Medium
SP	–	side population
TDTS	–	tissue-derived tumor spheres
TGF-β	–	transforming growth factor β
UAs	–	unsymmetrical bisacridines
ULA	–	ultra low attachment
VEGF	–	vascular endothelial growth factor

1. OBJECTIVES OF THE RESEARCH

For many years, neoplastic diseases have been the second leading cause of death in both Poland and globally. Cancer has a higher mortality rate than AIDS, tuberculosis, and malaria combined, and it is estimated that one in six deaths worldwide is now attributed to cancer. In the field of cancer, lung and colorectal cancers are among the most commonly diagnosed types in the world and the greatest contributor to cancer-related deaths worldwide is lung cancer, responsible for an estimated 1.8 million deaths in 2020. Following closely is colorectal cancer, causing roughly 0.9 million deaths over the same period. The significance of these numbers highlights the urgent need to continue efforts in cancer prevention, diagnosis, and treatment [American Cancer Society, 2018; Sung H. et al., 2021]. Therefore, a big challenge for modern medicine is the development of new, effective anticancer drugs, which, unfortunately, is a difficult task and involves a lot of costly and time-consuming research.

In the Group of Chemistry and Biochemistry of Anticancer Drugs at the Department of Pharmaceutical Technology and Biochemistry at Gdańsk University of Technology, the search for potential anticancer drugs has been carried out for many years now. Recently, new, promising antitumor compounds, unsymmetrical bisacridines (UAs), have been developed. These acridine derivatives, which have been patented in Europe, the USA, and Japan [Konopa J. et al., 2017; Konopa J. et al., 2019; Konopa J. et al., 2023], exhibit high cytotoxic and antitumor activity against numerous cancers, including human lung and colorectal cancers [Paluszkiewicz E. et al., 2020]. Preliminary studies of the distribution of HCT116 colorectal and H460 lung cancer cells in different phases of the cell cycle after UAs treatment, along with analysis of changes in the structure of cytoplasmic membrane indicated that UAs induced apoptosis in both cell lines. Therefore further experiments regarding cellular response were necessary, to prove that apoptosis is indeed the main type of cell death induced by UAs in HCT116 and H460 cells.

Three-dimensional cell cultures (spheroids) are gaining more and more interest in drug development and testing. An increasing number of studies have presented results obtained from comparisons of the effectiveness of anticancer drugs in 2D and 3D cell culture models. Among tested compounds there are natural extracts [Jamali T. et al., 2018; Muddineti O.S. et al., 2017], drugs already in clinical use [Herrmann R. et al., 2008; Selby M. et al., 2017; Ho W.Y. et al., 2012] or conjugates of these drugs with nanoparticles [Lu H. et al., 2018], but also newly synthesized compounds with promising mechanisms of action [Botchkina G.I. et al., 2010; Dhiman N. et al., 2020; Wernitznig D. et al., 2019]. The use of 3D spheroids has the potential to improve drug discovery research and bridge the gap between results obtained in preclinical phases and promising outcomes found in clinical trials. Therefore, I decided to apply this culture model in my studies concerning unsymmetrical bisacridines (UAs). Classic methods based on 2D monolayer cell cultures are very useful tools to show the biochemical and molecular effects of a new compound, but they cannot show the possibility and efficiency of a drug in tumor penetration and its potential action in the patients' tissues and body [Friedrich J. et al., 2007]. 3D cell cultures (spheroids) consist of different proliferation areas, determined by the presence of nutrients, metabolites, pH, and oxygen gradients, similar to those found in poorly or non-vascularized solid

tumors. Due to these gradients and the complex network of interactions with the extracellular matrix, neighboring cells, and proteins, spheroids act as a crucial bridge connecting the simplified structure of 2D monolayer cultures with the intricate and complex nature of tumors *in vivo* [Costa E.C. et al., 2018; Mikhail A.S. et al., 2013; Pinto B. et al., 2020]. According to most literature reports, many compounds have clearly limited effectiveness in 3D environments compared to the results obtained in 2D cultures. Thus, spheroids are a good tool for selecting chemotherapeutic agents with increased distribution and efficacy in environments similar to *in vivo* conditions and may help reduce unnecessary animal testing [Hirschhaeuser F. et al., 2010; Karlsson H. et al., 2012]. Therefore, the use of a 3D culture model in drug screening is recommended to support conventional 2D monolayer studies and prior to animal testing [Zanoni M. et al., 2016].

Among their many features similar to those found in tumors, spheroids show a more adequate content of cancer stem cells (CSCs) to that found *in vivo* than that observed in monolayer cultures. CSCs are a subset of tumor cells with stem cell-like properties, including the ability to self-renew and pluripotency, and therefore are responsible for resistance to conventional chemo- and radiotherapy, as well as act as a key factor in tumor progression, metastasis, and recurrence. This makes CSCs an attractive target for anticancer therapy in order not only to effectively treat cancer but also to prevent its relapse. Although there is hope in the development of novel compounds that target CSCs selectively, several drugs that have been shown to be specific for CSCs turned out to be either not very potent or excessively toxic to humans. Thus, while some attempts have been made to target CSCs, no effective treatment has yet been established, highlighting the need for new approaches to target these cells using more potent inhibitors with lower toxicity [Semov A. et al., 2012; Olejniczak A. et al., 2018; Katsura Y. et al., 2019].

One of the most recent advances in the study of CSCs is the application of three-dimensional (3D) cultures of cancer cells. Generally, there are four types of 3D cancer models, two of which are obtained from a single-cell suspension of an immortalized cell line: (a) multicellular spheroids, also known as cancer cell spheroids or multicellular tumor spheroids (MCTS), generated in the presence of serum, and (b) tumorspheres (tumor-derived spheroids), produced under serum-free conditions. The other two are obtained directly from a tumor tissue: (c) tissue-derived tumorspheres, by fine slicing of the tissue and partially dissociating it so that it contains primarily tumor cells, and (d) organotypic spheroids, by cutting the tissue into submillimeter pieces and maintaining them in the presence of serum and other supplements, without the dissociation [Ham S.L. et al., 2016; Ishiguro T.S. et al., 2017; Weiswald L.B. et al., 2015]. Most studies on CSCs are carried out using tumor-derived spheroids, which are typically enriched in cancer stem cells or cells with stem cell-related characteristics [Ishiguro T.S. et al., 2017]. However, multicellular spheroids, which have a myriad of advantages such as reproducibility, ease of initiation and maintenance, and simplicity of genetic manipulation, are considered the classical approach for 3D cell culture. Moreover, MCTS are very well characterized and can simulate the complex conditions present in a patient's tumor, such as oxygen, metabolic and proliferative gradients, as well as cell-cell interactions. As a result, they

show similar therapeutic responses and drug resistance to those observed *in vivo* [Ishiguro T.S. et al., 2017; Weiswald L.B. et al., 2015; Friedrich J. et al., 2009].

Therefore in my studies, besides an extension of research regarding apoptosis induction in colon and lung cancer cells, I decided to check whether selected cell lines, which showed high sensitivity to treatment with unsymmetrical bisacridines, would be able to form multicellular tumor spheroids that could be used as a functional model for the study of the biological response induced by UAs in cancer cells. Thus the aim of my research was the generation of 3D spherical cultures from selected tumor cell lines and the evaluation of the possibility of their potential application in studies concerning the cellular response induced by unsymmetrical bisacridines. Furthermore, I compared the cellular mechanism of action of UAs in selected cancer cells cultured in 2D and 3D conditions with an additional preliminary focus on the population of cancer stem cell-like cells.

In my studies, I focused on four unsymmetrical bisacridines: C-2028, C-2041, C-2045, and C-2053, the structures of which are presented in Figure 1.1. To facilitate a better comparison of my analyses, I also studied reference compounds frequently employed in the treatment of lung (cisplatin and etoposide) and colon cancer (irinotecan), which are also depicted in Figure 1.1.

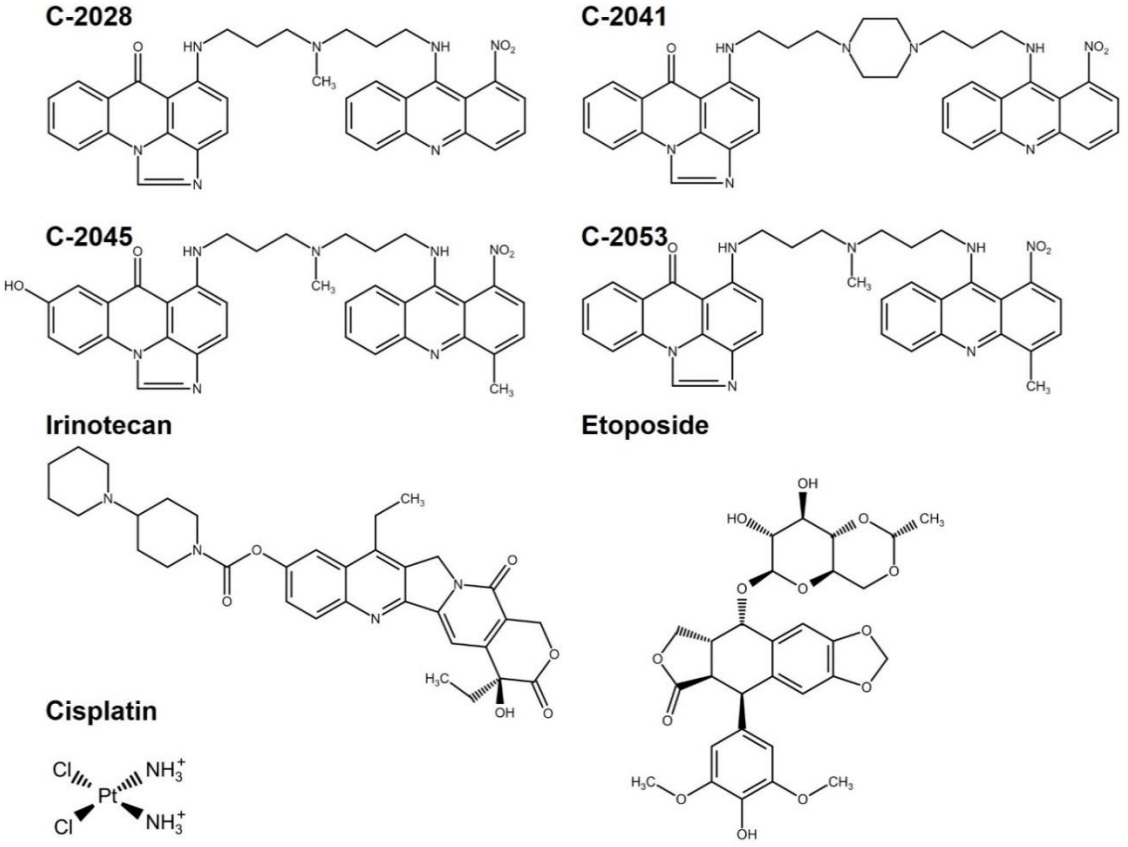

Figure 1.1. Chemical structures of studied compounds: four unsymmetrical bisacridines (UAs) – C-2028, C-2041, C-2045, and C-2053, together with the reference compounds – irinotecan, cisplatin and etoposide.

2. INTRODUCTION

2.1. Cell cultures in research of new chemotherapeutic agents

Cell culture-based assays are an essential part of the drug discovery process as they provide a simple, fast, and cost-effective tool to investigate the effects of a new drug on cells without resorting to large-scale animal testing, making them both ethically and financially favorable. To date, most *in vitro* experiments with new chemotherapeutics have been carried out using traditional two-dimensional (2D) culture methods, in which cells grow in a monolayer. Cultures obtained in this way are routinely used as initial models to evaluate the efficacy and safety of compounds with therapeutic potential, thanks to their ease of use, reproducibility, and cost-efficiency [Breslin S. and O'Driscoll L., 2013; Chaicharoenaudomrung N . et al., 2019; Edmondson R. et al., 2014; Waltz A. et al., 2014].

In the typical preclinical screening process of therapeutic agents, the success rate of compounds dramatically declines as they move from 2D cell culture systems and animal models to clinical trials. Ultimately, less than 5% of the therapeutics that undergo clinical trials are eventually approved for wide use. This failure could be attributed to the lack of consistent prediction of drug responses between 2D cell culture systems and human trials [Chaicharoenaudomrung N. et al., 2019].

One significant limitation of commonly used 2D culture systems is their inability to replicate the complex 3D environment in which virtually all cells in the human body exist. *In vivo*, cells interact with neighboring cells and extracellular matrix proteins, and this 3D context plays a crucial role in cellular behavior, including growth, differentiation, and metabolism. Unfortunately, 2D systems cannot properly reproduce these critical interactions and therefore do not accurately represent the function and phenotype of 3D tissues. As a result, data obtained from 2D cultures may not fully reflect the actual behavior of drugs in the complex environment of the human body, leading to potential discrepancies between preclinical and clinical outcomes [Breslin S. and O'Driscoll L., 2013; Lee J. et al., 2009].

2.2. Characteristics of spherical cultures

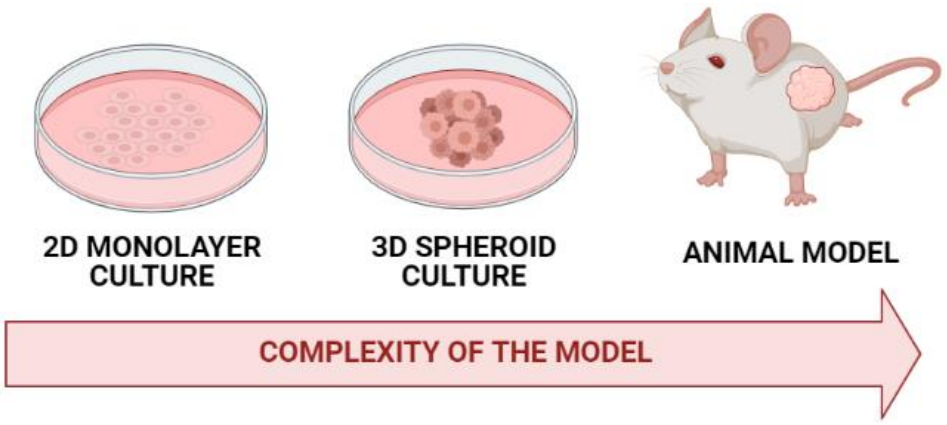

Figure 2.1. Comparison of the complexity of culture models. Created in BioRender.com

In response to the limitations of 2D monolayer cultures, researchers are increasingly turning to three-dimensional cell culture models (spheroids). Spheroids offer a more physiologically relevant alternative that serves as a link between the oversimplified structure of 2D cultures and the highly complex nature of tumors *in vivo* (Figure 2.1.). 3D cell cultures aim to recreate the natural microenvironment of cells, allowing them to organize into multicellular structures and maintain crucial interactions with the surrounding extracellular and intercellular matrix.

In simple terms, spheroids consist of an outer region of proliferating and migrating cells that surrounds an intermediate layer of dormant cells, and, if spheroids are large enough, a necrotic core (Figure 2.2). There may also be apoptotic cells in the peri-necrotic zone. This arrangement resembles the organization of the tissues that surround neoplastic blood vessels and is defined due to specific gradients of pH, oxygen, nutrients, and metabolites, similar to those found in poorly vascularized or avascular solid tumors [Costa E.C. et al., 2018; Devi G.R., 2016; Mikhail A.S. et al., 2013; Nath S. and Devi G.R., 2016, and Pinto B., et al., 2020].

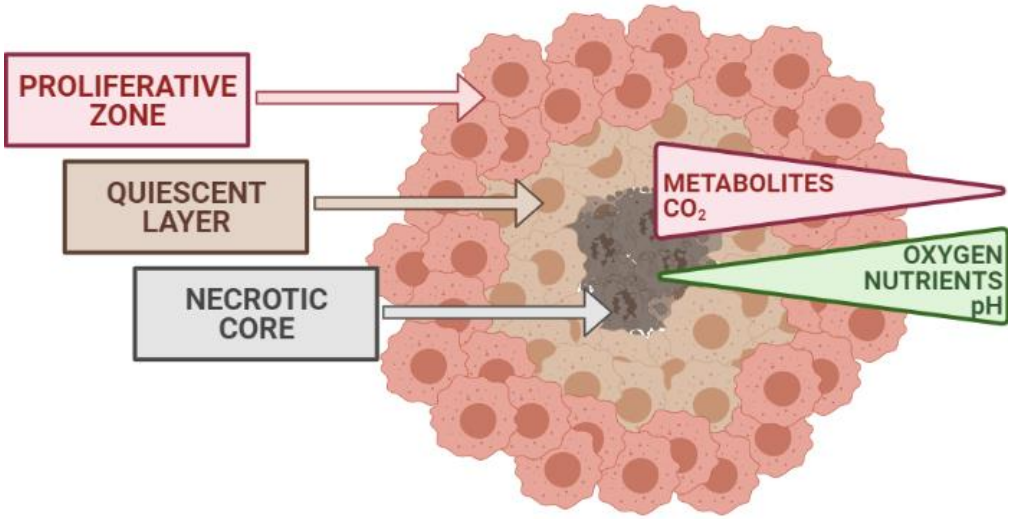

Figure 2.2. Schematic structure of the multicellular tumor spheroid. Visible cell layers (proliferative, quiescent, and necrotic) are present due to the existence of nutrients, oxygen, pH, CO_2, and waste gradients. Created in BioRender.com

This means that, much like *in vivo* tumors, spheroids contain simultaneously proliferating and dormant cells, normoxic and hypoxic cells, as well as living and apoptotic or necrotic cells. Using spheroids, therefore, allows researchers to study these various types of cells, providing valuable insights into tumor behavior and potential anticancer treatments [Waltz A. et al., 2014]. A brief summary of the most important differences between 2D monolayer and 3D spherical cultures is presented in table 2.1.

Table 2.1. Comparison of 2D monolayer and 3D spherical cultures based on Chaicharoenaudomrung N. et al., 2019; Costa et al., 2016; Costa et al., 2018; Fröhlich E., 2020; Thoma C. et al., 2014

Feature	Monolayer cultures	Spherical cultures
Structure	Cells grow in a single layer on a flat surface of a culture dish	Cells self-assemble into 3D spheroids, mimicking tumors *in vivo*
Growth kinetics	The fast growth of cells in culture	Slower than in 2D, similar growth pattern to *in vivo*, cell proliferation is mostly limited to the periphery of the spheroid
Cell-cell interactions	Limited cell-cell interactions	Enhanced cell-cell interactions
Interactions with extracellular matrix (cell-ECM interactions)	Minimal interactions with the ECM	Stronger interactions with the ECM, enhanced production and deposition of tumor ECM proteins, such as collagen, fibronectin, and laminin
Nutrient and oxygen availability	Equal exposition of all cells to nutrients and oxygen	Variable access to oxygen and nutrients, presence of specific gradients in culture similar to those observed in poorly vascularized or avascular tumors
Heterogeneity	Mostly uniform behavior of cells due to their low heterogeneity	Better representation of tumor heterogeneity and cellular diversity, reflecting *in vivo* conditions (presence of proliferating, quiescent, apoptotic, necrotic, and hypoxic cells)
Drug response	May not adequately predict the effects of drugs due to the simplicity of the culture and uniform drug penetration to cells - often no correlation between results for monolayer cultures and the responses *in vivo*	Potential for better prediction of drug responses, thanks to more heterogeneous drug penetration pattern - tumor cells in spheroids show similar drug resistance patterns to those observed in patients
Gene expression	Differential gene expression compared with *in vivo* tumors	The gene expression pattern is comparable to that observed in solid tumors
Cost and complexity	Simpler and generally cheaper, plenty of commercially available tests	More challenging to establish and maintain culture, often requiring specialized equipment, thus more expensive, fewer commercially available tests
Applications	Useful for initial screening of anticancer compounds, for evaluation of their activity, and study of their molecular and biochemical effects in cells	Valuable for studying tumor behavior, drug efficacy, penetration, and mechanism of action in more *in vivo*-like conditions

The usefulness of the 3D spherical model varies among different malignant tumors. For some cancers, such as leukemia, the lack of relevance of spheroids seems obvious, at least in terms of various pathophysiological parameters. Also, for melanoma, skin culture models are more suitable for reflecting the behavior of cancer cells at the primary tumor site, but spheroids may provide insight into metastatic growth. As long as a researcher recognizes the relevant limitations, spheroids can prove valuable tools for studying avascular metastasis. For solid tumors, in which avascular regions are crucial in tumor development and drug resistance, spheroids offer an accurate representation of these microenvironments. Despite certain limitations, spheroids remain a highly useful *in vitro* model, complementing the 2D monolayer system and helping to understand various aspects of tumor biology and drug response [Friedrich J., et al., 2009].

The size of the spheroids used in anticancer drug research clearly affects the response to treatment and must be defined at the beginning of the experiments. Interactions between cells and cell matrix occur already in spheroids with a diameter below 150 μm. Compared to 2D models, the expression of individual genes is changed even in such small spheroids, but in order to obtain characteristic chemical gradients (e.g. oxygen, nutrients, and metabolites) and differentiation in cell proliferation in individual regions of the spheroid, diameter within 200-500 μm is required. The necrotic core usually occurs in spheroids larger than 500 μm. The pathophysiological gradients and the distribution of heterogeneous populations of cells in the spheroid are cell-line dependent but mainly comparable to those found *in vivo* in avascular tumors, micrometastases, or inter-capillary microregions of solid tumors [Hirschhaeuser F. et al., 2010].

One of the problems that researchers face during anticancer compound testing is that some compounds require longer exposure times (over 6 days) to observe the effect on cell viability *in vitro.* For monolayer cultures, the incubation time with compounds is usually limited by the size of the culture vessel and the cell doubling time. Additionally, with long incubation times, monolayer cultures may exhaust the medium. Due to the gradient of oxygen and nutrients in the spheroids, cells multiply mainly at the periphery, close to the surface of the spheroid. This fact, together with the large surface area of spheroids, makes cell growth relatively slow compared to monolayer culture and enables long-term exposure to drugs, which is an important advantage of this culture model [Selby M. et al., 2017].

2.3. Classification of 3D culture models of cancer cells

Three-dimensional culture models vary in terms of cancer cell sources, cell handling protocols, and the time required to establish the 3D cultures. There are four main forms of 3D cancer models:

1) Multicellular tumor spheroids (MCTS), also referred to as cancer cell spheroids, or tumor spheroids – formed from a single cell suspension of immortalized cell lines in a conventional cell culture medium supplemented with serum. In this regard, MCTS can be considered an extension of the conventional 2D monolayer cultures of cancer cell lines. While they may not

fully resemble the histology of primary cancers, they do replicate the metabolic and proliferative gradients found in *in vivo* tumors. Moreover, MCTS exhibit clinically relevant chemoresistance, making them valuable models for studying cancer behavior and responses to treatment. Due to these advantages, MCTS remain the most classical approach in the use of 3D cultures [Friedrich J., et al., 2009; Ham S.L. et al., 2016; Ishiguro T.S. et al., 2017].

2) tumorospheres, or tumor-derived spheroids – produced similarly to MCTS from a single-cell suspension, but under serum-free conditions. Stem cell medium is instead supplemented with several factors that promote stem cell growth, such as basic fibroblast growth factor (bFGF), and epidermal growth factor (EGF). A subset of cancer cells capable of proliferating without the supplementation of serum are suggested to have stem cell-like properties, thus this model is mainly purposed for the enrichment of cancer stem cells (CSCs) or cells with stem cell-related characteristics. Tumorospheres are not intended to replicate cancer tissues but rather serve as a platform for studying CSCs properties. It is important to acknowledge that tumorospheres do not fully recreate the 3D structure and environment of an *in vivo* tumor [Ham S.L. et al., 2016; Ishiguro T.S. et al., 2017; Weiswald LB.. et al., 2015].

3) tissue-derived tumor spheres (TDTS) – generated by fine slicing and dissociation of tumor tissue, which is then cultured in a classical medium supplemented with serum. Tissue-derived tumorospheres faithfully represent the parent tumor concerning histological features, gene expression profiles, mutations, and tumorigenicity [Ham S.L. et al., 2016; Weiswald L.B. et al., 2015].

4) organotypic spheroids, or organotypic multicellular spheroids (OMS) – obtained by cutting tumor tissue fragments into submillimeter pieces and culturing them in a non-adherent vessel with the addition of serum or other supplements. The main difference from the tissue-derived tumor spheres is the lack of dissociation into single-cell suspension, thanks to which OMS appear to most closely resemble the *in vivo* tumors. They exhibit morphology similar to the original tumor and maintain its heterogeneity, including the presence of stromal components [Ham S.L. et al., 2016; Weiswald L.B. et al., 2015].

The first two approaches allow for easy initiation and maintenance of 3D cultures derived from various cell lines, are compatible with high-throughput drug screening, and enable extensive studies of many cancer-associated processes, such as tumor growth, migration, invasion, or drug resistance. MCTS and tumorospheres also offer the possibility of creating more complex models by including additional components of the tumor microenvironment, such as fibroblasts, immune cells, and ECM proteins. On the other hand, the latter two approaches offer a more accurate representation of tumors *in vivo*, but their initiation and expansion can be challenging, which prevents their use in some cases, such as for instance drug screening [Ham S.L. et al., 2016].

2.4. Methods for 3D spheroid generation

Spheroids, which are composed of neoplastic cells, show various morphologies depending on the nature of the cell and on the culture conditions [Ho W.Y. et al., 2012]. The ideal

method of obtaining spherical cultures should lead to the production of compact aggregates of the same size and uniform shape. To be able to use spherical cultures in large-scale screening tests, it is necessary to establish a simple methodology with a short time of spheroid culture and the possibility of process automation [Costa E.C. et al., 2018; Vinci M. et al., 2012; Ho W.Y. et al., 2012].

In the nearly 50 years that have passed since Sutherland et al. first used spheroids in cancer research, many methods for producing spherical cultures have been developed and optimized. Methods for spheroid generation are usually divided into two groups depending on the presence or absence of scaffolding. The most popular methods available for spheroid formation are shown in Figure 2.3. and described in the following sections.

2.4.1. Scaffold-based 3D culture methods

In scaffold-based methods, 3D cultures are obtained by stimulating cell growth on artificial three-dimensional structures to which cells anchor and fill the gaps present in the structures, where they then grow and divide [Breslin S. and O'Driscoll L., 2013; Nunes A.S. et al., 2019]. For spherical cultures, cells can be plated on a cell-free, solid 3D scaffold (e.g. sponges, foams, or membranes), on a solidified matrix (e.g. Matrigel™, methylcellulose) or seeded with the liquid matrix and embedded in it after gelling [Nath S. and Devi GR, 2016]. The three-dimensional scaffold geometry can act as a simple mechanical support to allow the formation of spheroids or have optimized properties that result in an architecture similar to that found in the native extracellular matrix of human tissues [Costa E.C. et al., 2016; Nunes A.S. et al., 2019].

The scaffolds used for spheroid generation can be made of biomaterials of natural origin, e.g. collagen or alginate, semi-synthetic biomaterials, e.g. chitosan, or synthetic ones, e.g. polycaprolactone, polyethylene glycol [Costa E.C. et al., 2016; Langhans S.A., 2018; Nunes A.S. et al., 2019]. The use of natural biomaterials for *in vitro* culture contributes to increasing cell viability and obtaining a cell phenotype similar to that observed *in vivo,* thanks to high biocompatibility, natural adhesive properties, presence of endogenous chemokines and growth factors [Langhans S.S., 2018; Nunes A.S. et al., 2019]. A natural hydrogel widely used in 3D cell cultures is called Matrigel™, which is a commercially available gelatinous mixture of proteins (mainly laminin, collagen, and entactin) and growth factors (including EGF - epithelial growth factor, bFGF - basic fibroblast growth factor, NGF - nerve growth factor, and TGF-β - transforming growth factor β) [Langhans S., 2018]. In the case of natural polymers, the content of endogenous factors may vary from batch to batch, thus reducing the reproducibility of results. Moreover, traces of undefined natural ingredients may hinder the formation of spheroids in some cell lines.

Scaffolds made of natural polymers have a low tensile strength, which can lead to rapid degradation of the matrix and may cause difficulties in long-term testing. In turn, the use of synthetic biopolymers allows the production of artificial 3D structures with high mechanical strength, which allows the cultivation of spheroids for a prolonged time. However, in order to mimic *in vivo* conditions, it is necessary to enrich the scaffold with biologically active molecules such as hormones or extracellular matrix proteins [Nunes A.S. et al., 2019]. The use of scaffolding culture

in the research of potential anti-cancer chemotherapeutic agents is sometimes problematic due to the possibility of some biomaterials interfering with the therapeutic effect of drugs. Difficulties with microscopic analysis of obtained spheroids may also occur, depending on the size of the scaffold and its transparency, as well as complications with isolation and transfer of spheroids for further studies [Costa E.C. et al., 2018].

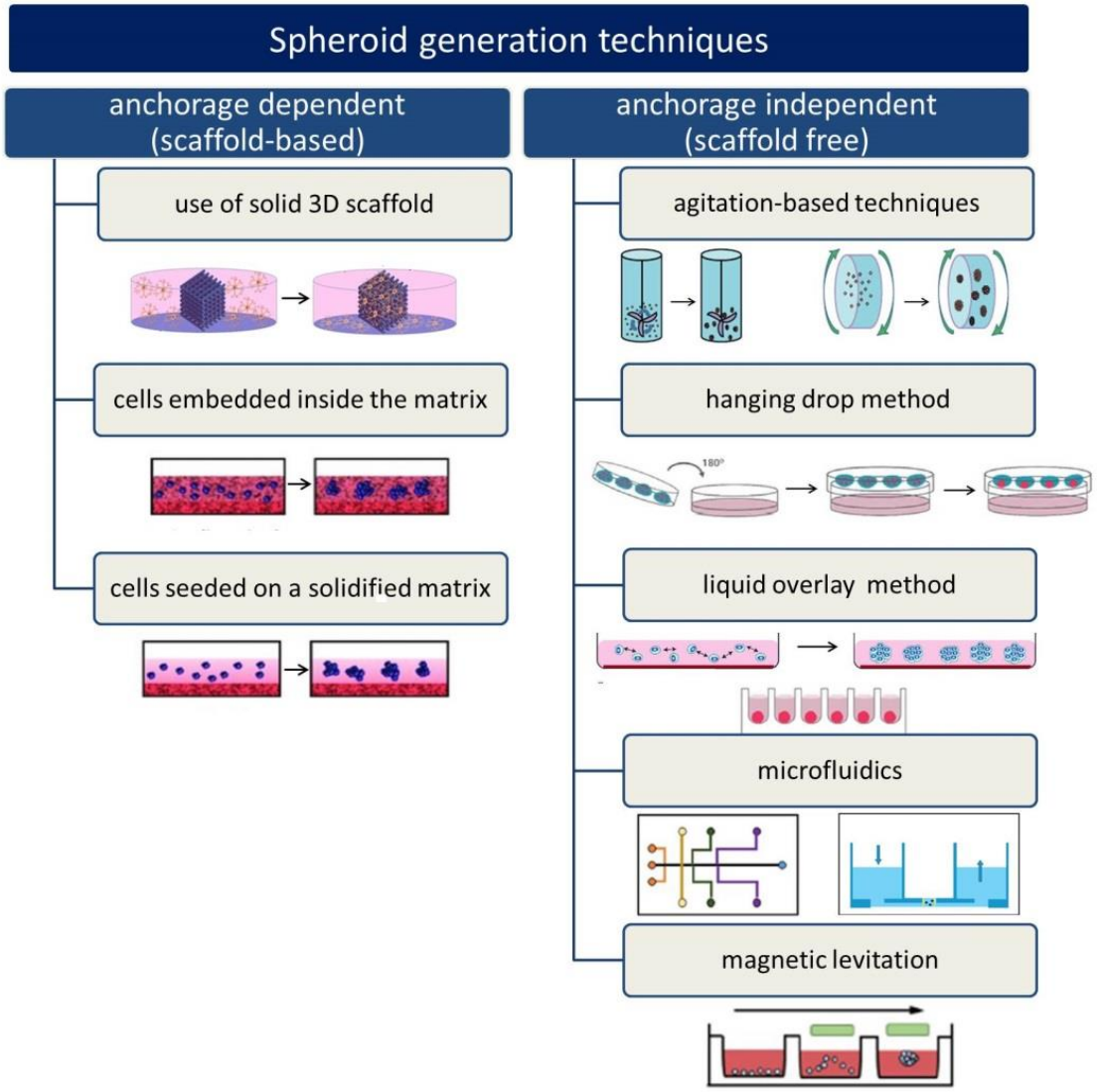

Figure 2.3. Methods for spheroid formation with schematic drawings for each of the techniques based on Breslin S. and O'Driscoll L., 2013; Hoarau-Vechot J. et al., 2018; Langhans S., 2018; Shoval H. et al., 2017

2.4.2. Scaffold-free 3D culture methods

The scaffold-free 3D culture methods allow cells to directly interact and aggregate based on biological signals, without exogenous platforms, and the extracellular matrix consists of proteins produced by cells during the formation of spheroids. Among the anchorage-independent 3D culture methods, the following can be distinguished: agitation-based spheroid formation techniques, the hanging drop method, forced-floating methods as well as microfluidics and magnetic levitation [Costa E.C. et al., 2016; Langhans S.A., 2018; Nath S. and Devi G.R., 2016; Nunes A.S. et al., 2019].

In agitation-based approaches for spheroid production, cell aggregation is achieved by keeping the cell suspension in constant motion, e.g. in a stirred flask, or by rotation of the culture flask around a horizontal axis. This continuous movement of the cell suspension prevents cells from adhering to the walls of the culture containers, allowing them to spontaneously aggregate and form spheroids. While both approaches are based on the same principle, the horizontally rotating flask method has been found to produce more homogenous spheroids compared to the spinner flasks with stirring [Breslin S. and O'Driscoll L., 2013; Fröhlich E., 2020; Kitel R. et al., 2013; Nunes A.S et al., 2018].

The hanging drop method is a popular 3D culture technique that uses the ability of cells to self-aggregate when no surface is available to form a monolayer culture. Hanging droplets are created by applying a small volume of cell suspension to the lid of the culture plate and inverting the plate to form a drop which, due to the surface tension, remains on the lid. Thanks to the action of microgravity, cells gather at the bottom of the droplet, where they form spheroids. Hanging drops can also be obtained using specialized plates with open, bottomless wells, but with longer cultivation times, due to the limited drop volume and the lack of possibility to replace the culture medium, it is necessary to transfer spheroids to plates with a non-adhesive surface [Bresciani G. et al., 2019; Breslin S. and O'Driscoll L., 2013; Kitel R. et al., 2013; Langhans S.A., 2018; Nunes A.S et al., 2018].

A relatively simple method for spheroid generation is to prevent cells from sticking to the bottom of the vessel by modifying its surface. Commercially available plates are divided into cell-repellant plates and Ultra Low Attachment (ULA) plates [Comley J., 2017; Froehlich K. et al., 2016]. These plates are usually made of polystyrene and the surface of the wells is covered with appropriate coatings that prevent cell adhesion. As a result, instead of cell-vessel interaction, intercellular interactions are promoted. Used coatings include natural polymers (e.g. agar and agarose) and synthetic polymers (e.g. PHEMA – 2-hydroxyethyl polymethacrylate) [Breslin S. and O'Driscoll L., 2013; Kitel R. et al., 2013; Langhans S.A., 2018; Selby M. et al., 2017]. Obtaining single spheroids of homogeneous size and similar morphology is possible thanks to the use of multi-well plates with concave (U-shaped) or conical (V-shaped) well bottoms. After the cell suspension is plated into the multi-well plate, the cells aggregate at the bottom of the well, and, due to gravitational sedimentation, they associate and form spheroids. In order to enforce the collocation of cells and thus accelerate the process of spheroid formation, the plates are often centrifuged, which also results in more compact aggregates. However, centrifuging or moving the plate should be an optimized and careful process, so as to promote cell aggregation without causing mechanical damage that could lead to cell death [Bresciani G. et al., 2019; Breslin S. and O'Driscoll L., 2013; Costa E.C. et al., 2018; Kitel R. et al., 2013].

To reduce the costs of cultivating spherical cultures on non-adhesive substrates, many people choose to coat the surface of the plates with polymers in the laboratory. While agar or agarose coatings are popular due to their low cost and easy accessibility, the plates coated with these polymers have a relatively short shelf life. On the other hand, coating with 2-hydroxyethyl polymethacrylate substantially prolongs the storage time of the prepared plates [Costa E.C. et al.,

2018]. Moreover, commercially available ULA plates have been found to yield spheroids with better compactness compared to plates coated with agarose [Vinci M., et al., 2012].

Microfluidic devices designed for cell culture are based on polydimethylsiloxane membranes and typically consist of microchannels and microchambers. Cells suspended in the culture medium flow through the microchannels and they accumulate in microchambers, forming spheroids. The use of microfluidics allows for precise control of the culture environment, making it possible to maintain conditions similar to those found in the organism's natural setting. This is achieved through a constant supply of oxygen and nutrients while effectively removing the byproducts of cellular metabolism [Breslin S. and O'Driscoll L., 2013; Fröhlich E., 2020; Nunes A.S et al., 2018; Langhans S.A., 2018].

Magnetic levitation uses superparamagnetic iron oxide nanoparticles (SPION), which guide the self-assembly of cells into spheroids under the influence of magnetic forces. Adherent cells are incubated overnight with nanoparticles, then seeded on low-adhesion plates, and a magnet is placed on the lid of the plates. Cells associated with nanoparticles are pulled up under the influence of magnetic forces and self-aggregate to form spheroids within a few hours [Langhans S.A., 2018; Nath S. and Devi G.R., 2016].

Just as scaffold-based methods of spheroid generation, each of the described scaffold-free techniques has its own advantages as well as disadvantages and limitations. Some of them are presented in Table 2.2.

Table 2.2. Advantages and disadvantages of different anchorage - independent 3D cell culture methods based on Breslin S. and O'Driscoll L., 2013; Costa E.C. et al., 2016; 2018; Nunes A.S. et al., 2019; Langhans S.A., 2018.

Spheroid generation method	Advantages	Disadvantages
spinner flasks and rotating systems	• easy large-scale production of spheroids • possibility of a long-term culture • medium exchange possible • the constant movement of the medium supports the transport of nutrients and metabolites • easy control of culture conditions (including pH, metabolite and nutrient concentration, and oxygen level)	• the amount of spheroids obtained is impossible to control • formation of spheroids with heterogenous sizes • possible influence on the physiology of cells due to the shear force generated by the agitation • specialized equipment required • large amounts of nutrients used
hanging drop method	• high throughput • easy to manufacture and low-cost • homogeneous spheroids of similar sizes • no specialized equipment required • formation of one spheroid per droplet	• the limited size of the spheroids produced due to droplet volume • higher costs when using specialized plates • transfer of spheroids is necessary for prolonged cultivation or further experiments (possible damage to spheroids) • impossible to replace the medium without transferring spheroids

Spheroid generation method	Advantages	Disadvantages
liquid overlay methods	• easy handling and large-scale production • relatively inexpensive • no specialized equipment required • easy access to spheroids during experiments • obtaining one spheroid per well, spheroids of uniform size and morphology (when using U-shaped / V-shaped bottom plates) • no need for spheroid transfer • changing the culture medium is relatively easy • very fast method (when using ready-made ULA plates) • high repeatability of experiments (ULA-plates)	• differences in the size, shape, and number of spheroids (only in plates with flat surfaces) • time-consuming (when self-coating plates) • difficulties in forming tight spheroids in some cell lines
microfluidics	• possible control of the size and shape of the generated spheres • easy to use in large-scale production of spheroids • high repeatability of experiments • constant supply of oxygen, nutrients, and drugs • long-term culture possible	• expensive method • specialized equipment is required • problems with further examination of spheroids • limitations in the generation of large spheroids due to the small sizes of microwells

In scaffold-free methods, the process of spheroid formation is divided into three subsequent phases: aggregation, compaction, and spheroid growth [Fröhlich E., 2020]. In the aggregation phase, the spheroid formation is initiated, through the interaction between extracellular matrix (ECM) components, particularly fibronectin, produced by cells, and integrin. This is followed by an upregulation of E-cadherins, which are type I transmembrane proteins. E-cadherin expression was found to be a crucial factor in spheroid formation, as it stabilizes cell contacts [Fröhlich E., 2020; Smyrek I., et al., 2019]. An intact F-actin network strengthens these intercellular contacts, while microtubules play a role in the accumulation of adhesion molecules in the plasma membrane. Cell arrangement is also crucial for spheroid formation, and microtubules help balance the formation and reorganization. Besides E-cadherin, connexins and pannexins, another transmembrane proteins, have been shown to facilitate spheroid formation, promoting intercellular communication [Fröhlich E., 2020].

2.5. Differences in spheroid formation ability

Despite following similar formation processes, various cells exhibit significant differences in their ability to form spheroids, as well as in the size and shape of the spheroids generated. Some cell lines show a preference for specific techniques, whereas others can form spheroids under various conditions [Fröhlich E., 2020]. Extensive research has been conducted to investigate the spheroid-forming capacity of different human cell lines, and interestingly, the ability to form spheroids does not seem to be correlated with the cells' tissue origin. For instance, in a study by Vinci M. et al., 40 tumor cell lines were tested using ULA plates, and among the five

colon cancer cell lines examined, only HCT116, HT29, and DLD-1 formed tight spheroids, while RKO and SW620 cells formed only loose aggregates [Vinci M. et al., 2012].

It is important to note that not all primary tumor cells or all established cell lines have the capability to form spheroids. Each specific case and every spheroid culture technique must be evaluated independently for their spheroid formation capacity [Friedrich J., et al., 2009]. In some cases, where the use of scaffold-free methods results in loose cellular aggregates instead of spheroid formation, researchers have explored the addition of certain supplements to facilitate cell aggregation and promote spheroid generation. These supplements include methylcellulose, ECM constituents (such as fibronectin, laminin, and collagen), and ECM protein mixtures like Matrigel™. While this approach expands the range of cancer cells that can form spheroids, it is important to consider the impact of matrix-driven alterations on cell growth, gene expression, and behavior of cells, including drug response [Costa E. et al., 2018; Friedrich J., et al., 2009]. For example, the addition of 2.5% Matrigel™ during the initiation of spheroid cultures of RKO and SW620 colon cancer cells led to improvements in their three-dimensional structure [Vinci M. et al., 2012].

Therefore, when applying spheroids in anticancer research, it is crucial to refer to the existing literature in order to select the most appropriate method for spheroid generation. This is to ensure that the chosen method is consistent with the specific characteristics and behavior of the target cell line, which will lead to more accurate and relevant experimental results.

2.6. 3D co-cultures

It is widely recognized that solid tumors exhibit a heterogeneous cellular composition, which means, that they consist not only of cancer cells, but also of nonmalignant stromal cells such as adipocytes, fibroblasts, immune cells (like lymphocytes and macrophages), lymphatic endothelial cells, vascular endothelial cells, and pericytes. Despite being nonmalignant, these cells play crucial roles in tumor development by interacting with each other and with cancer cells through the secretion of cytokines and growth factors. These interactions promote various events, including tumor angiogenesis, proliferation, invasion, metastasis, and mechanisms of therapeutic resistance [Nunes A. et al., 2018].

While spheroids composed of only one cell type can mimic certain aspects of cancer biology, such as for example micrometastasis, they cannot replicate the complex tumor microenvironment. To achieve a more accurate representation, co-cultures of cancer cells with other cell types are becoming widely used. Among the most commonly incorporated cell types there are immune cells, fibroblasts, and endothelial cells [Fröhlich E., 2020].

In recent years, cancer-associated fibroblasts (CAFs) have been recognized as crucial contributors to tumor development and progression, being present in most solid tumors. Studies involving fibroblasts isolated from tumor patients have provided valuable insights into the distinct characteristics of CAFs, setting them apart from normal fibroblasts. Cancer-associated fibroblasts typically originate from normal fibroblasts, activated by tumor-cell-derived factors such as transforming growth factor-β (TGF-β). Additionally, they can be derived from bone-marrow

progenitor cells and transdifferentiated epithelial cells. These specialized fibroblasts play a key role in supporting various tumor cell functions through paracrine signaling of factors such as for instance hepatocyte growth factor (HGF), fibroblast growth factor (FGF), epidermal growth factor (EGF), and interleukin-6. These factors promote tumor initiation, proliferation, epithelial-mesenchymal transition (EMT), and invasion, and also inhibit chemotherapy-induced apoptosis, contributing to poor prognosis [Ham S.L. et al., 2016]. Co-cultivation of cancer cells with CAFs has been shown to increase the expression of proliferation and invasive markers in spheroids, such as transforming growth factor beta 1 (TGF-β1), N-cadherin, and vimentin. Moreover, numerous studies have demonstrated that the addition of cancer-associated fibroblasts to cell culture directly influenced the efficacy of anticancer treatments. For instance, in 2D cultures, more than 90% of HN3, HN4, and HN9 head-and-neck cancer cells died after treatment with sorafenib or cisplatin, whereas in spheroids, over 60% of cells remained viable. This fraction was even higher when co-culture with CAFs was applied – the percentage of viable cells reached more than 90% [Nunes A. et al., 2018]. Thus, co-culturing fibroblasts with tumor cells in spheroids provides a more adequate representation of *in vivo* tumor microenvironment and helps researchers to investigate the drug responses to various chemotherapeutics more accurately [Fröhlich E., 2020].

The presence of macrophages in tumors is often associated with a poorer prognosis for a patient. Co-cultivation of breast cancer cells with macrophages resulted in a significant increase in the number of spheroids compared to monoculture. Interestingly, in certain cancers, the addition of macrophages to spherical cultures was proven to suppress tumor proliferation. For instance, in co-culture spheroids of human colorectal cancer cells with macrophages, the expression of genes related to proliferation was reduced, while apoptosis-associated genes were elevated. This indicates activation of the inflammatory pathway, which results in triggering the anti-tumor immune responses [Ham S.L. et al., 2016].

The application of tri-culture spheroid models, which comprise of cancer cells, macrophages, and fibroblasts can provide a close resemblance to tumor microenvironment *in vivo*. In a tri-culture of HT29 colon cancer cells with monocytes and fibroblasts, spheroids showed a 5-fold increase in cancer cell invasiveness compared to monoculture. Existing evidence from heterotypic spheroid models provides insight into the role of fibroblasts and immune cells in modulating cancer cell functions in the primary tumor [Ham S.L. et al., 2016].

The inclusion of endothelial cells in spheroid co-cultures is also significant as it can have the potential to partially mimic the formation of functional vessel equivalents within the spheroids, which can help to reduce the size of the necrotic core by enhancing oxygen and nutrient supply to the proliferating tumor cells. Therefore, co-culturing cancer cells with endothelial cells can provide valuable insights into angiogenesis and its influence on tumor growth and development, as well as help evaluate the pro- and anti-angiogenetic potential of drugs [Fröhlich E., 2020; Hirschhaeuser F. et al., 2010].

Understanding the impact of stromal components, both individually and collectively, on the functions of cancer cells is of significant importance. 3D spheroid cultures provide

a valuable tool for recreating important aspects of the tumor microenvironment and one of the main advantages of this culture model over animals is the flexibility of spheroids, which allows for easy modification of cellular components and complexity of the model [Ham S.L. et al., 2016]. Although co-cultures of multiple cell types in spheroids are useful for gaining a deeper understanding of tumor behavior, they may have limitations in drug screening. The variability in composition resulting from different cell proportions may affect the reproducibility and reliability of experiments regarding chemotherapeutics. Therefore, for drug testing purposes, researchers often rely on simpler spheroid models consisting of only one cell type. These single-cell-type spheroids still serve as valuable tools to study specific aspects of cancer biology, but may not fully capture the complexity of the tumor microenvironment that multi-cell-type spheroids can offer [Fröhlich E., 2020].

2.7. 3D cultures and drug resistance

One of the main benefits of 3D cell cultures is their ability to better reflect the complexity and heterogeneity of tissues within the human body. As a result, drug responses observed in 3D models are often more accurate and predictive of *in vivo* outcomes, making spheroids a promising tool to reduce the risk of late-stage drug candidate failures. According to the majority of literature reports, numerous compounds have clearly limited efficacy in the 3D environment compared to the results obtained from conventional 2D cultures. Therefore, spheroids can help in the selection of the most promising chemotherapeutic agents, thereby limiting the need for extensive animal testing and enabling the identification of potential drugs with increased distribution and effectiveness in an environment resembling *in vivo* conditions. Despite different mechanisms of action, many chemotherapeutic agents, highly active in monolayer cultures, exhibit a substantial reduction of their efficacy in spheroids. This highlights the importance of incorporating 3D cell cultures, like spheroids, to better assess the true potential of drug candidates [Hirschhaeuser F. et al., 2010; Karlssson H. et al., 2012].

The reduced efficacy of many chemotherapeutics in 3D spherical cultures compared to monolayer cultures may result from a combination of various factors related to the spatial organization and unique microenvironment of spheroids. The presence of specific gradients within spheroids also extends to differential drug exposure throughout spheroid layers, with the outer cells being more susceptible to treatment, while the inner cells are less affected due to limited drug diffusion. Therefore, the penetration and distribution of the drug in 3D spheroids may be significantly limited, reducing the overall efficacy of the drug in this culture model [Pinto B. et al., 2020].

Another factor that may influence the efficacy of drugs in 3D spheroids is the altered expression of numerous genes compared to monolayer cultures, especially those connected with metabolism and drug transport. For example, therapeutic resistance in spheroids may be connected with the high expression of the multidrug resistance gene 1 (*MDR1*), which encodes the P-glycoprotein, responsible for the active transport of foreign substances (including drugs) outside of the cell. Increased expression of this gene, as well as anti-apoptotic factors, such as

Bak, Bax, Bcl-2, and p53, and vascular endothelial growth factor (VEGF), is caused by a lack of sufficient access to oxygen in the inner regions of spheroids and associated with it upregulated expression of hypoxia-inducible family factors (HIF). A high concentration of HIF-1α protein was detected in spheroids derived from HeLa, MCF-7, and DU-145 cells and compared with monolayer cultures, where expression of genes encoding this protein was not observed or was negligible. Additionally, the resistance to anticancer treatment in spheroids may also be connected with the fact, that certain compounds, such as for example 5-fluorouracil, cisplatin, and irinotecan, require oxygen to induce an effective anticancer response through the generation of reactive oxygen species (ROS) that damage the cell's membrane and DNA. In response to resistance resulting from hypoxia in spheroids and solid tumors, a group of hypoxia-activated prodrugs (HAPS) has been developed. These are drugs that undergo chemical reduction and become active only under hypoxic conditions – they do not affect cells in an environment with normal oxygen levels [Nunes A.S. et al., 2019].

In addition to hypoxia, various other factors can influence drug resistance in spherical cultures, including:

1) changes in the cell energy metabolism – in the inner regions of spheroids, limited oxygen leads to anaerobic metabolism, causing overexpression of glucose transporter-1 (GLUT-1) and lactate dehydrogenase (LDH). This can result in drug resistance by altering the expression of multidrug resistance-associated protein 1 and P-glycoprotein,

2) acidic microenvironment – lactate production in spheroids promotes acidification of the core, leading to a low pH that affects drug cellular uptake, particularly in the case of weak basic drugs, which become protonated and have reduced uptake,

3) quiescence of cells – acidic pH, lack of oxygen and nutrients in spheroids induces a dormant state in cells and an increased number of cells are arrested in the G0-G1 phase of cell cycle compared to monolayer cultures. This nonproliferative state may lead to poor therapeutic efficacy for drugs that require cell proliferation to exhibit their antitumor activity,

4) heterogeneity of spherical cultures – as mentioned in subsection 2.6., presence of non-malignant cells in spheroids, such as fibroblasts, immune cells, and endothelial cells, may significantly affect the drug response,

5) presence of cancer stem cells – cancer stem cells are believed to be responsible for resistance to chemo- and radiotherapy. Spherical cultures typically have a more adequate proportion of cancer stem cells compared to monolayer cultures, which results in similar drug resistance to that observed *in vivo*,

6) cell-cell physical interaction – enhanced interactions between cells in the culture lead to higher expression of E-cadherins, which can influence the MDR1 levels through HIF-1α, contributing to poor response to anticancer therapy,

7) ECM proteins deposition – spheroids show increased expression of ECM proteins (e.g. fibronectin, collagens) compared to monolayer, which contributes to the establishment of a chemoresistant environment,

8) physical barrier – limited drug penetration and delivery to cells in spheroids due to increased tissue density [Ham S.L. et al., 2016; Nunes A.S. et al., 2019].

Although there are many features of 3D spherical cultures that may contribute to poorer drug response, it is essential to avoid generalizations about drug resistance of cells in 3D versus 2D conditions, as certain molecular targets and signaling pathways may exhibit unique or even exclusive roles in the 3D environment, potentially leading to increased activity of chemotherapeutic agents in spheroids compared to monolayer cultures [Hirschhaeuser F. et al., 2010]. Therefore, the relationship between cellular response and the specific microenvironment of 3D cultures may result in differential drug sensitivity, emphasizing the importance of considering the complexity of this system when evaluating the efficacy and drug resistance, and highlighting the need to study potential therapeutic candidates in both 2D and 3D models.

2.8. Cancer stem cells

2.8.1. Cancer stem cells characteristics

Cancer stem cells are a distinct subset of cells within tumors that share similarities with normal stem cells. They can self-renew, differentiate into multiple cancer cell types, and proliferate extensively. The exact origin of CSCs remains uncertain, as they could arise from various sources, such as normal stem cells or transformed progenitor cells. The malignancy level of tumors initiated by CSCs may vary depending on their degree of differentiation. Undifferentiated primary tumors are more prone to metastasize to distant organs, leading to disease progression, unfavorable prognosis, and increased resistance to existing therapies [Chen L. et al., 2012; Correia C. et al., 2022; Ham S.L. et al., 2016]. The occurrence of CSCs has been confirmed so far in leukemias [Lapidot T. et al., 1994] and many solid tumors, including, among others: breast [Al-Hajj M. et al., 2007], pancreas [Hermann P. et al., 2007], lung [Kim C. et al., 2005], colon [Ricci-Vitiani L. et al., 2009], and prostate [Collins A. et al., 2005].

Just like normal stem cells, CSCs have the remarkable ability to undergo an infinite number of symmetric divisions, enabling them to self-renew indefinitely and generate more daughter cells. Additionally, CSCs can also undergo asymmetric divisions, producing non-CSCs or heterogenous progenitor cells with different states of quiescence and activity. Cancer stem cells also exhibit distinct characteristics, not typically found in normal stem cells, such as hyper-efficient DNA repair mechanisms, resistance to hypoxic environments, and high expression of anti-apoptotic proteins and multidrug-resistance-type ATP-binding cassette (ABC) membrane transporters. That unique combination of features is believed to be a reason why CSCs play a significant role in cancer resistance to conventional antitumor therapies, as well as justify their involvement in cancer recurrence. Moreover, CSCs are considered to strongly

contribute to tumor initiation, progression, and metastasis (Figure 2.4) [Bielecka Z. et al., 2017; Chen L. et al., 2012; Ham S.L. et al., 2016]. Cancer stem cells are also referred to as tumor-initiating cells (TICs) but while these terms are often used interchangeably in the literature, it is essential to point out that TICs are described as cells containing oncogenic mutations before they transform into CSCs during the process of tumorigenesis [Bielecka Z. et al., 2017]. Though the cancer stem cell theory has been valuable, it may not explain all instances of cancer initiation, as evidenced by certain cancer types where CSCs have not been isolated (e.g. B-cell precursor acute lymphoblastic leukemia). Therefore, further research on cancer initiation and development remains crucial to improve cancer therapies [Chen L. et al., 2012].

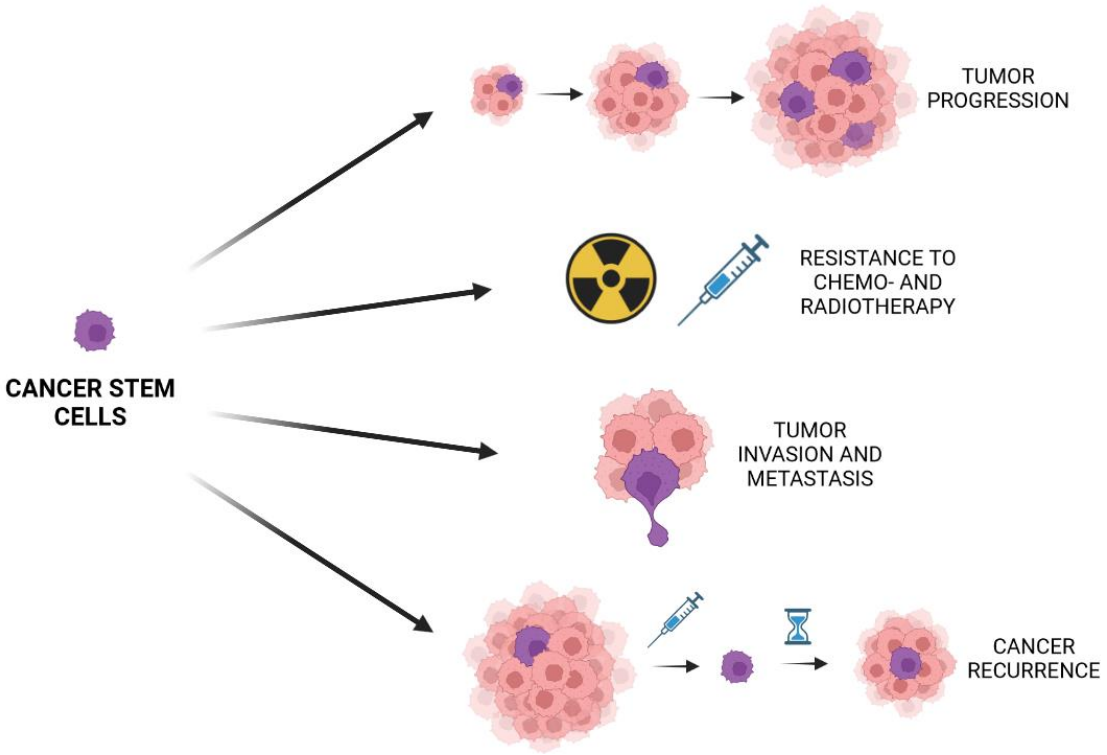

Figure 2.4. Fundamental roles of CSCs in cancer. Created in BioRender.com

2.8.2. Strategies to target CSCs

The presence of CSCs poses a challenge for anti-tumor therapy. The eradication of CSCs is of significant clinical interest due to their connection to the aggressive nature of cancer cells. Efficiently targeting and eliminating these cells is thus crucial for improving the outcome of drug treatment [Ishiguro T.S. et al., 2017]. So far, four approaches have been employed to target and eliminate cancer stem cells. These include increasing CSCs' sensitivity to conventional drugs, promoting CSC differentiation, disrupting CSC niches, and targeting and blocking relevant CSC signaling pathways [Chen L. et al., 2012].

Enhancing the sensitivity of cancer stem cells to conventional therapies is crucial for preventing cancer recurrence since CSCs can initiate tumors and are resistant to standard

treatments. Strategies like RNA interference-mediated downregulation of genes, especially anti-apoptotic genes, have a potential for future CSC eradication [Chen L. et al., 2012].

Promoting CSC differentiation into less tumorigenic cells could also improve the therapeutic outcomes and reduce the chance of cancer relapse. Cancer cells often originate from poorly differentiated cells, contributing to their tumorigenicity. In the case of CSCs, their unique ability to self-renew and differentiate makes them even more tumorigenic, thus inducing their changes may enhance the potential for their elimination [Chen L. et al., 2012].

An innovative approach to eliminate CSCs involves targeting the CSC-dependent stem cell niches, which play a crucial role in initiating and supporting tumor formation by activating signaling pathways and shielding CSCs from the effects of anticancer therapy. Thus the necessity to develop an effective CSC niche-targeting strategy is clear. The extracellular matrix and soluble factors in these niches present potential targets for the therapy [Correia C. et al., 2022; Chen L. et al., 2012]. In mouse models, combining vascular endothelial growth factor receptor 2 (VEGF2) antibodies with chemotherapeutic agents proved effective in reducing the population of CSCs [Folkins C. et al., 2007]. This suggests that such a comprehensive approach, including both the anti-CSC niche and antiangiogenesis therapies, holds promise for cancer treatment [Chen L. et al., 2012].

CSCs exhibit elevated expression of ABC transporters in various cells, which leads to reduced drug toxicity and increased chemoresistance. Targeting these transporters can effectively inhibit drug efflux, thereby facilitating the elimination of tumor cells, including CSCs. However, it is important to carefully use the ABC transporter inhibitors, as they may cause potential side effects on normal stem cells. Silencing CSC-related genes has also shown promise in inhibiting CSC growth and the ability to self-renew. Blocking functionally important components of the CSC signaling pathway, like Akt or STAT3, is recommended in some cases as a potential approach to help eradicate CSCs [Chen L. et al., 2012].

2.8.3. Approaches for CSCs identification and isolation

Cancer stem cells are identified and isolated based on distinctive properties that distinguish them from other cells in a tumor. There are two main sources for CSCs: established cancer cell lines and tumor tissues. Cancer cell lines are commonly used to study CSCs, but they may not fully represent all biological characteristics of primary CSCs due to cell adaptation to culture and the genetic alterations that occur during long-term subculture. Thus, caution is advised while interpreting results obtained from commercially available cell lines. On the other hand, generating primary cell lines from tumor tissues and isolating CSCs from these cells can provide valuable insight for research, but this approach is more complicated and requires time-consuming and problematic stabilization of a cell line [Akbarzadeh M. et al., 2018; Bielecka Z. et al., 2017].

Currently, several methods have been employed to specifically isolate cancer stem cells. Some methods rely on the expression pattern of cell surface markers, others focus on the functional aspects of CSCs, such as the spheroid formation assay, side population assay, or aldehyde dehydrogenase (ALDH) activity test [Akbarzadeh M. et al., 2018].

CSC markers are membrane proteins that are expressed on the surface of CSCs, including various receptors and antigens. However, the specific markers vary depending on the tumor type and no definite markers have so far been introduced. Numerous CSC surface markers have been discovered, but their accuracy remains uncertain, as some of them are also found on the surface of normal stem cells or differentiated cells. For instance, CD133, a glycoprotein initially considered a potential marker for CSCs, was regarded as not specific enough. Studies of glioblastoma multiforme (GBM) cells showed that both $CD133^+$ and $CD133^-$ GBM cells exhibited oncogenic properties, indicating the ambiguity of surface markers. Thus, researchers are constantly seeking specific and reliable markers to improve CSC identification and isolation techniques, as so far none of the known markers is universal and entirely accurate [Chen L. et al., 2012]. Nevertheless, compared to other methods, the identification of CSCs based on cellular markers has proven to be more specific [Akbarzadeh M. et al., 2018].

The drug-transporting function of ABC-transporters serves as a specific feature that can be used for isolating and studying hematopoietic stem cells. Unlike most cells that accumulate fluorescent dyes such as Hoechst 33342, stem cells do not retain these compounds due to their active efflux through ABC-transporters, which distinguishes them from the main population of cells. As a result, stem cells can be sorted by collecting cells with low levels of Hoechst 33342 fluorescence, commonly referred to as 'side population' (SP) cells [Bielecka Z. et al., 2017; Dean M. et al., 2005]. The main limitation of this method is the lack of precise staining protocols, which vary strongly in cell numbers, dye concentrations, and incubation times. Additionally, significant differences in individual cell-line-specific properties further limit its suitability for certain types of cells [Akbarzadeh M. et al., 2018].

Another notable approach for CSCs identification and isolation involves culturing CSCs in a serum-free media, allowing them to form tumorospheres. There are reports that cancer stem cell populations are particularly enriched, and in some cases, exclusively maintained in spherical cultures [Hirschhaeuser F. et al., 2010]. For example, Ricci-Vitiani et al. presented that CSCs from colorectal cancers could only be maintained in 3D culture without the addition of serum and that the transfer of cells to a culture medium supplemented with serum resulted in cell adherence, differentiation, and overall loss of tumorigenic potential [Ricci-Vitiani L. et al., 2009]. However, based on this, the conventional practice of using established cell lines grown in monolayers in culture media supplemented with serum raises doubts concerning its suitability for studies of new anticancer therapeutics. On the other hand, it is important to highlight that most established cancer cell lines exhibit tumorigenic properties in immunosuppressed mice, suggesting that these cell lines are capable of maintaining CSC populations even in the presence of serum [Hirschhaeuser F. et al., 2010].

2.8.4. Spheroids utilization in cancer stem cell research

Traditional 2D cell cultures lack the complexity and certain key features found in solid tumors, which limits their ability to fully reproduce the characteristics and behavior of cancer stem cells. Thus, researchers are increasingly focusing on studying spheroids to understand the role

of CSCs in the cancer microenvironment and shed light on the stubborn nature of solid tumors [Ishiguro T.S. et al., 2017]. Given the key role that CSCs play in tumorigenesis, including tumor growth and resistance to treatment, it becomes essential to incorporate 3D cell cultures to more accurately replicate and understand the complexity of these cells. Through the use of 3D models, valuable information can be gained to develop more effective strategies for targeting CSCs in anticancer treatment [Bielecka Z. et al., 2017; Zhang C. et al., 2020].

Tumorspheres serve as promising models widely used in CSC research. Methods for isolating and culturing CSCs as spheres are relatively consistent for various cancer tissue origins. Firstly, a single-cell suspension has to be obtained from a cancer cell line, or from a tumor tissue through mechanical and enzymatic dissociation. Then the suspension is cultivated in a specialized stem cell medium, under low-adherent conditions to facilitate extensive proliferation. Stem cell medium lacks fetal bovine serum but instead is supplemented with various factors that favor stem cell growth, such as basic fibroblast growth factor (bFGF), epidermal growth factor (EGF), hydrocortisone, insulin, progesterone, and heparin. Under these conditions, undifferentiated cancer cells proliferate and form spherical clusters, called tumorospheres. To enrich the CSC population and eliminate stromal cells, intermediate sorting steps may be applied, using CSC markers, such as CD133, CD44, ALDH, etc., however, as previously mentioned, no marker has yet turned out sensitive and specific enough to definitely identify CSCs [He J. et al., 2017; Weiswald L.B. et al., 2015].

Some studies indicate that CSCs respond differently to anticancer drugs *in vitro* and *in vivo.* Tumorospheres are widely used to study the response to chemotherapy, as remaining CSCs are believed to be responsible for the relapse after treatment. Researchers have shown that tumorospheres derived from patients' colon tumors are resistant to 5-fluorouracil and oxaliplatin due to the autocrine production of interleukin-4. Tumorospheres obtained from established cancer cell lines are also used to demonstrate CSC resistance in comparison to adherent cells, however, it is crucial to consider the 3D aspect of tumorospheres, as resistance observed may be due to the multicellular structure of 3D spheroids rather than being solely attributed to the intrinsic properties of CSCs. Few studies have analyzed the effect of anticancer drugs on organotypic multicellular spheroids (OMSs) due to the heterogeneity of OMSs derived even from the same tumor, making standardization challenging. On the other hand, studies on tissue-derived tumor spheres (TDTSs) show promise in predicting a patient's response to chemotherapy, making them a potential tool for implementing personalized treatment strategies [Weiswald L.B. et al., 2015].

Tumorospheres serve as a valuable model for enriching the CSC fraction, but they may not fully capture the intrinsic properties of CSCs, especially related to their 3D architecture. Many CSC studies rely heavily on tumorspheres, but when making interpretations and drawing conclusions, it is essential to consider that these models do not fully reproduce the *in vivo* tumor environment. Critical parameters such as culture duration, cell density, medium composition, volume, and surface area of the culture dish must also be taken into account while analyzing the results [He J. et al., 2017; Weiswald L.B. et al., 2015]. Interestingly, it has been observed that the

tumorosphere assay shows variable results in enriching the CSC population, depending on the specific cancer cell line. What is worth noting is that in certain cases, monolayer culture may actually better maintain the CSC phenotype [Calvet C. et al., 2014]. Therefore, while tumorospheres are very useful in CSC research, their limitations and context-specific aspects should be considered when planning, performing, and analyzing such experiments.

Overall, culturing cancer cell subpopulations in stem or progenitor cell conditions, including the use of sphere-forming assays, has provided valuable insights into tumor biology and plays an essential role in cancer research. 3D spheroid cultures offer unique insights into CSC biology and enable the identification of potential treatments targeting CSCs specifically [Ham S.L. et al., 2016; Hirschhaeuser F. et al., 2010].

3. MATERIALS AND METHODS

3.1. Materials

3.1.1. Tested compounds

The unsymmetrical bisacridines (UAs): C-2028, C-2041, C-2045, and C-2053 were synthesized as methanosulphonians (C-2028, C-2041, and C-2045) or monochloride (C-2053) in the Department of Pharmaceutical Technology and Biochemistry, Gdańsk University of Technology, according to a previously published procedure [Paluszkiewicz E. et al., 2020]. Both stock and working solutions were prepared in sterile deionized Mili-Q water. The reference compounds irinotecan, cisplatin, and etoposide were purchased from Sigma-Aldrich and the stock solution was prepared in dimethyl sulfoxide while working solutions were prepared in sterile, deionized Mili-Q water.

3.1.2. Cell lines

- A549 – human lung cancer cells (ATCC, Manassas, VA, USA),
- CCD 841 CoN – colon epithelial cells of human origin (ATCC, Manassas, VA, USA),
- DU 145 – human prostate cancer cells (ATCC, Manassas, VA, USA),
- H460 – human lung cancer cells (ATCC, Manassas, VA, USA),
- HCT116 – human colon cancer cells (ATCC, Manassas, VA, USA),
- HT29 – human colon cancer cells (ATCC, Manassas, VA, USA),
- MRC-5 – human lung fibroblasts (ATCC, Manassas, VA, USA).

3.1.3. Materials used for cell culture

- McCoy's 5A medium – for the cultivation of HCT116 and HT29 cells (SIGMA, St Louis, MO, USA),
- RPMI 1640 medium – for the cultivation of H460 cells (SIGMA, St Louis, MO, USA),
- MEM medium (Minimum Essential Medium Eagle) – for the cultivation of CCD 841 CoN, MRC-5, and DU 145 cells (SIGMA, St Louis, MO, USA),
- F12K medium (Kaighn's Modification of Ham's F-12 Medium) – for the cultivation of A549 cells SIGMA, St Louis, MO, USA),
- FBS (Fetal Bovine Serum) – heat-inactivated serum (Biowest, Kansas City, MO, USA),
- trypsin-EDTA 10x (5g trypsin/L 0.9% NaCl; 2g EDTA/L 0.9% NaCl) (SIGMA, St Louis, MO, USA),
- antibiotics: streptomycin (100 mg/L medium) and penicillin G (62.3 mg/L medium) (SIGMA, St Louis, MO, USA),
- $NaHCO_3$ – sodium bicarbonate (SIGMA, St Louis, MO, USA).

3.1.4. Chemical reagents

- CH_3COOH – acetic acid (POCH, Gliwice, Poland),

- CH_3OH – methanol (POCH, Gliwice, Poland),
- DMSO – dimethyl sulfoxide (POCH, Gliwice, Poland),
- KCl – potassium chloride (SIGMA, St Louis, MO, USA),
- KH_2PO_4 – dipotassium phosphate (SIGMA, St Louis, MO, USA),
- MTT – 3-(4,5-dimethylthiazol-2-yl)-2,5-diphenyltetrazolium bromide (SIGMA, St Louis, MO, USA),
- Na_2HPO_4, – disodium phosphate (SIGMA, St Louis, MO, USA),
- NaCl – sodium chloride (POCH, Gliwice, Poland).

3.1.5. Dyes

- 7-AAD – 7-aminoactinomycin D (Thermo Fisher Scientific, CA, USA),
- GIEMSA stain (SIGMA, St Louis, MO, USA),
- Hoechst 33342 (SIGMA, St Louis, MO, USA).

3.1.6. Laboratory solutions

- 5 x PBS (685 mM NaCl, 7 mM KH_2PO_4, 40 mM Na_2HPO_4, 13 mM KCl),
- Beckman Coulter™ ISOTON™ II Diluent (Beckman Coulter, Fullerton, CA, USA).

3.1.7. Experimental kits and buffers

- BD Cytofix/Cytoperm™ Fixation/Permeabilization Kit (BD Biosciences, San Jose, CA, USA),
- FITC Annexin V Apoptosis Detection Kit (BD Biosciences, San Jose, CA, USA),
- Flow Cytometry Mitochondrial Membrane Potential Detection Kit (BD Biosciences, San Jose, CA, USA),
- Stain Buffer BSA (BD Biosciences, San Jose, CA, USA).

3.1.8. Antibodies

- Alexa Fluor® 647 Mouse anti-Cleaved PARP (Asp 214) (BD Biosciences, San Jose, CA, USA),
- BB515 Mouse Anti-Human CD326 (BD Biosciences, San Jose, CA, USA),
- BB515 Mouse Anti-Human CD44 (BD Biosciences, San Jose, CA, USA),
- BB515 Mouse IgG1, $_K$ Isotype Control (BD Biosciences, San Jose, CA, USA),
- PE Mouse Anti-Human CD133 (BD Biosciences, San Jose, CA, USA),
- PE Mouse Anti-Human CD166 (BD Biosciences, San Jose, CA, USA),
- PE Mouse IgG1, $_K$ Isotype Control (BD Biosciences, San Jose, CA, USA).

3.1.9. Laboratory equipment

- 96-well BioRad iMark™ Microplate Reader (BioRad Laboratories, Hercules, CA, USA),
- Carl Zeiss light microscope TELAVAL 3 (Carl Zeiss, Jena, Germany),

- Eppendorf Centrifuge 5810 R (Eppendorf, Westbury, NY, USA),
- ESCO Biological Safety Cabinet (Esco Technologies, St Louis, MO, USA),
- FACS Accuri C6 Flow Cytometer (BD, San Jose, CA, USA),
- NUAIRE Biological Safety Cabinet (NuAire, Plymouth, MN, USA),
- NUAIRE IR Autoflow CO_2 Water-Jacket (NuAire, Plymouth, MN, USA),
- OLYMPUS BX60 fluorescent microscope, OLYMPUS U-RFL-T lamp, XC 50 camera (Olympus, Japan),
- OLYMPUS IX 83 fluorescent microscope, OLYMPUS U-HGLGPS lamp, XC 50 camera (Olympus, Japan),
- Z1 Coulter Particle Counter (Beckman Coulter, Fullerton, CA, USA).

3.2. Methods

3.2.1. Cell lines and culture conditions

Human cancer cell lines: A549, DU 145, HCT116, HT29, and H460 as well as normal cells: CCD 841 CoN and MRC-5 were purchased from the American Type Culture Collection and were tested negatively for mycoplasma. HCT116 and HT29 cells were cultured in McCoy's 5A medium, H460 cells in RPMI 1640 medium, A549 cells in F12K medium, and DU 145 in Minimum Essential Medium Eagle (MEM). These culture media were supplemented with 10% heat-inactivated fetal bovine serum (FBS), 100 µg/mL streptomycin, and 100 U/mL penicillin. CCD 841 CoN and MRC-5 cells were cultured in Minimum Essential Medium Eagle supplemented with 10% fetal bovine serum without the addition of antibiotics. Cells were incubated at 37 °C in a 5% CO_2 atmosphere. All the experiments were carried out with cells in the exponential phase of growth.

3.2.2. Observation of morphological changes of nuclei of cancer and normal cells treated with UAs

HCT116 and H460 cells were seeded onto 100 mm plates at a density of 1 x 10^6, while CCD 841 CoN and MRC-5 cells were seeded at densities of 1.6 x 10^6 and 1.2 x 10^6 cells, respectively. After overnight adherence, cells were incubated with C-2028, C-2041, C-2045, and C-2053 at 0.04, 0.05, 0.4, and 0.2 µM respectively for 24, 72, and 120 hours (only 120h for normal cells). Following treatment, the cells were collected into falcon tubes, centrifuged (1000 rpm, 4°C, 5 min.), and the resulting cell pellet was washed twice with 5 mL of cold PBS. Then the cell pellet was resuspended in PBS in a volume depending on the thickness of the pellet. 200 µL of this cell was centrifuged onto a glass slide using a cytocentrifuge (850 rpm, RT, 4 min.). Subsequently, cells were fixed for 15 minutes using Carnoy's solution (3:1 methanol: glacial acetic acid), washed in PBS, and stained in the dark with an aqueous solution of Hoechst 33342 fluorescent dye at a final concentration of 1 µg/mL for 15 minutes at RT. Stained cells were again washed with PBS and sealed with a coverslip after applying a drop of mounting buffer to the cell layer. Cells were visualized at 450 nm using an OLYMPUS BX60 fluorescence microscope, and images were

captured at 400x with a camera using CellSens software. The experiment was repeated twice for each tested cell line. (n=2-3)

3.2.3. Analysis of changes in the mitochondrial membrane potential of HCT116 and H460 cells

1 x 10^6 HCT116 or H460 cells were seeded onto a 100 mm plate and allowed to adhere overnight. Then the cells were incubated with 0.04, 0.05, 0.4, and 0.2 µM of C-2028, C-2041, C-2045, and C-2053 compounds, respectively, for 24, 72, and 120 hours. After treatment, 1 x 10^6 cells were collected into a falcon tube and centrifuged (400 x g, RT, 5 min). The resulting pellet was then suspended in 500 µL of the previously prepared JC-1 dye solution and incubated in the dark at 37°C for 15 minutes. After staining, cells were washed twice with warm diluted assay buffer, pelleted, and resuspended in 450 µL of buffer. Then cells were subjected to cytometric analysis using the FACS Accuri C6 and the acquired cytograms were analyzed using the BD Accuri C6 Software. Each experiment was repeated three to five times (n=3-5).

3.2.4. Investigation of the level of cleaved PARP protein in HCT116 and H460 cells

1 x 10^6 HCT116 or H460 cells were seeded onto a 100 mm plate and allowed to adhere overnight. Then the cells were incubated for 24, 72, and 120 hours, with C-2028, C-2041, C-2045, and C-2053 at 0.04, 0.05, 0.4, and 0.2 µM respectively. After treatment, 0.5 x 10^6 cells were collected, centrifuged (1000 rpm, 4°C, 5 min.), and washed twice with cold PBS. Next, cells were resuspended in 300 µL of BD Cytofix/Cytoperm solution and incubated on ice for 20 minutes. After fixation, cells were again centrifuged (1000 rpm, RT, 5 min.), then washed twice with previously diluted Perm/Wash BD solution. Afterward, the cells were resuspended in 50 µL of Perm/Wash buffer and 2 µL of Alexa Fluor® 647 Mouse anti-Cleaved PARP (Asp 214) antibody was added. Following a 30-minute incubation at RT in the dark, the suspension was diluted with 800 µL of Perm/Wash buffer. After a final centrifugation step, the cells were suspended in 250 µL of Perm/Wash buffer and analyzed by flow cytometry. Results were obtained from three to five independent experiments (n=3-5).

3.2.5. Establishment of seeding density for spheroid formation

For spheroid formation, 96-well Corning® Costar® Ultra-Low Attachment (ULA) round-bottomed plates were used. Five cancer cell lines were evaluated for their spheroid-forming capacity: HCT116, HT29, DU 145, H460, and A549. For each cell line, after initial trypsinization and counting, the cell suspension was centrifuged in order to remove trypsin, and a fresh culture medium was added to disperse the pellet. Then cell suspensions, prepared at various densities as outlined in Table 3.1, were seeded into the ULA plate using a multichannel pipette at 200 µL/well.

Table 3.1. HCT116, HT29, DU 145, H460, and A549 cell suspension densities used for spheroid formation in order to establish proper conditions for spheroid seeding

Cell line	Tested densities [cells/well]
HCT116	1000, 2000, 2500, 3000, 4000, 5000
HT29	2000, 3000, 4000, 5000
DU 145	2000, 3000, 4000, 5000
H460	1000, 2000, 2500, 3000, 4000, 5000
A549	2000, 3000, 4000, 5000, 6000, 7000

After seeding, the plate was centrifuged (1200 rpm, RT, 15 min.) to initiate cell aggregation and incubated at 37 °C in a 5% CO_2 atmosphere for 72 hours. Then images of each spheroid were captured using a 4x objective in OLYMPUS IX 83 inverted microscope with XC 50 camera and cellSens Dimension software. Following imaging, 100 µL of culture medium in each well was carefully replaced with fresh medium (this day is further referred to as day 0). Images of spheroids were taken daily for the next three days, the diameter of each spheroid was measured and the mean value was calculated. Each experiment was repeated two to three times (n=2-3).

3.2.6. Generation of HCT116, H460 and A549 tumor spheroids

After trypsinization and counting, the resulting cell suspension was centrifuged and fresh culture medium was added. Then, 200 µL of cell suspension at a density of 1 x 10^4 cells/mL for HCT116/H460 cells or 2.5 x 10^4 cells/mL for A549 cells was dispensed into each well of the ULA plate, using a multichannel pipette. After seeding, the plate was centrifuged for 15 min at 1200 rpm at room temperature and incubated at 37 °C in a 5% CO_2 atmosphere for 72 h before further experiments.

3.2.7. Cytotoxicity of UAs and etoposide against A549 cells

To estimate cell viability, the MTT assay was used. A549 cells were seeded into 24-well plates at the amount of 2 x 10^4 cells per well. Following 24 h of incubation at 37 °C in a 5% CO_2 atmosphere, unsymmetrical bisacridines or the reference compound (etoposide) were added at concentrations up to 10 µM for UAs and up to 100 µM for etoposide. After 72 h of incubation, 200 µL/well of 3-(4,5-dimethylthiazol-2-yl)-2,5-diphenyltetrazolium bromide at a concentration of 4 mg/mL was added and incubated for 3 h at 37 °C. Next, the culture medium from each well was removed, the formazan crystals were dissolved using DMSO, and the absorbance at 540 nm was measured. The concentrations of drugs required for inhibition of cell growth by 50% (IC_{50}), 80% (IC_{80}), and if possible 90% (IC_{90}) compared with untreated control cells were calculated from the curves plotting survival as a function of dose. Results were obtained from four independent experiments (n=4).

3.2.8. Spheroid size and morphology assessment

The spheroids were generated as described in section 3.2.6. First, 72 h after seeding, images of each spheroid were captured using a 4x objective in OLYMPUS IX 83 inverted microscope with XC 50 camera and cellSens Dimension software. Afterward, 100 µL of culture medium was carefully replaced with fresh medium in control spheroids, or fresh medium with UAs at concentrations corresponding to IC_{90} values or with reference compounds at IC_{50} values. Table 3.2. provides an overview of the concentrations of the tested compounds, used in all further experiments. In the case of HCT116 and H460 cells, these concentrations had been previously determined in our laboratory.

Table 3.2. IC_{90} values for UAs (C-2028, C-2041, C-2045, and C-2053) and IC_{50} values for reference compounds (irinotecan, cisplatin, and etoposide) used in presented experiments.

Compound	Drug dose	Drug concentration [µM]		
		HCT116	H460	A549
C-2028	IC_{90}	0.04	0.04	0.05
C-2041	IC_{90}	0.05	0.05	0.085
C-2045	IC_{90}	0.4	0.4	0.3
C-2053	IC_{90}	0.2	0.2	0.3
Irinotecan	IC_{50}	4.5	not applicable	not applicable
Cisplatin	IC_{50}	not applicable	3.0	not applicable
Etoposide	IC_{50}	not applicable	not applicable	5.6

Images of spheroids were captured every 2-3 days, up to 14 days after drug treatment, and each time the spheroid diameters were measured using the cellSens Dimension software. Results were obtained from four independent experiments (n=4). Within each experiment, no fewer than 8 spheroids were subjected to measurement, and the mean value of spheroid growth was calculated as shown below:

$$\%\ \boldsymbol{spheroid\ growth} = \frac{\boldsymbol{d_x}}{\boldsymbol{d_0}} * 100\%$$

where d_x is the mean diameter of at least 8 spheres at a given day of incubation and d_0 is the mean diameter of at least 8 spheres at day 0 (day of the drug treatment).

3.2.9. Cell death assay

For cell death evaluation, 7-aminoactinomycin D (7-AAD) dye was used. 7-AAD binds to the DNA of damaged cells, therefore allowing the distinction between living and dead cells.

In the initial phase, an analysis of control 2D and 3D cultures of HCT116, H460, and A549 cells was performed. For monolayer cultures, 1 x 10^5 of HCT116 and H460 cells or 1.4 x 10^5 of A549 cells were seeded onto a 100 mm plate and allowed to adhere overnight. Then, after 3 days, 0.5 x 10^6 cells were collected from plates, and centrifuged at 1000 rpm for 5 minutes at

RT, washed twice with PBS, pelleted, resuspended in 150 µl of PBS, and stained with 7-AAD dye (1 µg/mL) for 15 min in the dark at RT.

Spheroids were generated as described in section 3.2.6., then 72 h after seeding 100 µl of culture medium was changed and spheres were allowed to grow for 3 days. Afterward, spheroids were disaggregated to obtain a single-cell suspension for flow cytometry analysis. To achieve this, the spheroids were collected, centrifuged, washed with PBS, and incubated with 200 µL of trypsin to promote cellular detachment. During trypsinization, spheroid disruption was further aided through pipetting and/or vortexing. Next, fresh medium was added to neutralize trypsin, and cells were centrifuged, washed twice with PBS, suspended in 150 µL of PBS, and stained with 1µg/mL 7-AAD for 15 min in the dark at RT. After staining, the cells were analyzed using flow cytometry. Each experiment was repeated three to four times (n=3-4).

Cytometric analysis of spheroids seeded with different densities was also performed using the analogical methodology. 3 days after generation, spheroids derived from HCT116, H460, and A549 cell lines seeded with various densities presented in table 3.1. were collected into falcon tubes and then subjected to further analysis accordingly to the procedure described above.

When studying changes in the viability of cells after drug treatment similar conditions have been applied. In monolayer cultures, 1 x 10^6 of HCT116 cells were seeded onto a 100 mm plate (1 x 10^5 cells for 3 days and 1 x 10^4 for 7 days for untreated control) or 1.4 x 10^6 of A549 cells (1.4 x 10^5 for 3 days and 1.4 x 10^4 for 7 days for untreated control) and allowed to adhere overnight. Then, cells were treated for 3 or 7 days with UAs at concentrations corresponding to IC_{90} values or 5xIC_{90} values, while reference compounds were added at concentrations corresponding to IC_{50} or 5xIC_{50} values. After drug treatment and trypsinization, 0.5 x 10^6 cells were collected from plates, centrifuged at 1000 rpm for 5 min at RT, washed twice with PBS, pelleted and resuspended in 150 µL of PBS, and stained with 7-AAD dye (1 µg/mL) for 15 min in the dark at RT.

As for spheroids, their formation followed the procedure described in section 3.2.6. Then, 72 h after seeding, 100 µL of culture medium was changed, and cells were treated for 3 or 7 days with drugs at concentrations corresponding to IC_{90} or 5xIC_{90} values for UAs and IC_{50} or 5xIC_{50} values for reference compounds. After drug treatment, spheroids were collected, centrifuged, washed with PBS, and treated with 200 µL of trypsin. Next, fresh medium was added, and cells were centrifuged, washed twice with PBS, suspended in 150 µL of PBS, and stained with 1µg/mL 7-AAD for 15 min in the dark at RT. After staining, the cells were analyzed using flow cytometry. Each experiment was repeated three to eight times (n=3-8).

3.2.10. Colony formation assay

The ability of HCT116 and A549 cells to return to proliferation after treatment with UAs and reference compounds was evaluated through a colony formation assay. Cells were exposed to the tested compounds at concentrations corresponding to IC_{90} values (IC_{50} for irinotecan/etoposide) and after incubation for 24, 72, and 120h, cells were collected, counted, and

about 250 cells were seeded into each well of a 6-well plate containing fresh medium. Then the plate was incubated for two weeks, after which time, the colonies that had formed were fixed with 80% ethanol and stained with Giemsa dye. After staining the plates were photographed and the number of colonies in each well was counted. This experiment was repeated three times (n=3).

3.2.11. Establishment of the spherogenic potential of cells

To analyze the spherogenic potential, HCT116, and A549 cells were cultured in 2D (monolayer) and 3D (spheroid) conditions as described above. Then, after treatment with UAs and reference compounds for 3 days at IC_{90} doses (IC_{50} for irinotecan/etoposide), cells were collected into Falcon tubes, centrifuged, and resuspended in a fresh culture medium. Cells cultured as spheroids were disaggregated into a single cell suspension as explained in subsection 3.2.9. Then cells were counted and 200 µl of HCT116 cell suspension at 1 x 10^4 cells/mL or A549 at 2.5 x 10^4 cells/mL were dispensed into an ULA plate, which was then incubated at 37°C in a 5% CO_2 atmosphere for 3 days. After this time, 100 µL of culture medium was replaced with fresh medium, and plates were incubated for an additional two weeks. Throughout the course of this experiment, images of spheroids were captured on days 0, 7, and 14, and the diameters of formed spheres were measured using the cellSens Dimension software. The experiment was performed three to five times (n=3-5).

3.2.12. Annexin V/PI double staining

Changes in the cytoplasmic membrane of HCT116 and A549 cells were analyzed by flow cytometry using the FITC Annexin V Apoptosis Detection Kit (BD Biosciences, San Jose, CA, USA), according to the manufacturer's procedure. Briefly, after 3-day incubation of monolayer and spherical cultures of HCT116 and A549 cells with C-2045, C-2053, and IR/ETP at 5xIC_{90} doses (5xIC_{50} for reference compounds), 1x10^6 cells were collected into a falcon tube, centrifuged, washed twice with PBS, pelleted and resuspended in 100 µL of binding buffer containing Annexin V-FITC and propidium iodide (spheroids were dissociated into single-cell suspension beforehand). The cell suspension was then incubated for 15 min in the dark at RT, diluted with 400 µL of binding buffer, and analyzed by flow cytometry with FACS Accuri™ C6. Cells stained with only annexin V were considered early-apoptotic, cells both annexin V and PI-positive as late-apoptotic, and cells stained only with PI as necrotic. This experiment was repeated three to seven times (n=3-7).

3.2.13. Identification of CSC-like cells

The levels of the following surface biomarkers: CD44, CD133, CD166, and EpCAM were determined in 2D and 3D cultures of HCT116 and A549 cells using flow cytometry analysis. Cells cultured in both conditions after a 3-day incubation with C-2045, C-2053, and IR/ETP at 5xIC_{90} doses (5xIC_{50} for IR/ETP) were collected into a falcon tube. For monolayer cultures, 0.5 x 10^6 cells were analyzed, whereas for 3D culture all spheroids (no fewer than 16 for each compound) were pulled and after dissociation into a single-cell suspension subjected to further analysis. Then

cells were centrifuged, washed twice with Stain Buffer BSA (BD Biosciences, San Jose, CA, USA), and resuspended in Stain Buffer BSA containing the appropriate antibody: CD44-BB515, CD133-PE, CD166-PE or EpCAM-BB515 (BD Biosciences, San Jose, CA, USA). Following a 30-minute incubation at 4^{o}C in the dark, the cells were centrifuged, washed twice with Stain Buffer BSA, resuspended in it, and subjected to flow cytometry analysis. As a negative control, an isotype-matched labeled control was used for each antibody. This experiment was repeated three to seven times (n=3-7).

3.2.14. Statistical analysis

All results are presented as means ± SD from at least three independent experiments. Due to this, all the statistical analyses were performed using nonparametric statistics, exclusively. Differences between UAs (C-2028, C-2041, C-2045, C-2053) and reference compounds (irinotecan and etoposide) in comparison to the control group for each studied parameter were analyzed by Dunn's nonparametric multiple comparisons test, applied only if the nonparametric ANOVA (Kruskal-Wallis test) showed that the variability between group medians was significantly greater than expected by chance. Additionally – to assess the influence of time upon the size of spheroids for control, UAs, and reference compounds, the Jonckheere test for ordered alternatives was performed. Finally, the Mann-Whitney U test was used to analyze the differences between the results of the selected experiments for 2D and 3D samples. Two statistical packages were used: GraphPad InStat v. 3.0 and KyPlot v. 2.0. For all the statistical analyzes, the differences of $p < 0.05$ between the two groups were considered statistically significant: * $p < 0.05$, ** $p < 0.01$, *** $p < 0.001$.

4. RESULTS

4.1. Morphological changes of nuclei triggered by UAs in cancer and normal cells

In our laboratory, previous investigations into the cellular response induced by unsymmetrical bisacridines (UAs) in colon HCT116 and lung H460 cells were conducted. These prior studies have established their effects on the cell cycle distribution, along with the cytometric analysis of the changes in the cytoplasmic membrane structure and the presence of active caspase-3. These experiments indicated that UAs induce apoptosis in both cell lines tested. Thus, to further prove that apoptosis indeed represents the main type of cell death triggered in HCT116 and H460 cells by UAs, I performed an analysis of the nuclei morphology of HCT116 and H460 cancer cells. Cells were treated with 0.04, 0.05, 0.4, and 0.2 μM of C-2028, C-2041, C-2045, and C-2053 compounds, respectively, and after fixation, cells were stained with Hoechst 33342 and visualized under fluorescent microscopy. At the same time, I conducted an adequate experiment for normal CCD841 CoN and MRC-5 cells to evaluate the effect that UAs might have on normal tissues (Figure 4.1).

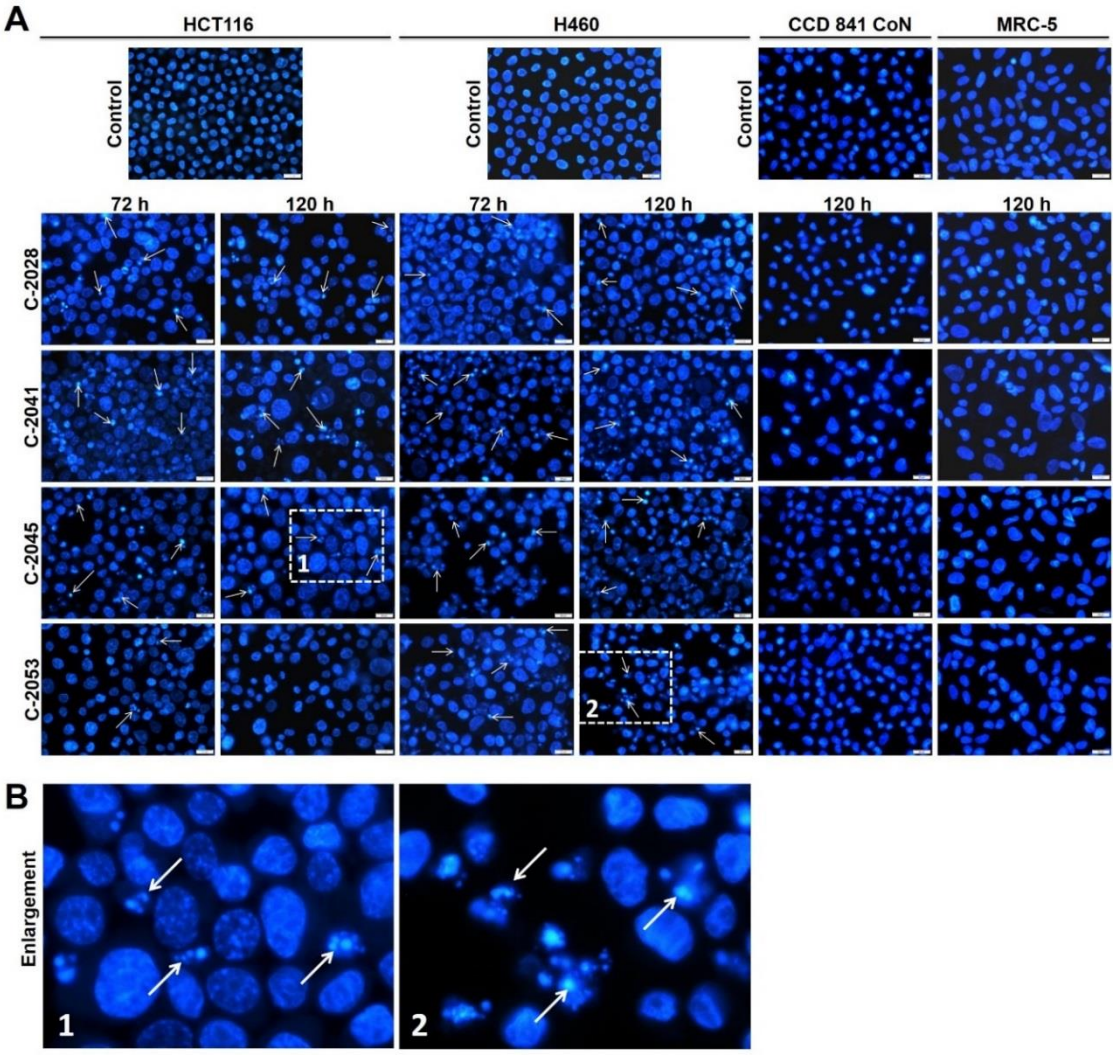

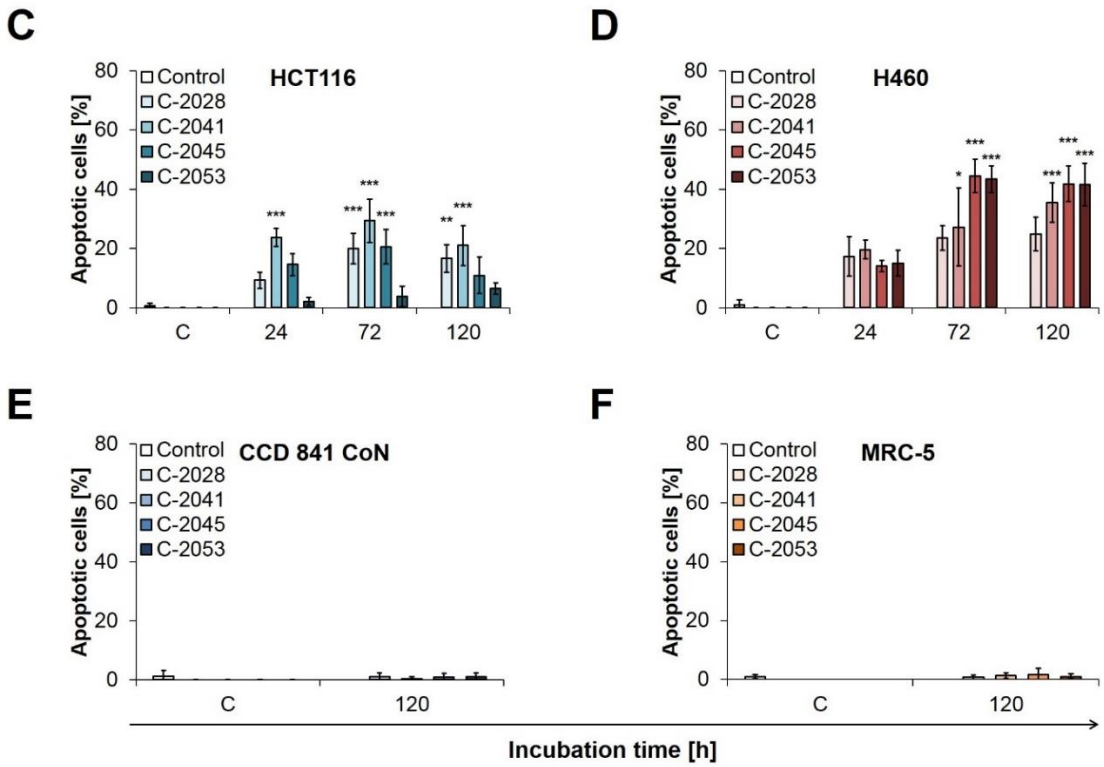

Figure 4.1. Morphological changes of nuclei of cancer and normal cells treated with UAs. (**A**) Representative pictures presenting changes in nuclear morphology of HCT116, H460, CCD 841 CoN, and MRC-5 cells treated with 0.04, 0.05, 0.4, and 0.2 μM of C-2028, C-2041, C-2045, and C-2053 compounds. Cells were stained with Hoechst 33342 (1 mg/mL) and visualized under a fluorescent microscope (400x magnification). Arrows point cells with nuclei changes characteristic to apoptosis (condense, intensely stained fragmented chromatin) (**B**) Enlarged fragments of pictures with indicated changes characteristic of apoptosis. (**C-F**) Bar graphs show quantified data, expressed as the percentages of nuclei with apoptotic features. White scale bars presented on images correspond to 20 μm. Data are presented as the means ± SD of two to three independent experiments. Statistical analysis was performed using Dunn's nonparametric multiple comparisons test. Significantly different from control at: * $p < 0.05$, ** $p < 0.01$, *** $p < 0.001$. (n=2-3)

Following exposure to UAs, notable alterations in the morphology of cell nuclei were observed. Among these changes, the most profound was the appearance of features characteristic of apoptosis: chromatin condensation, fragmentation of the cell nucleus, and the presence of apoptotic bodies. Importantly, the number of apoptotic cells depended on the duration of exposure to UAs for both HCT116 and H460 cells, with longer incubation correlating with an increase in the appearance of nuclei showing distinctive signs of apoptosis.

In HCT116 cells, the strongest induction of apoptosis was observed after exposure to C-2041 and C-2045. In turn, C-2053 treatment led to a very limited appearance of apoptotic cells. Over extended incubation times, some nuclei showed substantial enlargement – this was observed to the highest extent in cells treated with C-2041 and C-2045 for 120h, which may indicate partial induction of necrosis in these cells. Additionally, a few polyploid cells (a characteristic feature of mitotic catastrophe) could be found in HCT116 cells treated with C-2045.

Microscopic observations revealed that the nuclei of H460 cells exposed to UAs underwent many alternations. Compared to HCT116, the H460 cells exhibited a larger proportion of cells with apoptotic features, as indicated by the numerous cell nuclei with condensed

chromatin and the presence of apoptotic bodies. The most profound induction of apoptosis was observed in H460 cells treated with C-2045 and C-2053, while treatment with C-2028 caused changes to the least extent. Furthermore, exposure of H460 cells to C-2028 and C-2053 led to an enlargement of nuclei in these cells compared to control and cells treated with C-2041 and C-2045, which was particularly evident after 72 h of incubation.

In the case of normal CCD 841 CoN colon epithelial cells and MRC-5 lung fibroblasts, after a 120-hour incubation with bisacridines, no apparent changes in the morphology of the nuclei were observed compared to control cells. While chromatin condensation was visible in a few nuclei, these changes do not apply to a wide population of cells and were also detected in control cells. The nuclei of both normal cell lines displayed a slight increase in size after treatment with C-2041.

4.2. Changes in mitochondrial membrane potential of HCT116 and H460 cells after UAs treatment

One of the typical hallmarks of an apoptotic cell is the alteration in the mitochondrial transmembrane potential. The reduction of the electrochemical potential $\Delta\psi_m$ occurs even before DNA fragmentation, and its decrease below a critical threshold indicates that mitochondrial mega-channels have been opened and pro-apoptotic factors have been released from mitochondria, which directs the cell toward apoptosis. In order to detect cells with decreased mitochondrial potential, lipophilic fluorescent molecules of JC-1 are used. When the mitochondrial membrane maintains polarization, aggregates are formed, which emit light in the orange fluorescence range. As the mitochondrial potential declines, the amount of aggregates decreases and the molecules remain in monomeric form, and consequently, green fluorescent light is emitted. The fluorescence intensity can be measured using flow cytometry or fluorescence microscopy [Borowa-Mazgaj B., 2016; Rudnicka K.W. et al., 2011].

Compared to control cells, the mitochondrial potential reduction was evident in both HCT116 and H460 cells treated with the tested compounds (Figure 4.2). Changes in the mitochondrial potential started as early as 24 hours after exposure to bisacridines and as the time of treatment with UAs was extended, the number of cells with reduced mitochondrial potential gradually increased. This observation was consistent across all compounds and both cell lines.

In the case of the HCT116, the highest increase in cells with reduced $\Delta\psi_m$ was observed after treatment with C-2041 – following a 120-hour incubation with this compound, the number of cells emitting green fluorescence reached 63%. H460 cells were generally more sensitive to treatment with tested compounds and changes in the mitochondrial potential were observed in a larger population of cells than in HCT116. The only exception was C-2041, which after 120 hours of incubation caused a decrease in transmembrane potential in about 47% of H460 cells – over 15% less than in the HCT116 cells. The most pronounced depolarization of mitochondrial potential membrane was detected in lung cancer cells exposed to C-2053, where the number of cells with reduced $\Delta\psi_m$ after 120 hours of incubation with the compound was approx. 68%.

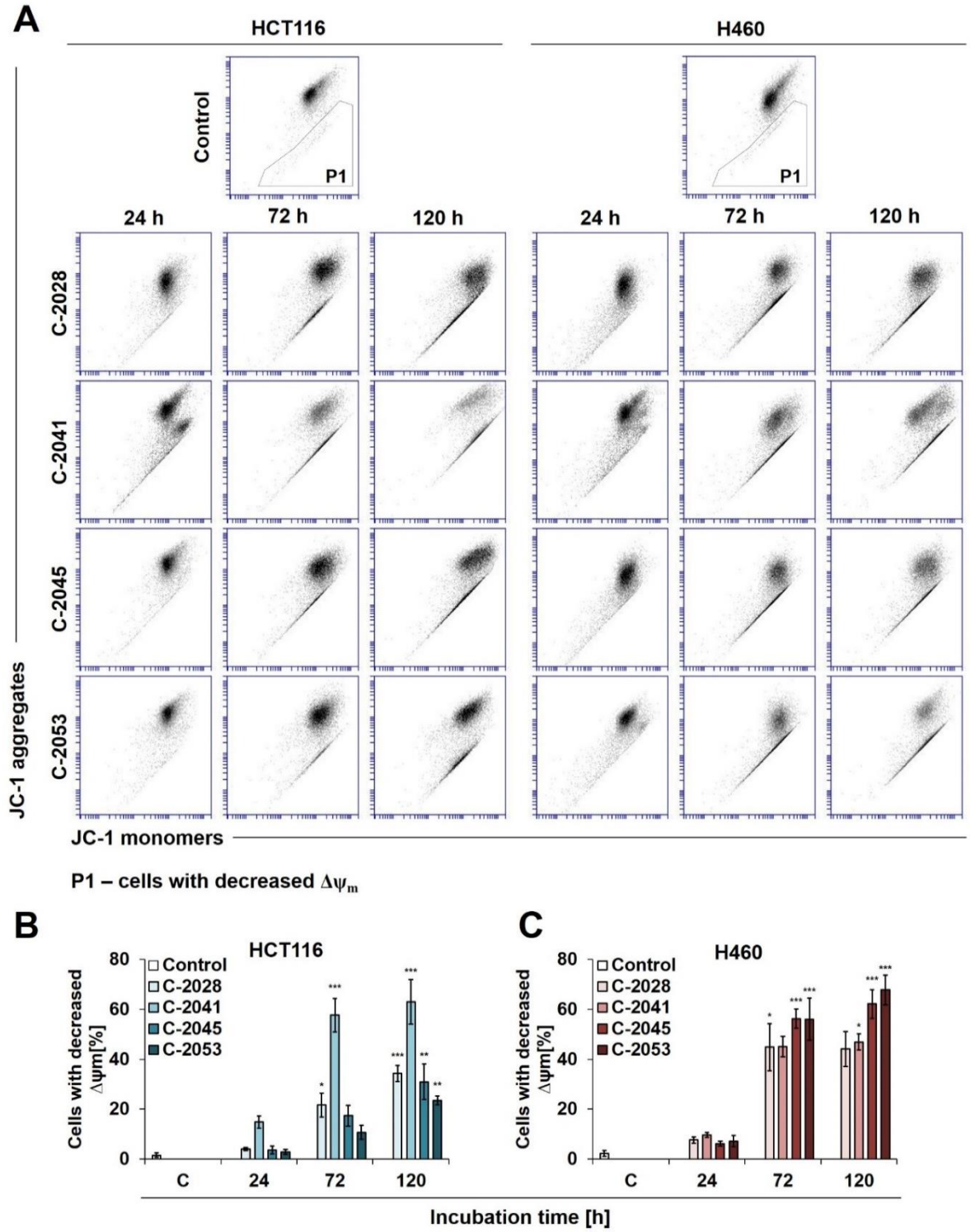

Figure 4.2. Changes in the mitochondrial potential of HCT116 and H460 cells after unsymmetrical bisacridines treatment. Cells were incubated with 0.04, 0.05, 0.4, and 0.2 μM of C-2028, C-2041, C-2045, and C-2053 respectively for 24, 72, and 120 h. Then after staining with JC-1 dye cells were subjected to flow cytometry analysis. **(A)** Representative cytograms showing changes in the mitochondrial potential of HCT116 and H460 cells after UAs exposure. Bar graphs showing the mean percentage of HCT116 **(B)** and H460 **(C)** cells with reduced mitochondrial potential after incubation with UAs. Data are presented as the means ± SD of three to five independent experiments. Statistical analysis was performed using Dunn's nonparametric multiple comparisons test. Significantly different from control at: * $p < 0.05$, ** $p < 0.01$, *** $p < 0.001$. (n=3-5)

4.3. The effect of bisacridines on the level of cleaved PARP protein in HCT116 and H460 cells

PARP-1, or Poly (ADP-ribose) polymerase, is a 113 kDa long chromatin-associated enzymatic protein. During apoptosis, caspase-3 and caspase-7, enzymes that are activated, cleave the PARP-1 protein into fragments of 24 and 89 kDa, which is a distinctive hallmark of this type of cell death. Therefore, the presence of the 89 kDa PARP-1 fragment in cells is regarded as a marker of apoptosis [Gobeil S. et al., 2001].

After treatment of HCT116 and H460 cells with UAs, a monoclonal antibody conjugated to the Alexa Fluor 647 fluorescent dye was used to detect cells with the 89 kDa fragment of the cleaved PARP-1 protein.

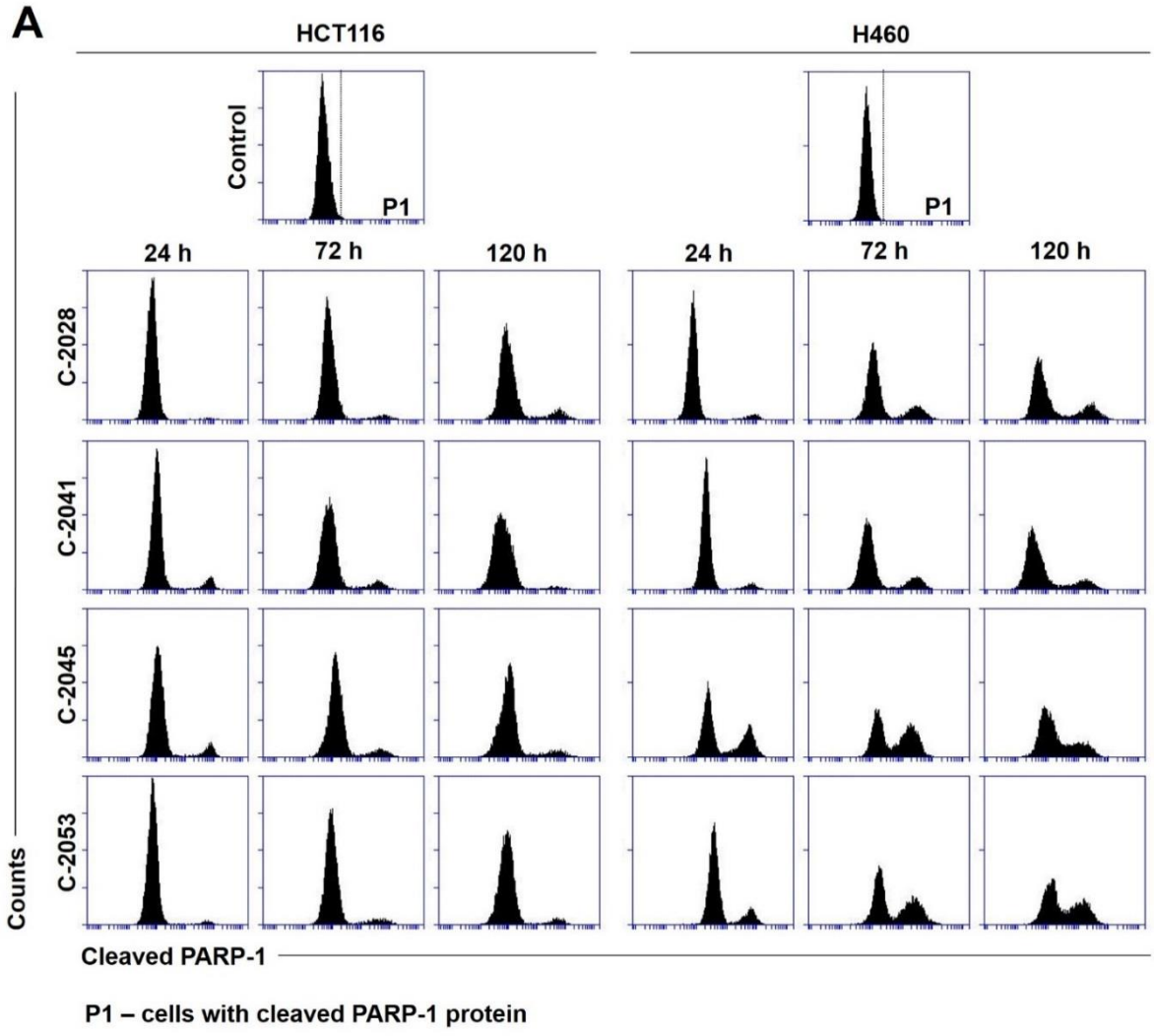

P1 – cells with cleaved PARP-1 protein

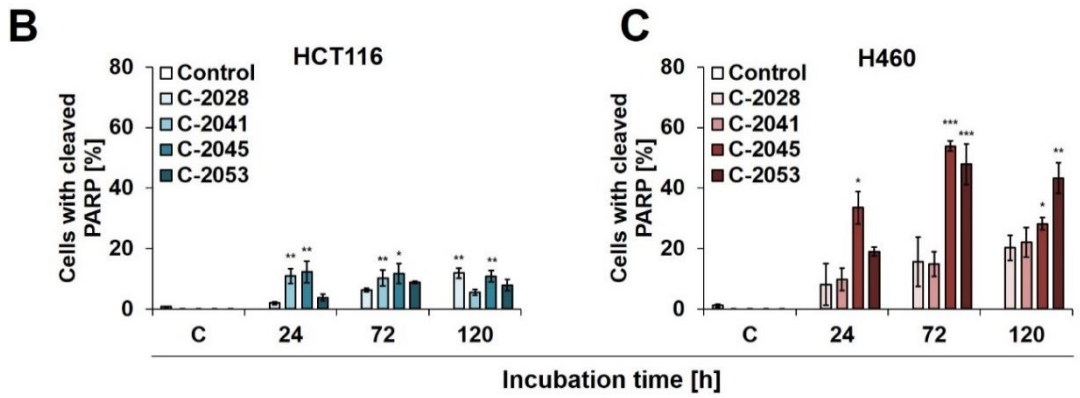

Figure 4.3. Cleavage of PARP-1 protein in HCT116 and H460 cells after UAs exposure. Cells were incubated for 24, 72, and 120 h with C-2028, C-2041, C-2045, and C-2053 at 0.04, 0.05, 0.4, and 0.2 μM respectively, fixed and incubated with anti-cleaved PARP antibody conjugated with Alexa Fluor 647 and analyzed with flow cytometry. **(A)** Representative histograms showing changes in the number of cells with cleaved PARP-1 protein after treatment with UAs. Bar graphs showing the mean percentage of HCT116 **(B)** and H460 **(C)** cells with cleaved PARP-1 protein after incubation with UAs. Data are presented as the means ± SD of four to six independent experiments. Statistical analysis was performed using Dunn's nonparametric multiple comparisons test. Significantly different from control at: * $p < 0.05$, ** $p < 0.01$, *** $p < 0.001$. (n=4-6)

Compared to control cells, the degradation of the PARP-1 protein occurred in both HCT116 and H460 cells treated with bisacridines, which resulted in the appearance of an 89 kDa protein fragment, the presence of which is characteristic of apoptotic cells (Figure 4.3). The cleavage of PARP by caspase-3 in HCT116 cells stayed at a relatively low level and did not exceed 12% for all tested compounds, even after 120 h. However, it was observed that the amount of cleaved PARP was slightly higher in cells incubated with C-2041 and C-2045 than with C-2028 or C-2053.

In the case of H460, the number of cells with the 89 kDa fragment of PARP was notably higher than in HCT116 cells. In H460 cells, the highest fraction of cells displaying cleaved PARP was observed after exposure to C-2045 (53.9%) and C-2053 (47.8%) compounds for 72 h.

The population of HCT116 and H460 cells in which the PARP-1 protein was cleaved after UAs treatment increased or remained consistent when the incubation time was extended. However, some exceptions were noted: HCT116 cells incubated with C-2041, where after 24 and 72 hours of incubation the number of cells with a degraded form of protein remained constant at around 10%, and after 120 hours it decreased to 5.5%; and H460 cells incubated with C 2045, where after 24 hours of incubation the number of cells with cleaved PARP-1 protein was approx. 33%, and after 72 hours it increased to approx. 54%, then after 120 hours it dropped by more than 25% reaching the value of 28.2%.

4.4. Generation of tumor spheroids derived from various cell lines

Since 3D spherical cultures are a very promising tool in drug development and testing, which may help to bridge the gap between results obtained *in vitro* and *in vivo*, I decided to apply this model in studies of biological response induced in cancer cells by unsymmetrical bisacridines.

First, I focused on establishing the appropriate spherical cultures which would be suitable for further analyses. To achieve that, I tested the spheroid-forming ability and monitored the initial

growth of five cell lines (HCT116, HT29, DU 145, A549, and H460), which had previously proven to be sensitive to UA treatment.

Microscopic observations showed, that four studied cell lines, namely HCT116, DU 145, H460, and A549 formed circular spheroids with different morphometric features. The HCT116 spheres were condensed, had a nearly perfect spherical shape, and a smooth, even periphery (Figure 4.4.A). H460 spheres in turn were slightly bigger and presented a more irregular shape (Figure 4.7.A). A549 cells formed spheroids with a bit uneven periphery and when concerning the same seeding densities much smaller than HCT116 or H460 spheres (Figure 4.6.A). DU 145-spheres were the smallest and had a jagged periphery (Figure 4.8.A). Spheroids derived from this cell line did not grow over time. Instead, they decreased slightly in size, regardless of seeding density (Figure 4.8.B). In HCT116-, H460- and A549-spheres gradual, almost linear, increase in diameter was observed in the first 4 days after formation (Figure 4.4.B, 4.7.B and 4.6.B).

Despite using various seeding densities for HT29 cells, efforts to obtain spheroids from this cell line proved unsuccessful. The cells did not aggregate and remained scattered at the bottom of the ULA plate (Figure 4.5.).

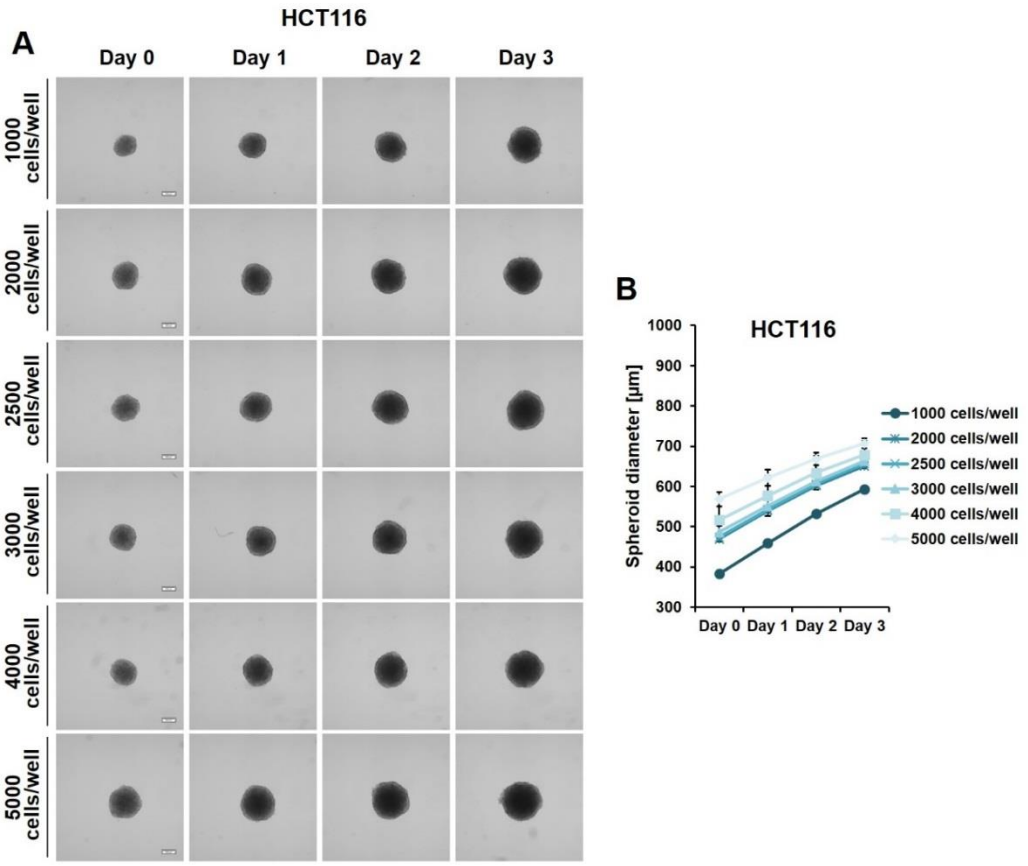

Figure 4.4. Establishment of seeding conditions for generation of HCT116 spheroids. Cell suspensions with various densities were seeded into ULA plates and incubated for 72h to allow spheroid formation. Then for 3 days images of spheroids were taken and diameters measured. **(A)** Representative microscopic images of HCT116-spheres obtained from various seeding densities. **(B)** HCT116 tumor spheroid growth curves. Values are mean ± SD (n=3).

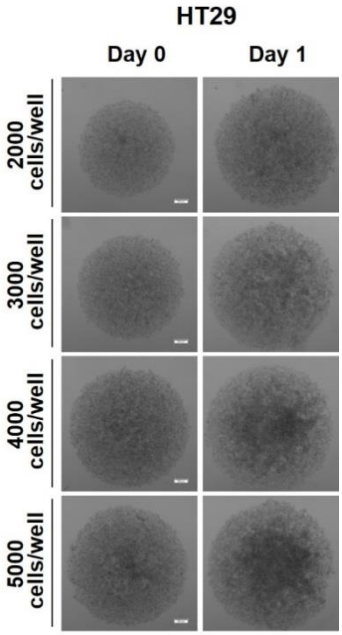

Figure 4.5. Establishment of seeding conditions for generation of HT29 spheroids. Cell suspensions with various densities were seeded into ULA plates and incubated for 72h to allow spheroid formation. Then images of spheroids were taken (n=2).

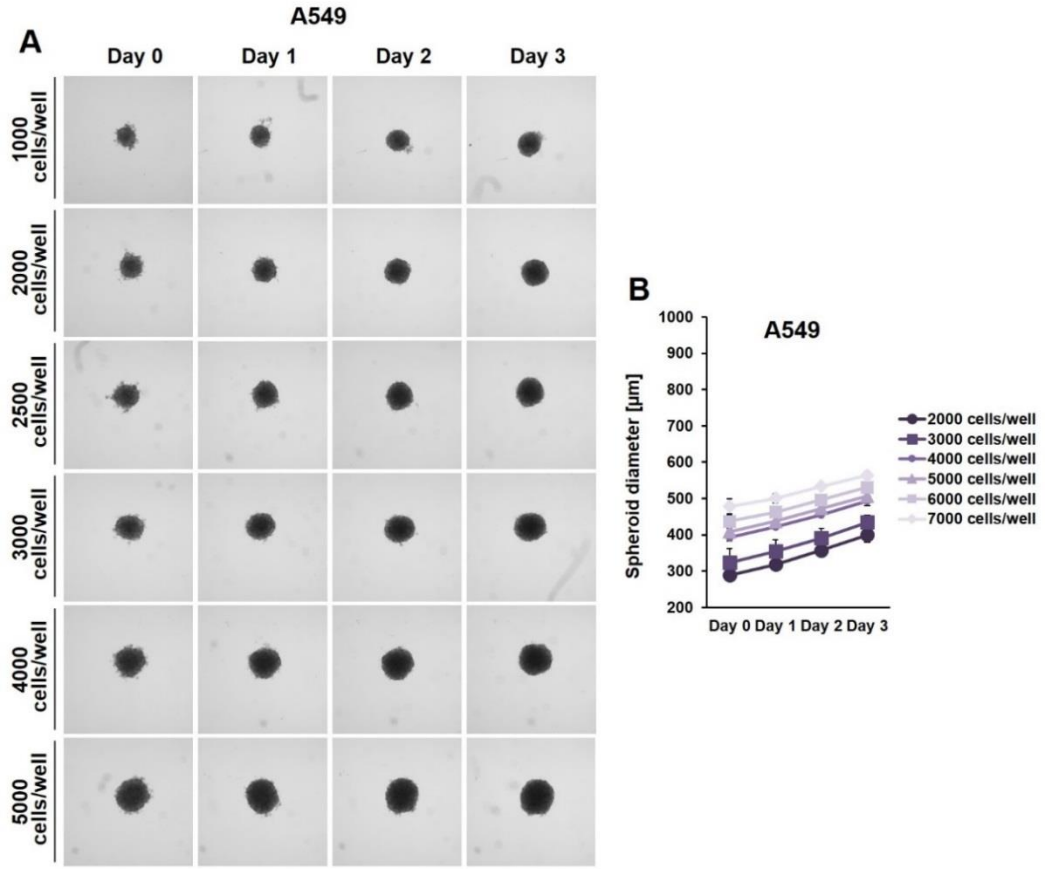

Figure 4.6. Establishment of seeding conditions for generation of A549 spheroids. Cell suspensions with various densities were seeded into ULA plates and incubated for 72h to allow spheroid formation. Then for 3 days images of spheroids were taken and diameters measured. **(A)** Representative microscopic images of A549-spheres obtained from various seeding densities. **(B)** A549 tumor spheroid growth curves. Values are mean ± SD (n=3).

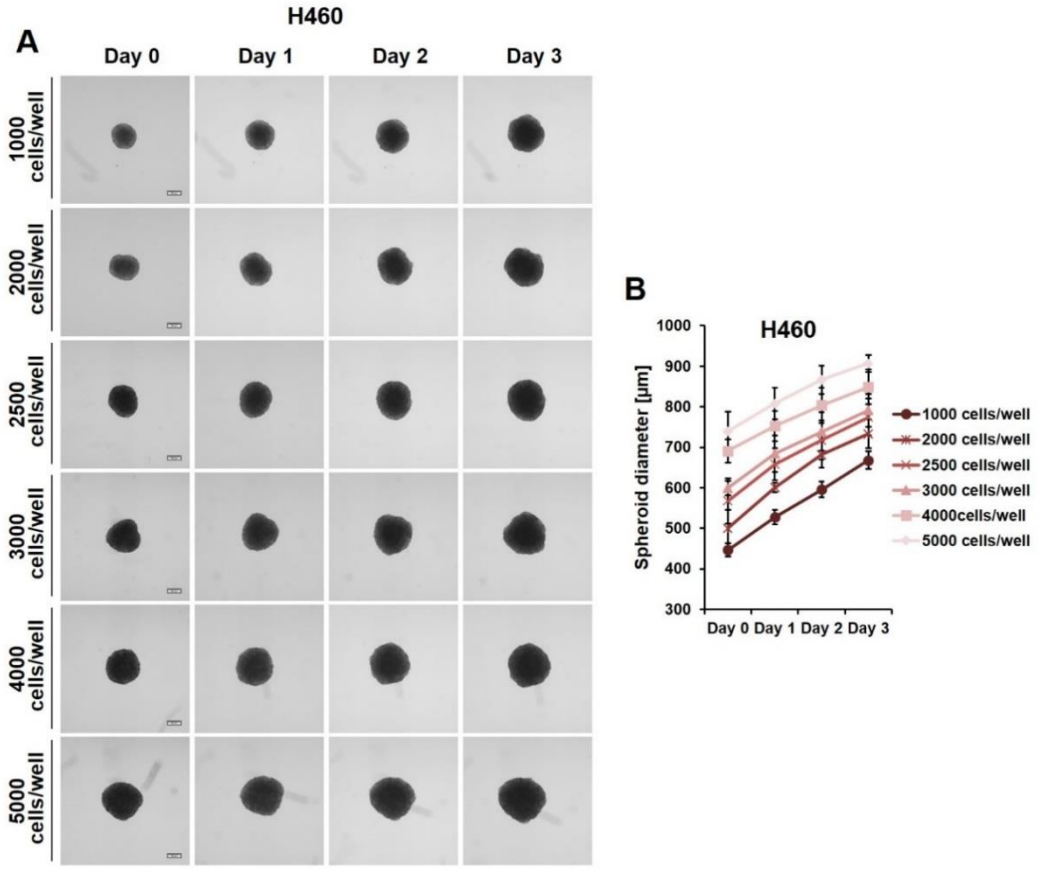

Figure 4.7. Establishment of seeding conditions for generation of H460 spheroids. Cell suspensions with various densities were seeded into ULA plates and incubated for 72h to allow spheroid formation. Then for 3 days images of spheroids were taken and diameters measured. **(A)** Representative microscopic images of H460-spheres obtained from various seeding densities. **(B)** H460 tumor spheroid growth curves. Values are mean ± SD (n=3).

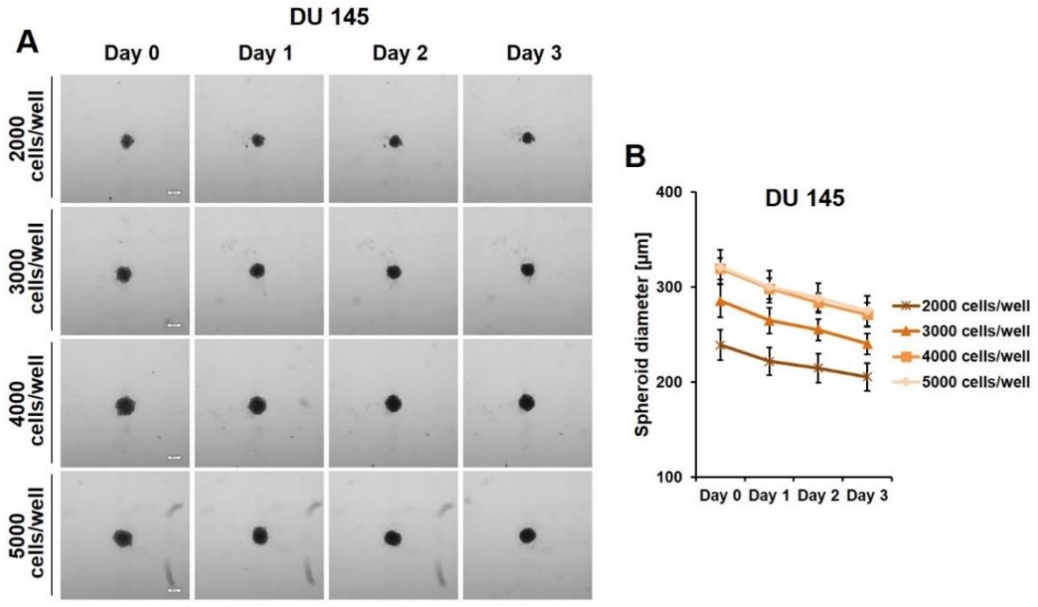

Figure 4.8. Establishment of seeding conditions for generation of DU 145 spheroids. Cell suspensions with various densities were seeded into ULA plates and incubated for 72h to allow spheroid formation. Then for 3 days images of spheroids were taken and diameters measured. **(A)** Representative microscopic images of DU 145-spheres obtained from various seeding densities. **(B)** DU 145 tumor spheroid growth curves. Values are mean ± SD (n=2).

Due to these observations, in further experiments, HCT116, H460, and A549 cells were used. In order to obtain spheres with diameters between 300 and 500 μm, which is suggested as the preferred range for experiments with spheroids [Amaral R.F.L. et al., 2017; Mittler F. et al., 2017; Vinci M. et al., 2012], seeding densities of 1 x 10^4 cells/mL for HCT116 and H460 cells and 2.5 x 10^4 for A549 cells were chosen.

4.5. Cytotoxic effects of UA compounds and etoposide against A549 cells

Since the cytotoxicity of tested compounds against HCT116 and H460 was previously established in our laboratory, there was no need to repeat those experiments. Therefore, I evaluated the cytotoxic activity of C-2028, C-2041, C-2045, C-2053, and etoposide, as reference compound, against A549 cells using the MTT assay. This method is based on the assumption that only viable cells contain functional mitochondria, in which the yellow, water-soluble MTT dye can be reduced to water-insoluble, purple formazan crystals. The amount of precipitated crystals is therefore directly proportional to the number of living cells.

A549 cells were incubated for 72 hours with increasing concentrations of UAs up to 10 μM or etoposide up to 100 μM, which resulted in concentration-dependent inhibition of cell proliferation. The obtained growth inhibition curves, with determined drug concentrations required to inhibit cell growth by 50, 80, and 90% (IC_{50}, $IC_{80,}$ and IC_{90} values) are presented in Figure 4.9.

All four bisacridine compounds exhibited very high cytotoxicity against A549 cells, with concentrations required to inhibit cell proliferation in 90% below 0.35 μM. Notably, C-2028 and C-2041 derivatives inhibited the proliferation of lung cancer cells at very low concentrations: their IC_{50}, $IC_{80,}$ and IC_{90} values did not exceed 0.024, 0.053, and 0.085 μM, respectively. Considering IC_{90} values, C-2045 and C-2053 were around 3.5 times less active than the previous two compounds. In contrast, A549 cells demonstrated much lower sensitivity to treatment with the reference compound, etoposide, than to UAs. The IC_{50} value for etoposide (5.59 μM) was over 120 times higher than the IC_{50} value for any UA compound and still at least 17 times higher than IC_{90} values for UAs.

Given the substantial differences between the doses established for UAs and the reference compound, and the fact, that for etoposide in some repetitions, the IC_{90} value was impossible to determine, for further experiments I have selected the IC_{50} dose for reference compounds and IC_{90} for the UAs. The choice of these concentrations for unsymmetrical bisacridines was based on the preliminary investigations conducted in our laboratory, which highlighted that the remarkable changes observed in the cellular response after treatment with UAs occurred at higher concentrations than IC_{50}. Moreover, these preliminary studies indicated a notable similarity in the extent of induced apoptosis in the 2D monolayer culture of HCT116 cells between irinotecan at its IC_{50} concentration and UAs at their IC_{90}. This further supported my rationale for using these doses in further experiments.

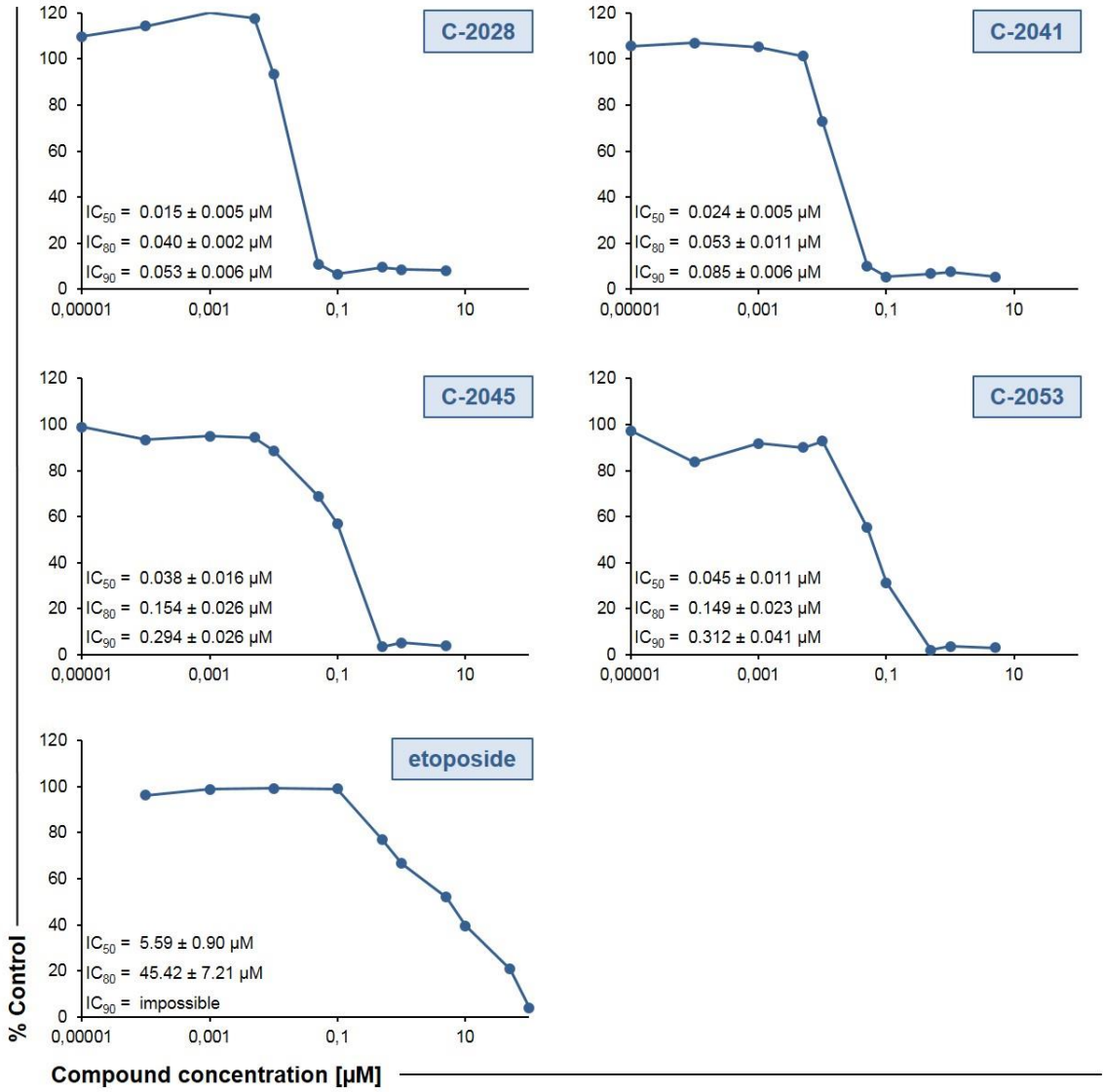

Figure 4.9. Cytotoxicity of UA compounds and etoposide against A549 cells. Cells were incubated with increasing concentrations of tested compounds for 72h and cytotoxic activity was assessed using the MTT assay. Data represented are the averages of four independent experiments with standard deviation. (n=4)

4.6. Changes in morphology and size of HCT116-, H460- and A549-derived spheroids

A widely used and straightforward approach to assess a drug's influence on spheroids is to monitor the diameters of the spheroids exposed to the compound over increasing time of treatment. In this context, I decided to investigate the influence that UAs and reference compounds have on the morphology and size of spheroids derived from HCT116, H460, and A549 cancer cells.

Microscopic observation of obtained spheroids and their growth over time presented that there are noticeable distinctions among spheroids derived from each cell line in terms of both morphology and size. These differences were evident not only between control spheroids and those subjected to the tested compounds but also across the various cell lines themselves (Figure 4.10.A, 4.11.A, 4.12.A).

Over time, control spheres of all cell lines exhibited slightly different growth kinetics. HCT116 sphered displayed a more rapid increase in size and reached bigger diameters

(Figure 4.10). Spheroids derived from that cell line retained their circular rim up to day 7, and after 9 days of incubation, an incohesive peripheral cell layer appeared. In contrast, H460 spheres (Figure 4.11), exhibited slower and more limited growth. Moreover, even after 14 days of incubation, they preserved a clearly defined periphery, and no diffuse outer layer was observed after day 7. Over time, H460 spheres evolved into heterogenous and lobular shapes. A549 spheroids (Figure 4.12), which have grown over time to the least extent, demonstrated a heightened ability to retain their circularity during longer incubation times. Remarkably, almost no visible changes in the spheroid periphery of A549 were observed even on day 14.

The treatment of 3D spheroid cultures with the tested bisacridines and reference drugs caused visible changes in the morphology of spheroids. HCT116 spheres subjected to the tested compounds exhibited a transition from a smooth periphery to a jagged one, and after prolonged exposure, a diffuse outer layer of cells emerged. It was, however, more condensed than the cell layer present in control spheroids, and even after 14 days, the core of HCT116 spheres treated with UAs and irinotecan remained compact and well-defined (Figure 4.10.A).

In the case of H460 spheres after 9 days of incubation with cisplatin and 11 days with C-2041, spheroids began to take slightly lobular shapes similar to those observed in control. Spheres incubated with C-2028, C-2045, and C-2053 did not show such features - they had condensed cores with cells sprouting at the periphery (Figure 4.11.A).

A549-derived spheroids incubated with UAs showed minimal changes in their morphology. Even after 14 days, all spheres retained their circular rim and there were no visible cells sprouting at the periphery. Interestingly, A549 spheroids treated with C-2041 or etoposide during extended exposure periods appeared to have acquired more well-defined edges compared to the control spheres (Figure 4.12.A).

In the case of HCT116 cells, a gradual reduction in spheroid size was observed after 4 days of incubation with all compounds except C-2041, with C-2053 demonstrating the most pronounced reduction. Notably, spheroids incubated with this compound after 14 days were about 10% smaller than on day 0. A similar, slightly stronger effect was observed for the reference compound – the spheroids incubated with irinotecan after 14 days were almost 20% smaller in diameter than the spheroids on day 0.

H460 spheres began to decrease in size after 7 days of incubation with the UAs, yet even after two weeks, neither compound led to a reduction in spheroids size below their initial baseline. Similarly to the observations in HCT116 spheres, in the case of H460-derived spheroids, the growth inhibition after treatment with C-2041 derivative was the least pronounced among the tested UAs. The other bisacridines, namely C-2028, C-2045, and C-2053, demonstrated comparable effects on H460 spheres. Moreover, spheroids incubated with those derivatives reached smaller sizes than those exposed to the reference compound, cisplatin.

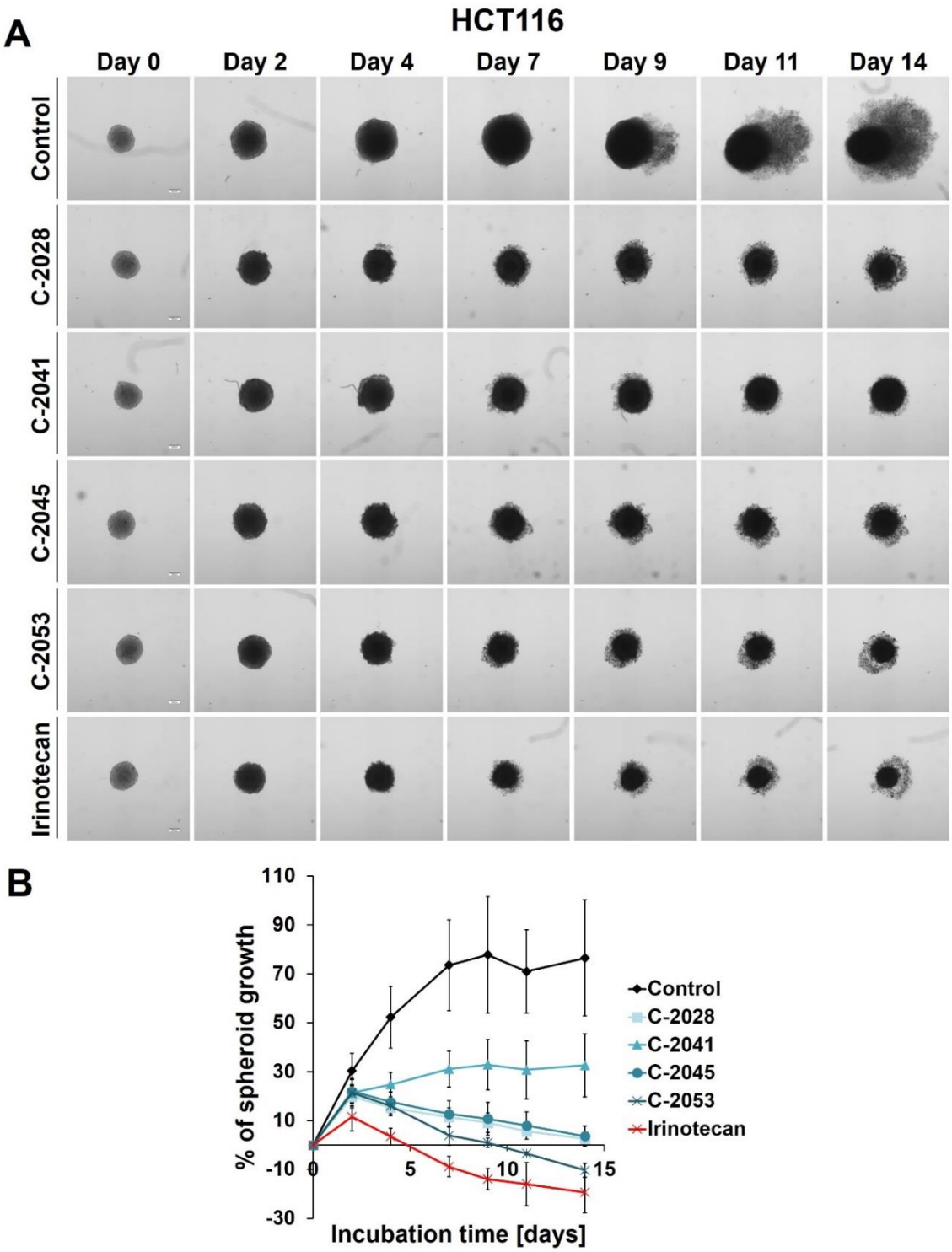

Figure 4.10. HCT116 spheroid morphology and kinetics. Spheroids were incubated with UAs at concentrations corresponding to IC_{90} values and irinotecan at IC_{50} dose for 14 days. Every 2–3 days, images of spheroids were taken and diameters were measured. **(A)** Representative images of the HCT116 control spheroids and spheroids treated with tested compounds. **(B)** Growth kinetics presented as a graph of percentages of spheroid growth over time. Data represent the averages of four independent experiments with standard deviation. Scale bar 200 µm. (n=4)

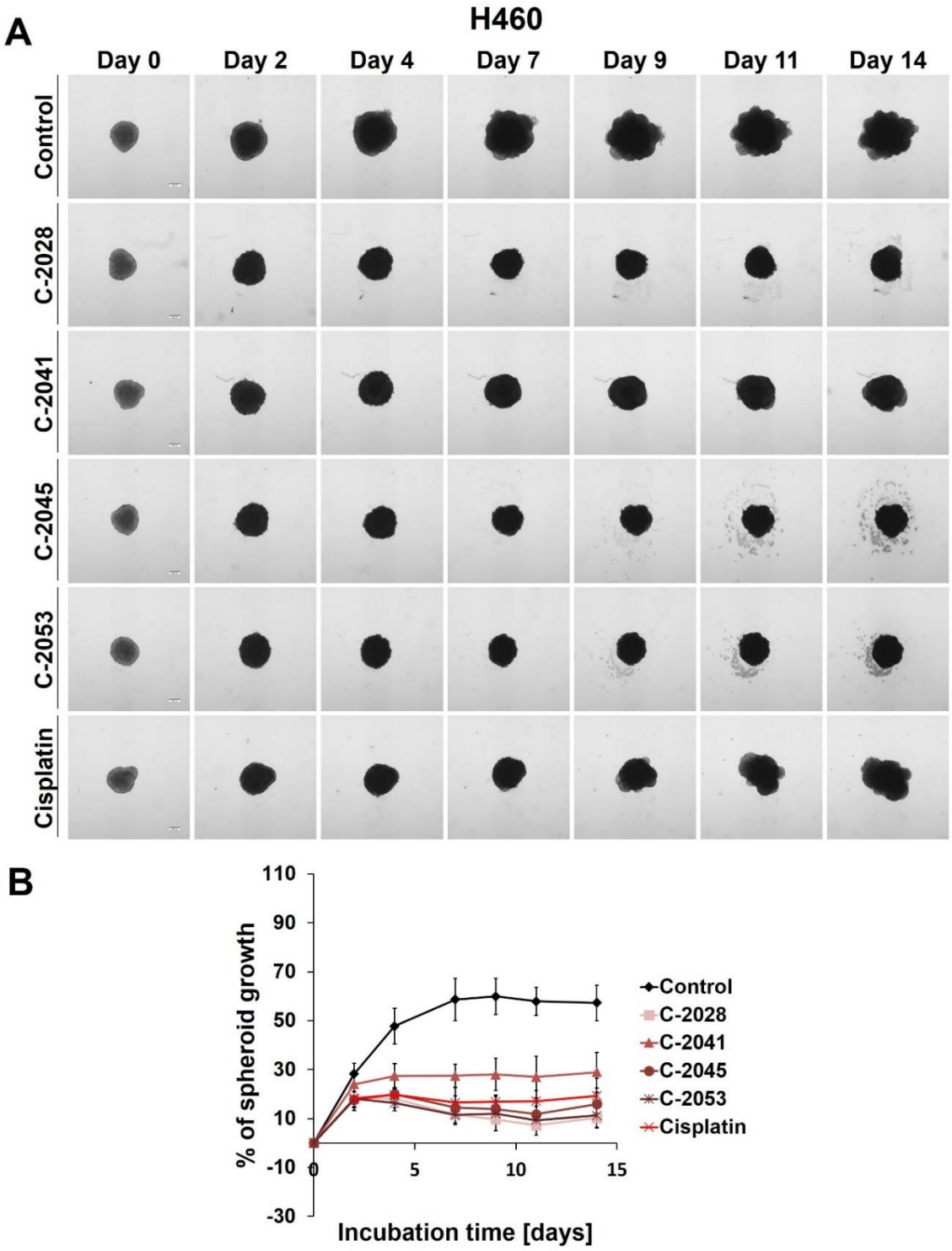

Figure 4.11. H460 spheroid morphology and kinetics. Spheroids were incubated with UAs at concentrations corresponding to IC_{90} values and cisplatin at IC_{50} dose for 14 days. Every 2–3 days, images of spheroids were taken and diameters were measured. **(A)** Representative images of the H460 control spheroids and spheroids treated with tested compounds. **(B)** Growth kinetics presented as a graph of percentages of spheroid growth over time. Data represent the averages of four independent experiments with standard deviation. Scale bar 200 µm. (n=4)

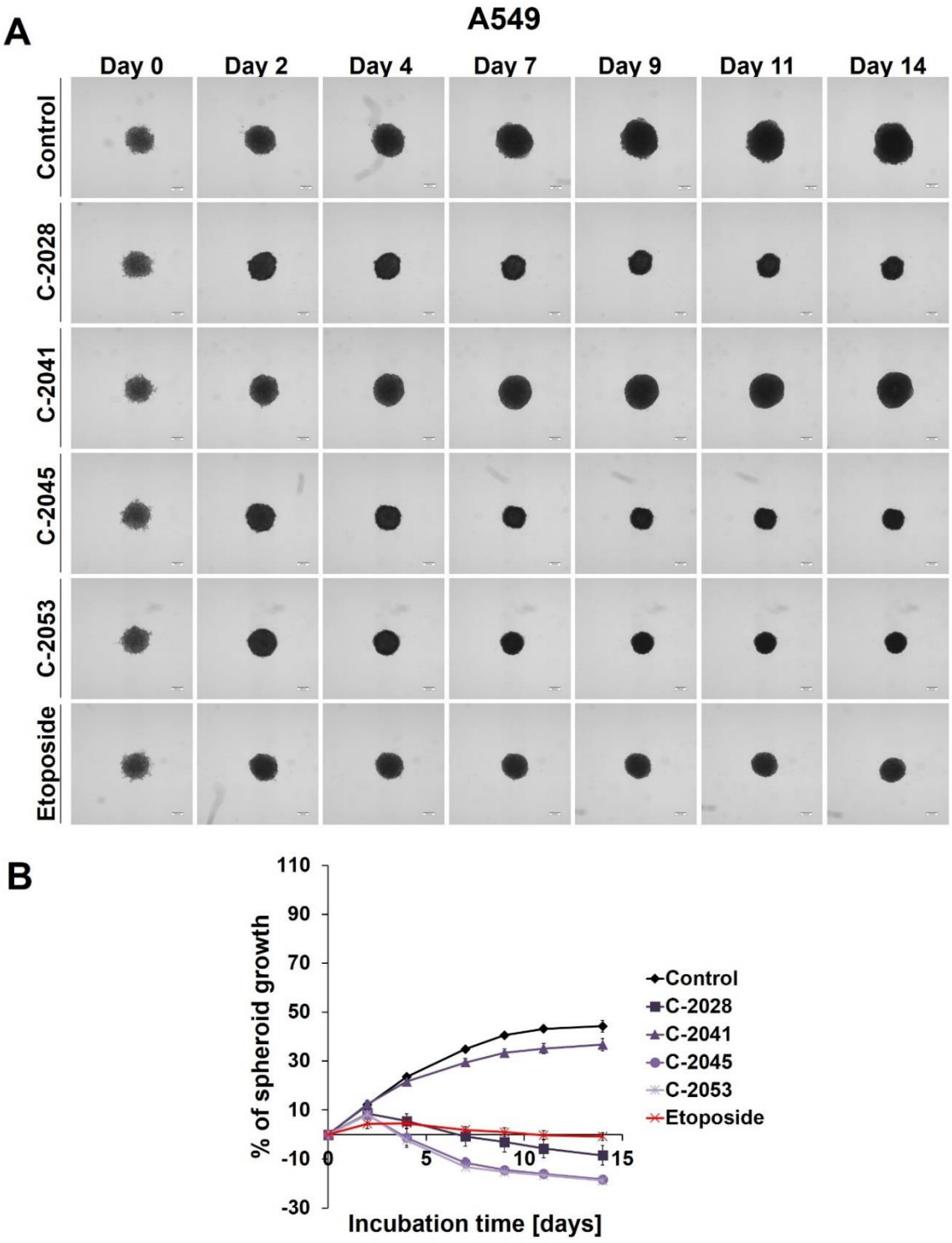

Figure 4.12. A549 spheroid morphology and kinetics. Spheroids were incubated with UAs at concentrations corresponding to IC_{90} values and etoposide at IC_{50} dose for 14 days. Every 2–3 days, images of spheroids were taken and diameters were measured. **(A)** Representative images of the A549 control spheroids and spheroids treated with tested compounds. **(B)** Growth kinetics presented as a graph of percentages of spheroid growth over time. Data represent the averages of four independent experiments with standard deviation. Scale bar 200 µm. (n=4)

In the case of A549 spheres, a gradual reduction in spheroid size was already evident after just 2 days of incubation with reference compound (etoposide) as well as with three tested UAs, namely C-2028, C-2045, and C-2053. C-2041 derivative had a negligible impact on spheroid

size, with only slight inhibition of their growth observed. Spheroids treated with C-2028, C-2045, and C-2053 reached smaller sizes than those incubated with etoposide. While the reference compound effectively inhibited spheroids' growth, it didn't cause a reduction of spheroids below baseline sizes. On the other hand, spheroids exposed to C-2028, C-2045, and C-2053 after 14 days were 8.53, 18.32, and 18.84% smaller, respectively, than on day 0.

4.7. Viability of cells in 2D and 3D cell cultures of HCT116, H460, and A549

The assessment of the viability of HCT116, H460, and A549 cells in both monolayer and spherical cultures was a crucial step in the determination of the 3D model's suitability for investigating unsymmetrical bisacridines. The proportion of live and dead cells was established using 7-aminoactinomycin D (7-AAD) – a dye that binds to the DNA of cells with compromised cell integrity, therefore allowing to distinguish between viable and non-viable cells.

Flow cytometry analysis of HCT116, H460, and A549 cells showed that when grown in monolayers, all studied cell lines exhibited high fractions of 7-AAD negative (alive) cells. Interestingly, the H460 cell line cultured in 3D conditions differed substantially from the other two lines in the number of viable cells (Figure 4.13.). In the case of HCT116, both monolayer culture and spheroids showed consistency in maintaining a minimal population of dead cells, constituting less than 10% of the total cell count. Similarly, the A549 monolayer culture displayed a comparable fraction of dead cells, while a slightly higher number was observed in A549 spheroids (13%). In contrast, the H460-derived spheres exhibited markedly reduced viability, with only about 52% alive cells. This percentage was nearly 40% lower than that observed in the adherent model of this cell line.

To determine whether spheroid seeding density has an impact on the percentage of alive cells in this culture model, a similar analysis was performed using spheroids derived from HCT116, H460, and A549 cells seeded with various amounts of cells per well. 3 days after formation, the spheroids were disaggregated, stained with 7-AAD, and subjected to flow cytometry analysis. In the case of spheroids derived from these three cell lines, no significant variations in cell viability were observed under our experimental conditions when different seeding densities were used. Spheroids derived from the HCT116 cell line presented consistency in maintaining a markedly high percentage of alive cells (approximately 90%). Likewise, the viability of A549 cells in spherical culture remained similar at all seeding densities tested and accounted for at least 80% of all cells. In contrast, for H460 cells, regardless of the seeding density, I was unable to obtain spheres with a higher fraction of alive cells than 55%.

The high proportion of dead cells (7-AAD$^+$) within the H460 spheres makes the 3D model derived from this cell line not as suitable for analysis of the cellular response induced by anticancer compounds as the spheroids derived from HCT116 and A549 cell lines. While it remains possible to employ these H460 spheroids as controls in experimental setups, the interpretation of results would be much more complicated. It might be challenging to distinguish between the natural cell death occurring so extensively in these spheroids and the mechanism of action triggered by the compounds tested. Furthermore, my initial attempts at cytometric analysis

of H460 spheres after exposure to unsymmetrical bisacridines encountered complications, therefore, given these challenges, the H460 spheroid model was not used in further experiments regarding UAs. Instead, I concentrated my efforts on studying UAs and their impact on HCT116 colon and A549 lung cancer cells in 2D and 3D conditions.

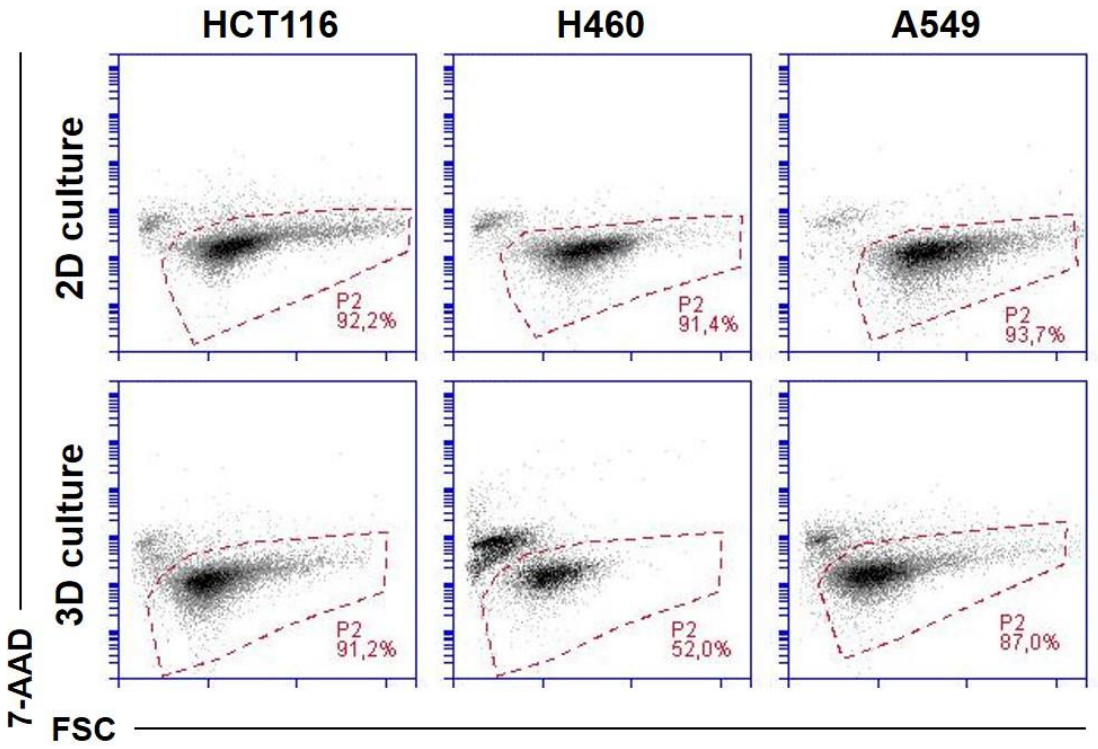

Figure 4.13. Viability of HCT116 (left), H460 (middle), and A549 (right) cells cultured in 2D and 3D conditions. Cells after 3 days of culture in both culture systems were stained with 7-AAD and subjected to flow cytometry analysis. P2: fraction of the 7-AAD negative cells (alive). Presented cytograms are representative of four independent experiments. (n=4)

4.8. Changes in the viability of HCT116 and A549 cells cultured in 2D and 3D conditions after drug treatment

4.8.1. Viability of HCT116 cells in 2D and 3D cultures after treatment with UAs and irinotecan

To assess the influence of the tested compounds on the viability of HCT116 cells cultured in monolayer and as spheroids, the cells were treated for 3 or 7 days with IC_{90} or $5xIC_{90}$ concentrations of UAs and IC_{50} or $5xIC_{50}$ concentrations of irinotecan. Then, the cells were stained with 7-AAD and analyzed by flow cytometry. The obtained results showed that 2D and 3D culture models differed in the intensity of the observed cellular response (Figure 4.14.).

When grown in monolayer, after 3 days of treatment with UAs at IC_{90} doses, HCT116 cells showed at least three-fold higher percentages of dead cells than the untreated control. Among the tested compounds, the C-2041 derivative exhibited the most pronounced impact, inducing cell death in HCT116 cells to the highest extent – after 72 h of incubation with this compound at IC_{90} dose, the fraction of non-viable cells reached 38.1%. Comparatively, the C-2028 and C-2045 demonstrated slightly lower potency, affecting colorectal cancer cells on a similar level to irinotecan, with the proportion of 7-AAD^+ cells being just above 30%. In the

case of the C-2053 derivative, after 72 h of incubation with this compound, only 21.4% of all the HCT116 cells were dead.

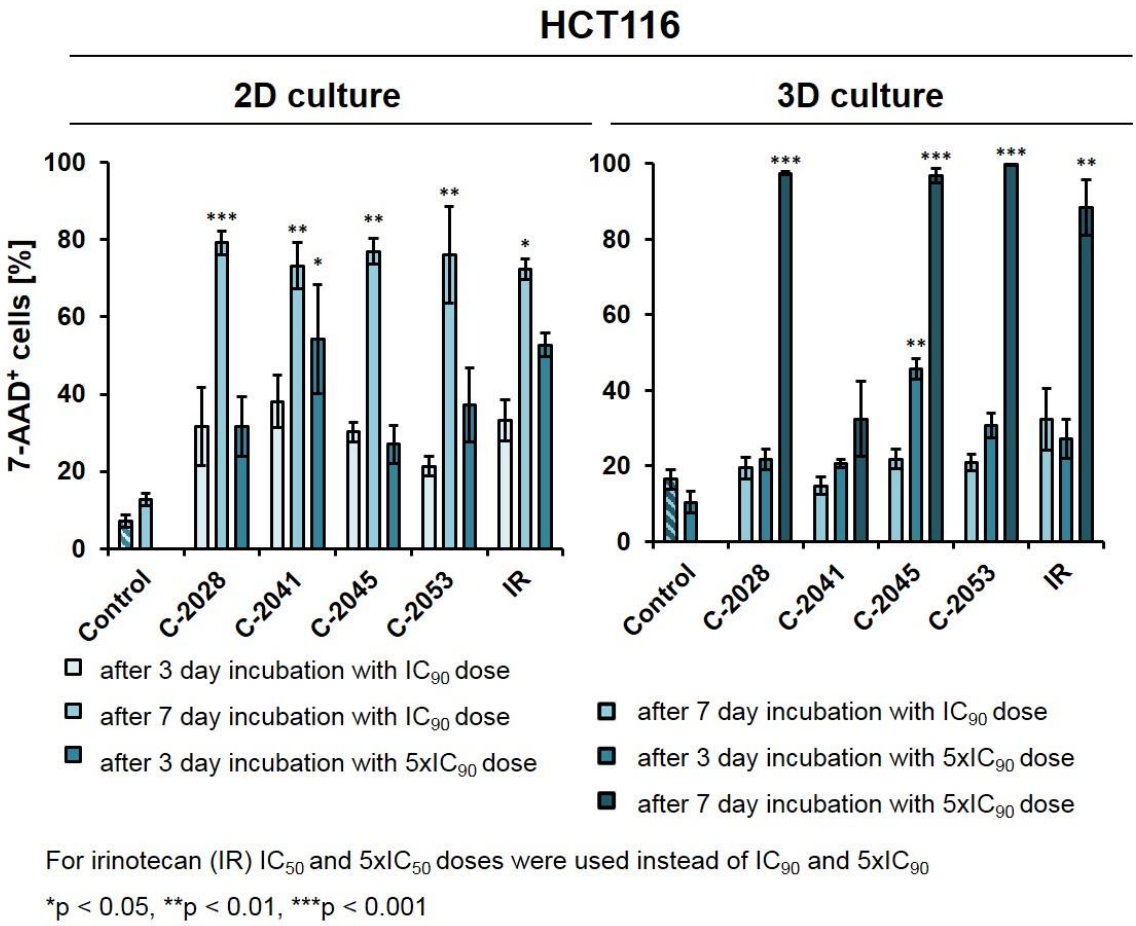

Figure 4.14. Effects of C-2028, C-2041, C-2045, C-2053, and irinotecan on cell viability in HCT116 cells cultured in 2D and 3D conditions. Cells were incubated with tested compounds at concentrations corresponding to IC_{90} and $5xIC_{90}$ values (IC_{50} and $5xIC_{50}$ for irinotecan) for 3 or 7 days, stained with 7-AAD, and subjected to flow cytometry analysis. Bar graphs show quantified data, expressed as the percentages of 7-AAD$^+$ (dead) cells after incubation with tested compounds in 2D (left) and 3D (right) cell cultures. Data are presented as the means ± SD of three to eight independent experiments. Statistical analysis was performed using Dunn's nonparametric multiple comparisons test. Significantly different from control at: * $p < 0.05$, ** $p < 0.01$, *** $p < 0.001$. (n=3-8)

Since the 3-day incubation with UAs and irinotecan at IC_{90} and IC_{50} doses resulted in only a moderate effect on HCT116 cells grown in a monolayer, I decided not to analyze the cellular response under these conditions in spheroids. Instead, I have selected two modifications in experimental conditions for further investigations – I extended the incubation period to 7 days and increased the doses of tested compounds five-fold.

For both UAs and irinotecan, the fractions of 7-AAD$^+$ (dead) cells were much higher in 2D culture than in 3D after 7 days of incubation with the compounds at IC_{90} doses. In monolayer culture, over 70% of cells treated with the tested compounds were non-viable, while in spheroids, these fractions were notably lower: 19.5, 14.8, 21.8, 20.5, and 32.3% for C-2028, C-2041, C-2045, C-2053, and irinotecan, respectively. Furthermore, this trend was maintained when treatment was carried out with compounds at $5xIC_{90}$ concentrations. After 3 days of incubation, the presence of dead cells was more pronounced in the 2D versus 3D cultures. The most apparent discrepancy

was visible in the case of the C-2041 derivative, where the fraction of dead cells after 72 h of exposure in 2D culture reached 52%, which was more than 2.5 times higher than that in 3D culture (20.3%). Importantly, the only exception was noted when the cells were treated with the C-2045, where 27% of all cells were dead in 2D culture, while in spheroids this population reached almost 45%. This intriguing finding suggests that this compound may be more effective in 3D culture than in 2D.

Extending the incubation period from 3 to 7 days at 5xIC_{90} concentrations within 3D cultures resulted in a marked increase in the number of 7-AAD^+ cells. This adjustment, however, was not implemented for cells grown in a monolayer because in this culture model, after 7 days of treatment, even at IC_{90} doses, a very high fraction of 7-AAD^+ cells was observed. Moreover, in adherent cultures, cells are evenly exposed to equal concentrations of tested compounds. This creates challenges in maintaining prolonged exposure to high doses in this model, which are not observed in spheroids and tumors *in vivo*, where a characteristic gradient is present. Consequently, long-term treatment with high doses of compounds in 2D conditions would inevitably lead to an extensive death of cells, complicating cell collection for subsequent analysis.

In HCT116 spheres, after 7 days of incubation with 3 tested bisacridines (C-2028, C-2045, and C-2053) at 5xIC_{90} doses, the fraction of non-viable cells was very high, reaching over 96%. A slightly weaker effect was observed for irinotecan, where exposure to a 5xIC_{50} concentration for 7 days resulted in 88.4% of cells being dead. A surprising observation was made for HCT116-spheres treated with C-2041 derivative, where even after a full week of exposure, more than 67.5% of all cells within spheroids remained viable. Under these conditions, only 32.5% of cells were dead, which was still less than the non-viable cell population in a 2D monolayer culture of HCT116 cells after a 3-day incubation with the IC_{90} dose of C-2041 (38%), proving that this compound, while highly effective in 2D, loses much of its potential when applied in HCT116 spheroids.

4.8.2. Viability of A549 cells in 2D and 3D cultures after treatment with UAs and etoposide

In a manner analogous to the HCT116 cells, A549 cells cultured in monolayer and as spheroids were incubated for 3 or 7 days with tested compounds at concentrations corresponding to the IC_{90} or 5xIC_{90} values for UAs and IC_{50} or 5xIC_{50} for etoposide. Following the treatment, the cells were subjected to 7-AAD staining and analyzed by flow cytometry. The obtained results are presented in Figure 4.15.

In monolayer culture of A549 cells, 3-day treatment with UAs at IC_{90} doses resulted in a clear increase in the number of 7-AAD^+ (dead) cells compared to control, with the fraction of non-viable cells reaching 40.1, 21.0, 23.2, and 28.3% for C-2028, C-2041, C-2045, and C-2053, respectively. In contrast, this fraction reached only 18.3% after exposure to etoposide. Considering the experiments on HCT116 and this relatively moderate effect on A549 cells, here I also decided to test and compare two variants in 2D and 3D: one with IC_{90} doses (IC_{50} for ETP) with an extended incubation time of 7 days, and the other with a 3-day treatment time but a fivefold increase in compound doses to 5xIC_{90} (or 5xIC_{50} for ETP).

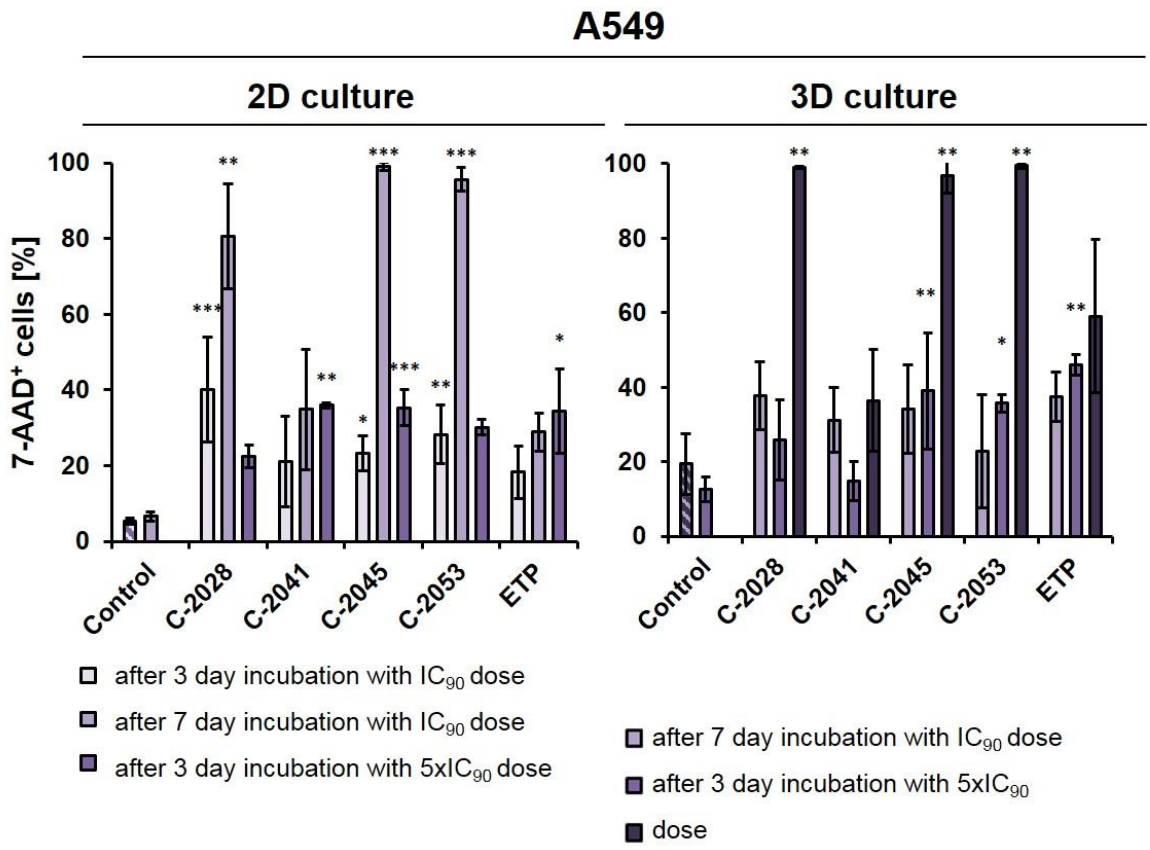

Figure 4.15. Effects of C-2028, C-2041, C-2045, C-2053, and etoposide on cell viability in A549 cells cultured in 2D and 3D conditions. Cells were incubated with tested compounds at concentrations corresponding to IC_{90} and $5xIC_{90}$ values (IC_{50} and $5xIC_{50}$ for etoposide) for 3 or 7 days, stained with 7-AAD, and subjected to flow cytometry analysis. Bar graphs show quantified data, expressed as the percentages of 7-AAD$^+$ (dead) cells after incubation with tested compounds in 2D (left) and 3D (right) cell cultures. Data are presented as the means ± SD of three to seven independent experiments. Statistical analysis was performed using Dunn's nonparametric multiple comparisons test. Significantly different from control at: * $p < 0.05$, ** $p < 0.01$, *** $p < 0.001$. (n=3-7)

After treatment with UAs for 7 days at IC_{90} doses, the number of non-viable A549 cells was much higher in 2D culture (about 80-98% of 7-AAD$^+$ cells) than in 3D (23-38%), with the exception of C-2041 derivative, for which this fraction of cells remained similar in both culture conditions (34.9% in 2D and 31.2% in 3D). Notably, when subjected to a 3-day treatment with C-2028, C-2045, and C-2053 at $5xIC_{90}$ doses, the proportion of dead cells in 3D (25.8, 39.0, and 35.8, for C-2028, C-2045, and C-2053, respectively) was very similar to that observed in 2D (22.3, 35.3 and 30.1%) but slightly higher. In contrast, for the C-2041 derivative, this fraction was more than 20% lower in spherical culture, compared to monolayer. In the case of etoposide, regardless of whether A549 cells were exposed to an IC_{50} dose for 7 days or with a $5xIC_{50}$ dose for 3 days, the percentage of 7-AAD$^+$ cells was about 10% higher in the 3D culture compared to the 2D.

Similarly to HCT116 cells, here I also decided to extend the incubation period for A549 spheroids treated with $5xIC_{50}$ doses from 3 to 7 days, to see how this would affect the observed cellular response in lung cancer cells. Once again, this was not done in monolayer cultures, where it is very challenging to sustain prolonged treatment with high concentrations of compounds.

In A549 spheroids treated with 5xIC_{90} doses of UAs (5xIC_{50} for ETP), extending the exposure time resulted in a marked increase in the number of dead cells, which for three of the examined UAs (C-2028, C-2045, and C-2053) reached over 97%. Interestingly, a considerably weaker effect was observed for etoposide, where even after a 7-day treatment with a 5xIC_{50} dose, over 40% of cells remained viable. Similar to previous observations, C-2041 demonstrated the least considerable impact, and treatment with this derivative resulted in the death of less than 37% of cells.

4.9. Colony formation

To determine the potential for HCT116 and A549 cells to return to proliferation following exposure to UAs and irinotecan/etoposide, a colony formation assay was performed. After treatment with the tested compounds, cells were collected, counted, and approximately 250 were incubated for 14 days in a fresh medium, after which their ability to form colonies was evaluated (Figure 4.16).

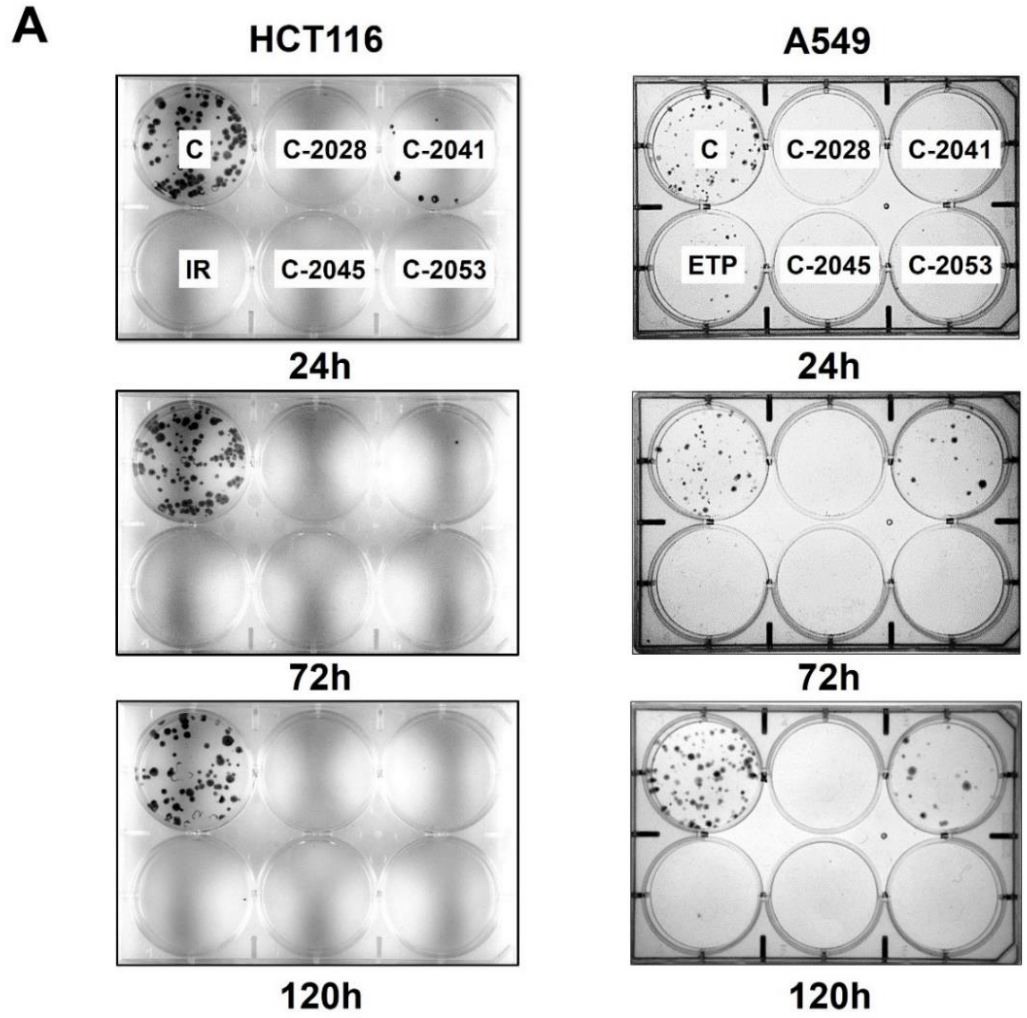

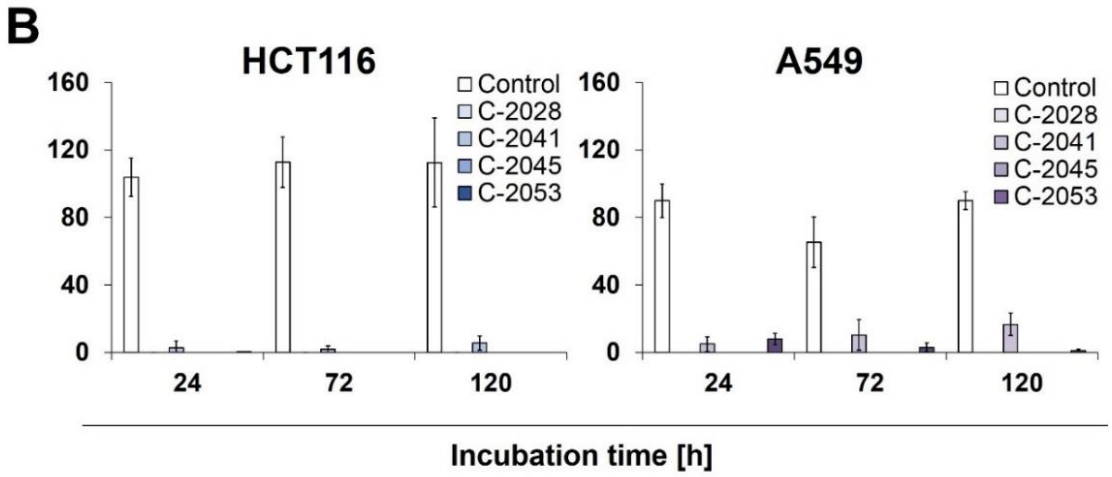

Figure 4.16. The ability of HCT116 and A549 cells to return to proliferation after UAs exposure. Cells were treated with IC_{90} doses of C-2028, C-2041, C-2045, and C-2053 compounds (IC_{50} for irinotecan and etoposide). After the indicated drug exposure, approximately 250 cells were cultured for two weeks in a fresh medium and the number of colonies was counted. (**A**) Representative pictures of HCT116 (right) and A549 (left) cells after postincubation and Giemsa staining. (**B**) Bar graphs show quantified data, expressed as the number of colonies ± SD for HCT116 (left) and A549 (right) cells (n=3).

Following exposure to C-2028, C-2045, and C-2053, HCT116 and A549 cells displayed a complete inhibition of proliferation, which was apparent already after 24 h of treatment with these compounds, as evidenced by the complete absence of colonies. Meanwhile, C-2041 only partially blocked cell division, as both HCT116 and A549 cells were able to form colonies even after 120 h of incubation with this derivative, with an average of 6 HCT116 and 16 A549 cells undergoing mitosis. Interestingly, while no HCT116 colonies were observed after exposure to irinotecan, treatment of A549 cells with etoposide did not completely stop the cells' ability to proliferate and a few colonies appeared even after 120 h of exposure to the reference compound.

4.10. Spherogenic potential of HCT116 and A549 cells

The ability of HCT116 and A549 cells to generate spheroids following exposure to tested compounds was determined after treatment of cells cultured in 2D and 3D conditions with IC_{90} doses of UAs and IC_{50} doses of reference compounds for 3 days. Captured images of formed spheroids on day 0 (3 days after seeding) and on day 14 together with the graphs illustrating the mean diameters of spheroids obtained are presented in Figure 4.17.

In the case of HCT116 cells, control spheroids generated from cells cultured in 2D and 3D (secondary spheres) exhibited nearly identical characteristics, both in terms of size and morphology. A549 cells, however, when cultured as spheroids after disaggregation into a single-cell suspension, were unable to reproduce spherical cultures on day 0. After 14 days of incubation, spherical forms reappeared in some cases, but they were still less defined compared to the spheres generated from cells cultured in 2D. Their shapes were not perfectly spherical, the periphery was uneven, and slightly lobular shapes appeared. As a result, an accurate and definitive measurement of A549 secondary spheres was not entirely possible, especially on day 0, and the diameters that I have determined using the count and measure extension in cellSens

Dimension software are only indicative and approximate, hence the high standard deviation values for this condition.

After incubation with the tested compounds, generally, the spheroids generated were smaller and grew less in time when treatment was applied in 2D cultures of HCT116 and A549 cells compared to 3D. HCT116 cells were able to form spheroids approximately 250-300 μm in diameter after exposure in 2D to C-2028, C-2045, C-2053, and IR, and in the case of C-2045, C-2053, and IR they did not grow over time. Spheroids generated after treatment with C-2041 although substantially smaller than control spheres at day 0 (about 330 μm versus 485 μm) grew to similar sizes over time (780 μm for C-2041 and 830 for control). HCT116 secondary spheroids after UAs treatment for all compounds except C-2041 were considerably smaller than control on day 0, but by day 14, spheroids formed after treatment with C-2028 and IR had reached similar diameters to control. The lowest increase in the diameters of HCT116 secondary spheroids was observed after exposure to the C-2053 derivative, followed by C-2045.

As with HCT116, in A549 cells cultured in 2D, treatment with the C-2041 derivative did not significantly inhibit the spherogenic potential of the cells. The spheroids generated exhibited sizes comparable to the control and displayed a similar growth pattern. Notably, the spheroids formed after incubation with C-2045, though only slightly smaller than the control on day 0, over time became more compact and their size decreased considerably, while the periphery became much more defined. A similar effect was observed for spheres obtained after exposure of 2D culture of A549 cells to etoposide. Interestingly, treatment with C-2028 and C-2053 derivatives completely inhibited the spherogenic potential of A549 cells cultured as monolayers, and no spherical forms were observed even after 14 days.

As mentioned above, secondary sphere formation in the case of A549 cells is difficult to analyze. Nevertheless, several general observations can be made. Firstly, as in control, A549 cells, following treatment with all tested compounds, proved unable to recreate spheroids after the primary spherical forms were disintegrated. Yet, on day 14, some distinctions were visible between the control and the spheres obtained after exposure to tested compounds. Most notably, it is worth mentioning that as in 2D conditions, after treatment of 3D spheroids with C-2053, this derivative completely inhibited the ability of A549 cells to form spheroids. None of the other compounds tested presented such activity, including the reference compound. Furthermore, secondary spheres formed after treatment of A549 spheres with the C-2045 derivative were also considerably smaller than those incubated with ETP. A similar observation was made in the case of C-2028, although here the contrast in size was less pronounced. The largest spheroids were generated following exposure to C-2041 derivative, once again highlighting the minimal effect of this derivative on A549 cells.

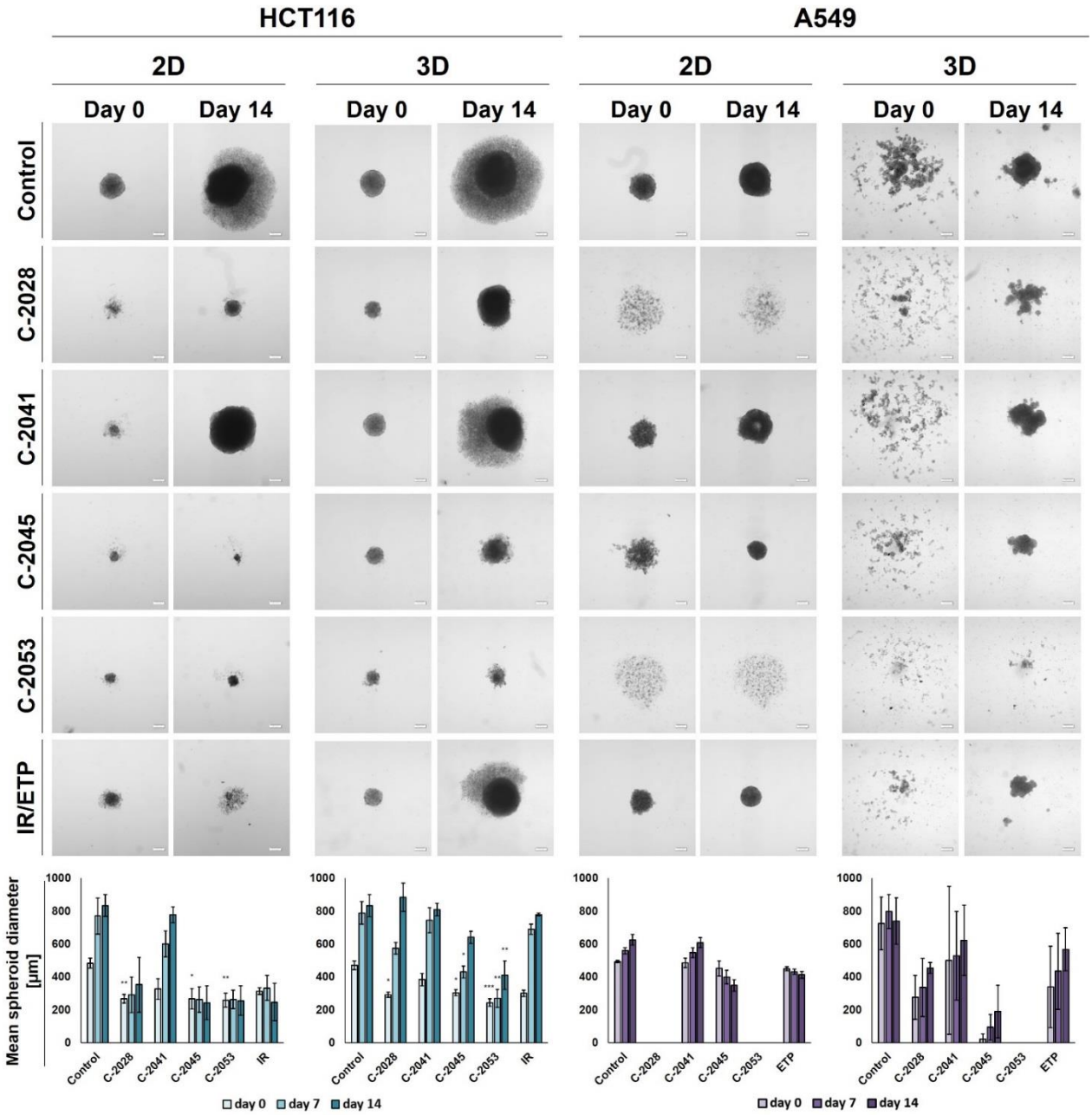

Figure 4.17. Spherogenic potential of HCT116 (left) and A549 (right) cells cultured in 2D and 3D (secondary sphere formation) conditions after incubation with UAs and reference compounds. Cells cultured as monolayer and spheroids were incubated with C-2028, C-2041, C-2045, C-2053, and irinotecan (IR)/etoposide (ETP) at concentrations corresponding to IC_{90} values (IC_{50} for IR/ETP) for 3 days and then were seeded onto ULA plates. Pictures of generated spheroids were taken 3 days after seeding (day 0), and then two weeks later (day 14). Scale bar 200 µm. Bar graphs show quantified data, expressed as the mean diameters of spheroids at day 0, day 7, and day 14. Data are presented as the means ± SD of from 3 to 5 independent experiments. Statistical analysis was performed using Dunn's nonparametric multiple comparisons test. Significantly different from control at: * $p < 0.05$, ** $p < 0.01$, *** $p < 0.001$. (n=3-5)

4.11. Analysis of the changes in the asymmetry and integrity of the cytoplasmic membrane of HCT116 and A549 cells

To test whether the type and intensity of the observed UAs-induced biological response in the studied cells depend on the culture method, I performed a flow cytometry analysis of the changes in the asymmetry and integrity of the cell membrane of HCT116 and A549 cells. The

cells were grown in monolayers and as spheroids and after 72h incubation with selected UA derivatives: C-2045 and C-2053, at concentrations corresponding to 5xIC_{90} doses, and with reference compounds: irinotecan and etoposide, at 5xIC_{50} doses, double staining with annexin V/PI was performed, and cells were subjected to flow cytometry analysis (Figure 4.18).

I have selected the two UA derivatives (C-2045 and C-2053) due to the most promising results with these compounds from previous experiments (morphology and size analysis, 7-AAD staining, and spherogenic potential assessment). The decision to use doses of 5xIC_{90} (5xIC_{50} for reference compounds) was based on the analysis of the cell viability after treatment, which was determined by 7-AAD staining).

In both culture systems, HCT116 and A549 control cells exhibited comparable levels of dead cells of less than 8%. After incubation with studied compounds, the number of apoptotic cells increased considerably, both in 2D and 3D. For HCT116 cells cultured in 2D, the apoptotic cell number after treatment with C-2045 and C-2053 derivatives amounted to about 20-25%, and for C-2053, this level stayed consistent (27.20%) also in the spherical model. Remarkably, for C-2045, this fraction of cells doubled, from 20.47 in 2D to 40.23% in 3D. In the HCT116 monolayer culture, the most profound induction of cell death was observed after exposure to the reference compound, where 43.53% of cells underwent apoptosis. In contrast, when applied in the spherical culture of colon cancer, irinotecan induced apoptosis in merely 19.27% of cells.

It is worth noting that in A549 cells, the fraction of annexin V positive cells for both tested UA derivatives was higher in 3D (about 40 and 35% for C-2045 and C-2053, respectively) than in 2D (33 and 25%). On the other hand, etoposide, for which the percentage of cells with translocated phosphatidylserine in 2D was similar to C-2053 (24.28%), induced apoptosis in only 11.10% of treated cells in the spherical culture of A549.

Interestingly, for both cell lines tested, a higher percentage of late-apoptotic cells was observed in 2D monolayer culture following incubation with UAs compared to early-apoptotic cells. However, in 3D conditions, this trend was quite the opposite – the vast majority of apoptotic cells were in the early phase of apoptosis and only about 5-10% of cells showed both phosphatidylserine translocation and cell membrane disruption. In 2D cultures, the fraction of A^+/PI^+ cells was about 12-18% for HCT116 and 10-12% for A549 cells. In contrast, early apoptotic cells after treatment with UAs accounted for about 22-34% of HCT116 and 25-30% of A549 cells cultured in 3D, while in 2D this population was only 8% for HCT116 cells and 15-20% for A549 cells. Necrosis was induced in a small percentage of cells cultured in 3D and no significant difference compared to control was observed for either cell line. In the monolayer culture of HCT116, a slight increase in the number of PI-positive cells was observed after treatment with tested compounds, but the number of necrotic cells still did not exceed 6%.

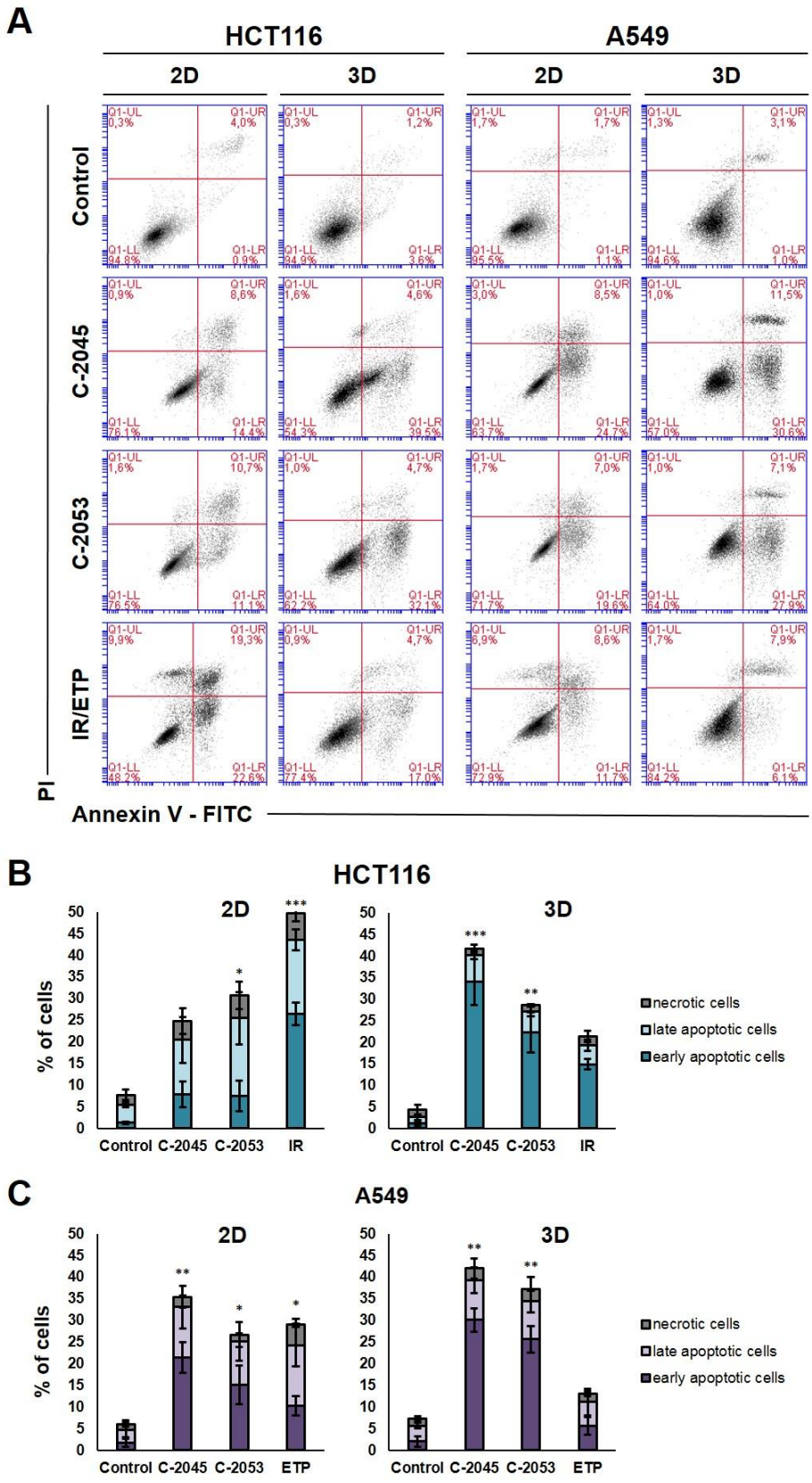

Figure 4.18. Phosphatidylserine externalization and membrane disruption in HCT116 and A549 cells treated with C-2045, C-2053, and reference compounds: irinotecan (IR) and etoposide (ETP). Cells were exposed to C-2045, C-2053, and IR/ETP at concentrations corresponding to 5xIC_{90} values (5xIC_{50} for IR/ETP) for 72h, stained with annexin V–fluorescein isothiocyanate (FITC) and propidium iodide (PI), and analyzed using flow cytometry. (**A**) Representative bivariate flow cytometry histograms of annexin V–FITC signal versus PI signal are shown. The bottom left quadrant represents living cells (annexin V negative,

PI negative); the bottom right quadrant represents early apoptotic cells (annexin V positive, PI negative); the top right quadrant represents late apoptotic cells (annexin V positive, PI positive); the top left quadrant represents primary necrotic cells (annexin V negative, PI positive). (**B, C**) Bar graphs show quantified data, expressed as the percentages of HCT116 (**B**) and A549 (**C**) early apoptotic, late apoptotic, and necrotic cells in 2D and 3D cell cultures. Data are presented as the means ± SD of three to seven independent experiments. Statistical analysis was performed using Dunn's nonparametric multiple comparisons test. Significantly different from control at: * $p < 0.05$, ** $p < 0.01$, *** $p < 0.001$. (n=3-7)

4.12. Cancer stem cell-like population

In order to test whether the 3D spherical cell culture model I have established for my studies differs significantly in the number of cells with cancer stem cell-like characteristics from the monolayer culture, I determined the levels of the following surface biomarkers: CD166, EpCAM, CD44, and CD133, all of which have been identified in colon and lung cancer stem cells [Walcher L., et al., 2020; Butler S. et al., 2017]. I conducted these experiments in both 2D and 3D cultures of HCT116 and A549 cells. Furthermore, I tested two previously selected UAs (C-2045 and C-2053), along with irinotecan and etoposide, for their ability to affect cancer stem cells in both culture conditions. The results of the flow cytometry analysis are presented in Figure 4.19.

In the HCT116 monolayer culture, the levels of all tested CSC markers were similar, ranging from 87 to 96%. In colon spheroids, the number of $CD166^+$ and $CD44^+$ cells was comparable to 2D, but for EpCAM and CD133, the number of positive cells was much lower than in adherent culture, at 80.4 and 56.6%, respectively (Figure 4.20.B). In A549 cells, high levels of only two of the CSC markers tested, CD166 and CD44, were observed. $CD166^+$ and $CD44^+$ cells accounted for about 92-96% of A549 cells, regardless of whether the cells were grown in 2D or 3D conditions. In the A549 monolayer culture, 5.1% of cells were CD133 positive, while in 3D, this fraction was even lower, reaching less than 1%. Notably, $EpCAM^+$ cells were not identified in either the 2D or 3D cultures of A549 cells and the percentage of cells expressing this marker was less than 1.5% in both cases (Figure 4.19.C).

Treatment of HCT116 cells with tested compounds resulted in a marked reduction in the number of cells with CSC markers in both culture systems. In the monolayer culture, incubation with UAs led to a decrease of $CD166^+$, $EpCAM^+$, and $CD44^+$ cells by about 15-20%, while $CD133^+$ cells were reduced to as little as 2.4 and 0.8% for C-2045 and C-2053, respectively. Meanwhile, after exposure of HCT116 cells in monolayer culture to irinotecan, the number of cells expressing CSC markers decreased to comparable levels for all four markers tested, and the number of positive cells after treatment was 67.1, 58.9, 63.1, and 50.6% for CD166, EpCAM, CD44, and CD133, respectively.

In the 3D culture of HCT116 following treatment with both UAs and IR, the reduction in the number of cells with CD166 and CD44 markers was less pronounced compared to the 2D. In contrast, a more substantial decrease in the proportion of EpCAM+ and CD133+ cells was noted after exposure to tested compounds in the HCT116-spheres than in monolayer culture. The number of EpCAM-positive cells in colon cancer spheroids reached approximately 55-60%, while CD133-positive cells were reduced to only less than 3% of all cells after treatment.

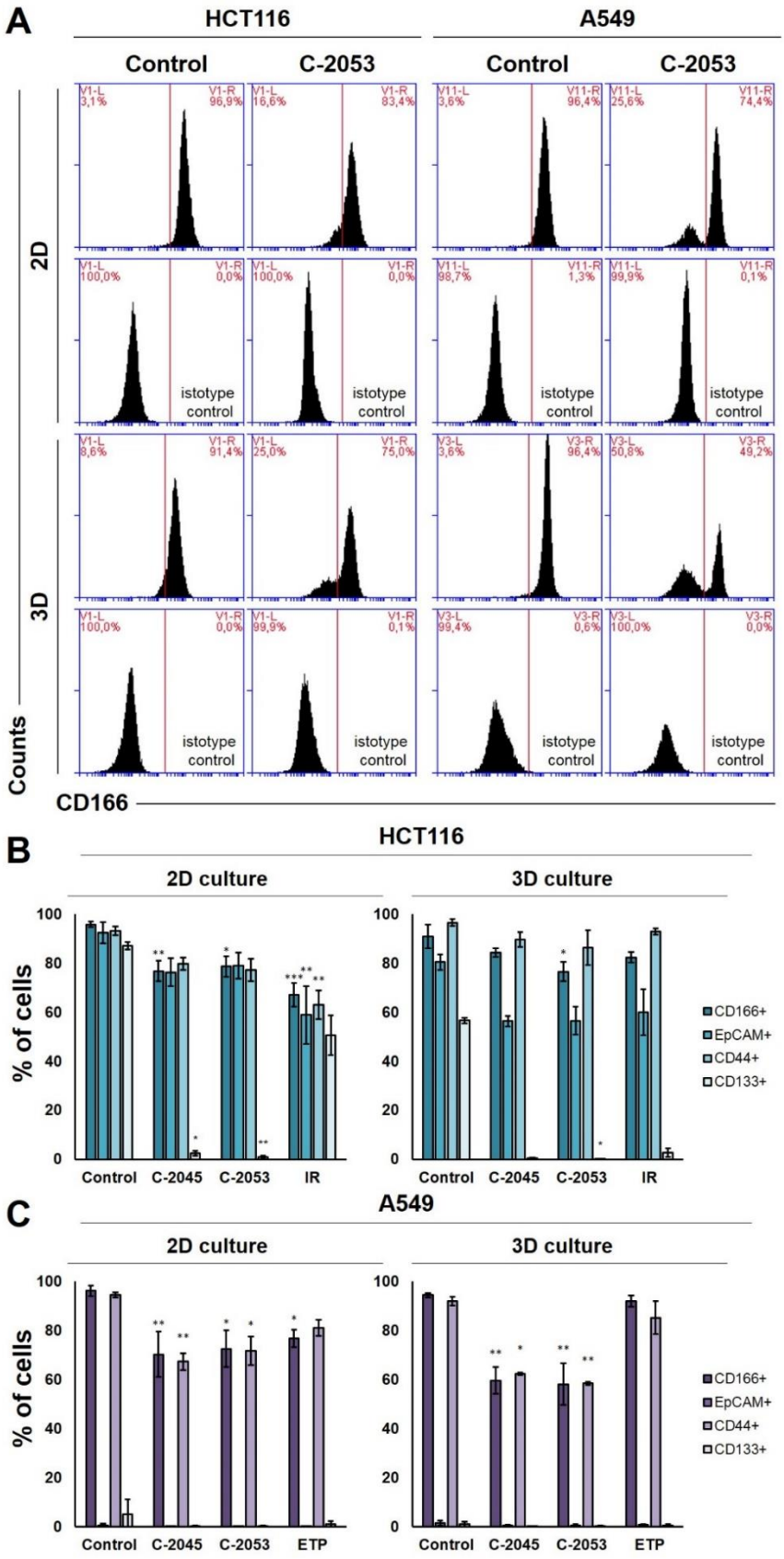

Figure 4.19. Levels of selected cancer stem cell markers in HCT116 colon and A549 lung cancer cells cultured in monolayer and as spheroids. Cells were treated with C-2045, C-2053, and reference compounds (IR/ETP) at concentrations corresponding to 5xIC_{90} doses (5xIC_{50} for IR/ETP) and then the levels of CD166, EpCAM, CD44, and CD133 positive cells were determined cytometrically. (**A**) Representative histograms of the level of CD166 in HCT116 (left) and A549 (right) cells treated with

C-2053 in 2D and 3D conditions (with isotype control). (**B, C**) Bar graphs presenting quantified data, expressed as the percentages of HCT116 (**B**) and A549 (**C**) $CD166^+$, $EpCAM^+$, $CD44^+$, and $CD133^+$ cells in 2D and 3D cell cultures. Data are presented as the means ± SD of three to seven independent experiments. Statistical analysis was performed using Dunn's nonparametric multiple comparisons test. Significantly different from control at: * $p < 0.05$, ** $p < 0.01$, *** $p < 0.001$. (n=3-7)

In A549 cells, a notable reduction in the number of CD166 and CD44-positive cells was observed in both 2D and 3D conditions following exposure to UAs. Although incubation with etoposide caused a 15-20% decrease in the percentage of cells with CSC markers in monolayer culture, the number of $CD166^+$ and $CD44^+$ cells in spheroids after treatment with this compound remained comparable to the control. In contrast, C-2045 and C-2053 exhibited a more pronounced effect in 3D than in 2D, and the cell number with both markers after exposure to UAs in A549 spheroids was about 60%, whereas in monolayer culture of this cell line, it was approximately 10% higher (about 70-73%).

5. DISCUSSION

For many years, one of the primary objectives in the fields of pharmacy and medicine has been to develop effective anticancer drugs with limited adverse effects. Additionally, there has been a significant effort to establish more accurate and predictable cellular models for testing drug sensitivity, while limiting the reliance on animal testing for the evaluation of the pharmacokinetic properties of studied compounds. Despite the fact that traditional methods based on 2D monolayer cell cultures remain the standard approach for the *in vitro* testing of new therapeutic agents since the 1950s, these models, while very useful in showing the biochemical and molecular effects of new compounds, exhibit notable limitations in recreating the complexity and pathophysiology of cancer tissues. Furthermore, adherent cultures cannot show the possibility and efficiency of a drug to penetrate the tumor and its possible action in the patients' tissues and body. Presently, much attention is directed towards designing improved *in vitro* models that can bridge the gap between outcomes in preclinical research and success in clinical trials. Three-dimensional (3D) cultures are becoming valuable tools in testing and identifying promising drug candidates. They are turning into indispensable research instruments in the realm of anticancer drug development, as they complement conventional 2D monolayer studies and reduce the need for unnecessary animal testing. Spheroids may serve as a tool for the negative selection of drugs that lose their efficacy in a 3D pathophysiological environment and conversely, have the potential to identify compounds that exhibit greater activity in 3D than in 2D [Costa E.C. et al., 2018; Friedrich J. et al., 2007; Friedrich J. et al., 2009; Zanoni M. et al., 2016].

As previously demonstrated in our laboratory, the selected derivatives of unsymmetrical bisacridines: C-2028, C-2041, C-2045, and C-2053 show high cytotoxic activity in monolayer culture against HCT116 colorectal cancer cells and H460 lung cancer cells. In this work, I presented that A549 lung cancer cells are also sensitive to UAs treatment and that all tested derivatives were able to inhibit cell proliferation at remarkably low concentrations (IC_{90} values ranged from 0.05 to 0.3 μM). In contrast, the reference compound (etoposide) demonstrated considerably lower cytotoxicity against A549 cells, with an IC_{50} dose of about 5.6 μM. Notably, the IC_{50} doses determined for the UAs did not exceed 0.06 μM, so they were approximately 100 times lower than for the reference compound. The IC_{50} dose established for ETP was comparable to the values reported by other researchers [Davou G.I. et al., 2019; Kanintronkul Y. et al., 2011] and similar to the IC_{50} for irinotecan in HCT116 cells (about 4.5 μM) and cisplatin in H460 (3.0 μM), both of which have been previously determined in our laboratory.

Initial investigations carried out by fellow researchers in our laboratory on HCT116 and H460 cells indicated that UAs induced apoptosis in these cells. Therefore, I performed further in-depth studies to prove that this is the main death pathway in these cells. Microscopic analysis of the changes in nuclei morphology showed that indeed apoptosis occurs in both cell lines after incubation with UAs (Figure 4.1). Following treatment with C-2028, C-2045, and C-2053, the number of cell nuclei exhibiting features characteristic of apoptosis (chromatin condensation, fragmentation of the nuclei, and presence of apoptotic bodies) was considerably higher in H460 cells than in HCT116. On the other hand, in the case of normal CCD 841 CoN and MRC-5 cells,

alterations in the morphology of the nuclei following 120 h of UAs exposure were evident only in a very small population of cells, which allows the conclusion that the tested compounds do not have a strong pro-apoptotic effect on these cell lines.

The decrease of mitochondrial transmembrane potential (Figure 4.2) along with the cleavage of PARP-1 protein (Figure 4.3) provided further confirmation that HCT116 cells are less sensitive to the pro-apoptotic effects of unsymmetrical bisacridines compared to H460 cells. Interestingly, in the case of the H460 cell line, the fraction of cells with cleaved PARP was lower than the number of cells with decreased $\Delta\Psi_m$. This can be explained by the fact, that the reduction in mitochondrial potential in apoptosis usually occurs prior to caspase activation. Caspase-mediated apoptosis is executed through the cleavage of key proteins required for cell proliferation, including PARP-1, which normally is engaged in routine DNA damage repair in response to cellular stressors [Chaitanya G.V. et al., 2010]. Additionally, an alternative rationale might be that the decrease in $\Delta\Psi_m$ has been observed not only in apoptotic but also in necrotic forms of cell death, thus not all cells exhibiting green fluorescence after JC-1 staining are necessarily apoptotic and some may indeed be undergoing necrosis [Kinnally K.W., 2011; Lemasters J.J. et al., 1998].

3D spheroids are widely used as a valuable tool in the development of novel anticancer drugs, because they closely mimic the main features of tumors *in vivo*, such as their structural organization and the presence of specific gradients [Nunes A.S., et al., 2018]. Therefore applying this culture method in my studies concerning unsymmetrical bisacridines seemed like a logical next step in the biological evaluation of these potential antitumor compounds. Besides the previously tested HCT116 and H460, I evaluated three additional cell lines: HT29 colon, DU 145 prostate, and A549 lung cancer cells for their ability to form spheroids. Out of these cell lines, three demonstrated the capability to generate functional multicellular tumor spheroids suitable for further experiments: HCT116, H460, and A549. According to the 2017 classification of 60 human cancer cell lines by Selby et al., spheroids were divided into four categories, based on their morphology and the degree of intercellular adhesion. Spheroids formed by HCT116 and A549 cells were classified into the first group, i.e., condensed spheroids - tight and round spheres with smooth and even edges. In turn, the H460 spheres were classified into the second group, i.e., non-condensed spheroids - generally rounded structures with a rougher perimeter [Selby M. et al., 2017]. The morphology of the spheroids I obtained from HCT116 and H460 cells was consistent with this classification and observations. While the periphery of A549 spheroids was not as smooth and defined as in HCT116-spheres, the shape of spheres remained predominantly circular. Conversely, the shape of H460 spheroids occasionally varied slightly from the ideal spherical form, unlike the consistently round profile of A549 and HCT116 spheroids.

The first step in evaluating a drug's influence on spherical cultures is the measurement of spheroids diameter after exposure to the compound with increasing time of incubation. Among the tested bisacridines, C-2028, C-2045, and C-2053, distinctly managed to inhibit the growth of HCT116, H460, and A549 spheroids (Figure 4.10, Figure 4.11, and Figure 4.12). Starting from the fourth day of incubation, these compounds caused a gradual and continuous reduction of the

diameter of spheroids derived from both HCT116 and A549 cells. Importantly, HCT116 spheroids following treatment with C-2053 became even smaller than their initial size before the addition of the UAs. This observation highlights the usefulness of 3D multicellular tumor spheroids as valuable tools for exploring the effects of potential anticancer drugs, especially those that may require extended exposure times to induce biological responses in cells. In colon cancer cells, a substantial reduction in spheroid size occurred after 10 days of incubation with C-2053. Such prolonged incubation time would not be possible in traditional monolayer cultures, due to the limitations related to the surface of the culture dish, cell doubling time, and the amount of culture medium. The slower cell growth in 3D models, in contrast to 2D, makes longer incubation time experiments possible and enables the evaluation of slower-acting anticancer agents.

In A549-spheres, a reduction of spheroids diameter below their initial sizes was observed after incubation with C-2028, C-2045, and C-2053. Noteworthy, in this case, the decrease in spheroid dimensions occurred much sooner – C-2045 and C-2053 managed to reduce A549 spheroid sizes below their baseline measurements already on day 4 after drug exposure, while C-2028 achieved this outcome by day 7. For H460-spheres, exposure to C-2028, C-2045, and C-2053 also led to a decrease in size over time, however, with extended incubation periods, the spheroids either maintained their size or even began to grow again.

Among the tested UAs, the C-2041 derivative exhibited the least prominent inhibitory effect on spheroid growth across all three cell lines. Notably, when A549-spheres were incubated with this compound, their growth pattern closely resembled that observed for the control. In HCT116 and H460 spheroids, while treatment with this derivative did result in an inhibition of spheroid growth, it was notably the least pronounced among all tested compounds.

Regarding the reference compounds, in HCT116-spheres, irinotecan proved slightly more effective in inhibiting spheroid growth compared to the UAs tested. In contrast, when considering spheroids derived from H460 and A549 cells, C-2028, C-2045, and C-2053 exhibited a notably greater reduction in spheroid size compared to the reference compounds used for these cell lines: cisplatin for H460 and etoposide for A549.

Assessing the viability of cells in control spheroids revealed, that H460 spheres consisted of a very high amount of dead cells - 3 days after the generation of spheroids only 52% of the cells remained viable, while at the same time, HCT116 and A549 spheres contained about 90% alive cells. The high content of dead cells in H460 spheres may result from their heightened sensitivity to hypoxic conditions and subsequent induction of cell death. Thus, I did not continue the studies concerning the cellular response to treatment with UAs for this cell line, and in further experiments, I focused on HCT116 and A549 cells cultured in 2D and 3D conditions.

Analysis of the influence of UAs on the viability of HCT116 and A549 cells in 2D and 3D cultures showed that the four UA derivatives behaved differently in spheroids compared to monolayers. Both models of cell culture differed significantly in the number of viable cells after UAs treatment. Earlier experiments carried out on the 2D monolayer culture of HCT116 cells (Figure 4.1, 4.2) together with the analysis of the effect of UAs on the cell viability in 2D culture performed parallel to 3D conditions (Figure 4.15 - left panel) pointed that C-2041 should be the

derivative with the strongest impact on HCT116 cell viability. However, 7-AAD staining of cells cultured as spheroids revealed that in MCTS, this compound was the least potent, and even when the time of treatment with 5xIC_{90} dose of UAs was extended to 7 days, C-2041 derivative induced death in only 32.5% of HCT116 cells. At the same time, after exposure to other UAs, at least 95% of cells were non-viable, which was slightly higher than the effect observed for reference compound - irinotecan (88.4%). Also in the case of A549 cells, the C-2041 derivative had the least pronounced effect on cell viability. However, this trend for A549 was observed even in the 2D monolayer conditions and remained unchanged in the 3D context.

When considering the same incubation times and doses, it is evident that in most cases, the population of 7-AAD^+ (dead) cells was higher in monolayer culture compared to spheroids after drug exposure (Figure 5.1.A and 5.2.A left panel). This is an expected observation, due to distinct characteristics of 3D cultures that affect their susceptibility to drug treatment. Nonetheless, it is worth noting that this pattern was not consistent for every compound across all conditions. For instance, when HCT116 cells were treated for 3 days with C-2045 derivative at 5xIC_{90} dose, cell death was induced in a significantly ($p<0.01$) larger population of cells in 3D spherical culture (44,9%) than in 2D monolayer (27%) (Figure 5.1.A. right panel). Similarly, in A549 cells, a slightly higher fraction of dead cells was observed after incubation with C-2045 and C-2053 in the 3D culture than in the 2D, though this discrepancy was less pronounced in this case (Figure 5.2.A. right panel).

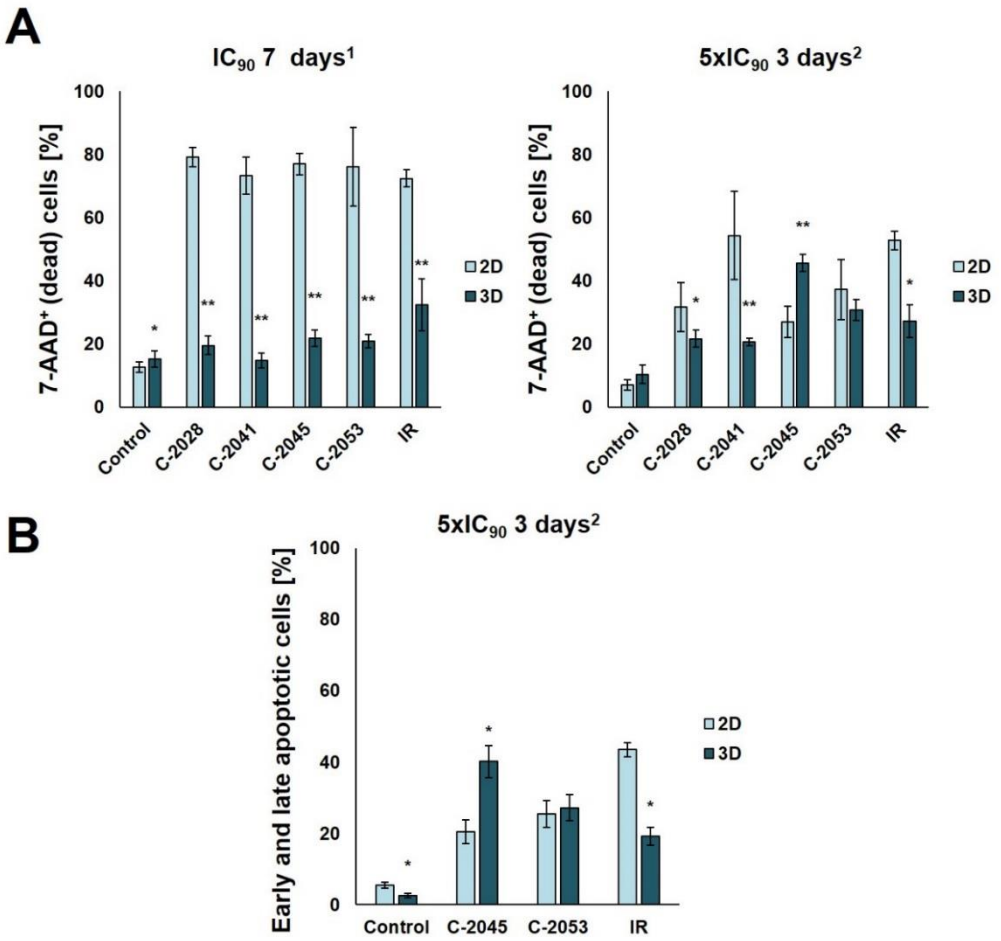

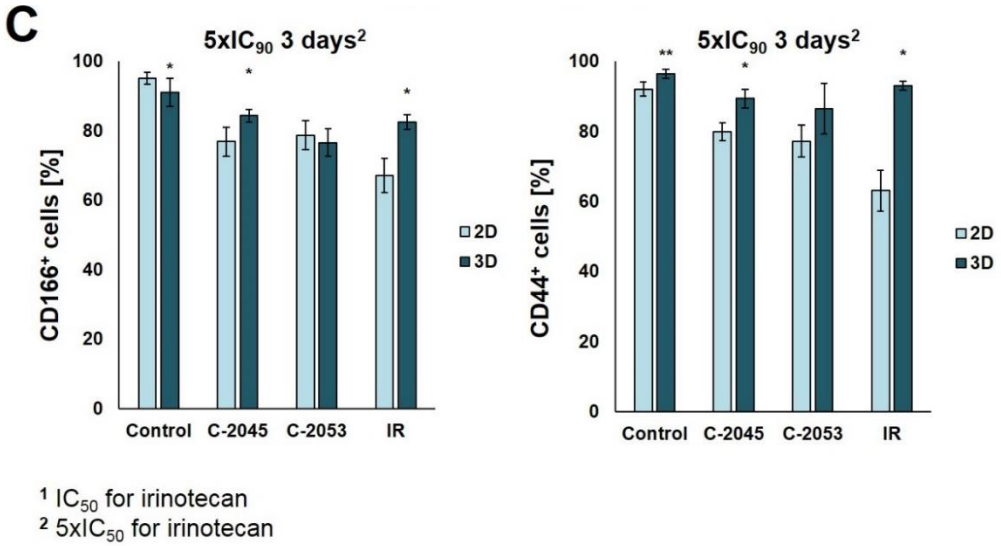

Figure 5.1. Comparison of the effects of UAs and irinotecan on HCT116 cells cultured in monolayer (2D) and spherical (3D) cultures. (**A**) The number of dead HCT116 cells in 2D and 3D after treatment with UAs and irinotecan under the indicated conditions. (**B**) The number of early and late apoptotic cells (annexin V-positive) in both monolayer and spherical cultures after incubation with C-2045, C-2053, and irinotecan at $5xIC_{90}$ doses ($5xIC_{50}$ for IR) for 3 days. (**C**) The number of $CD166^-$ (left) and $CD44^-$ (right) cells in 2D and 3D following treatment with C-2045, C-2053, and IR at $5xIC_{90}$ doses ($5xIC_{50}$ for IR) for 3 days. Data are presented as the means ± SD of three to eight independent experiments. 2D vs. 3D comparisons between the controls and for each compound were performed using the Mann-Whitney U test. Significantly different from control at: * $p < 0.05$, ** $p < 0.01$, *** $p < 0.001$. (n=3-8)

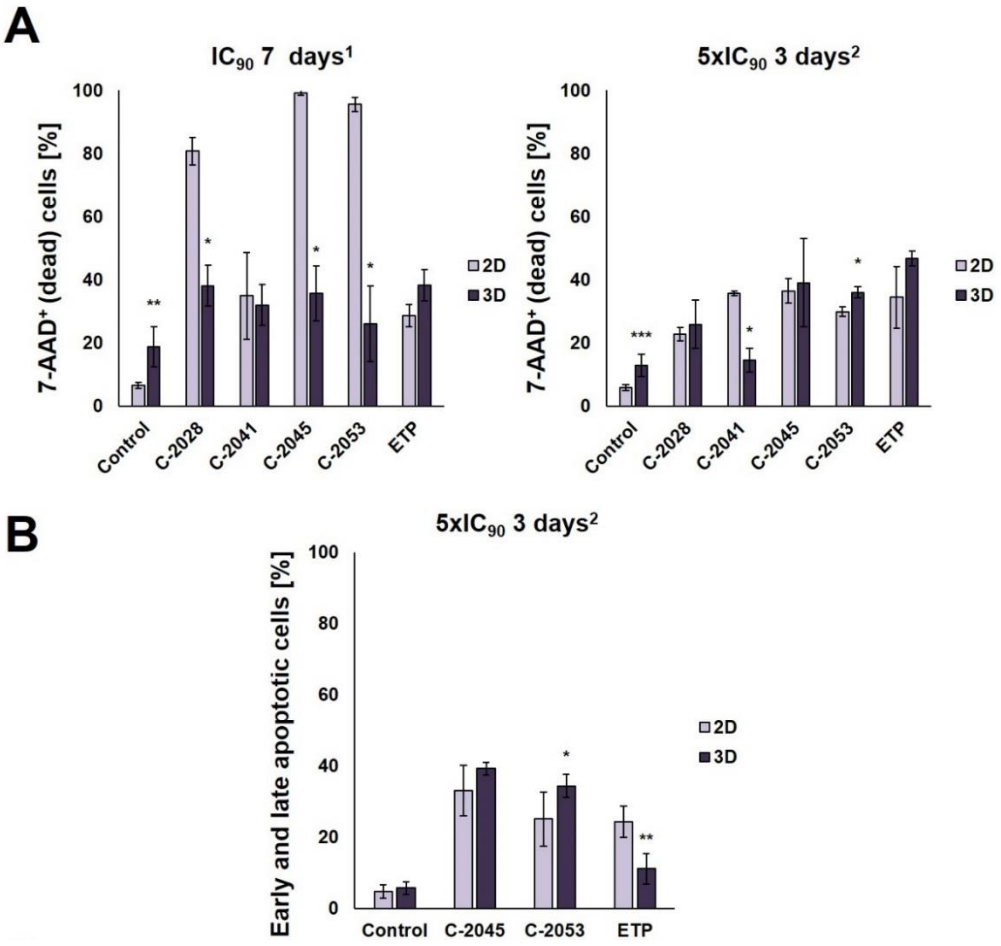

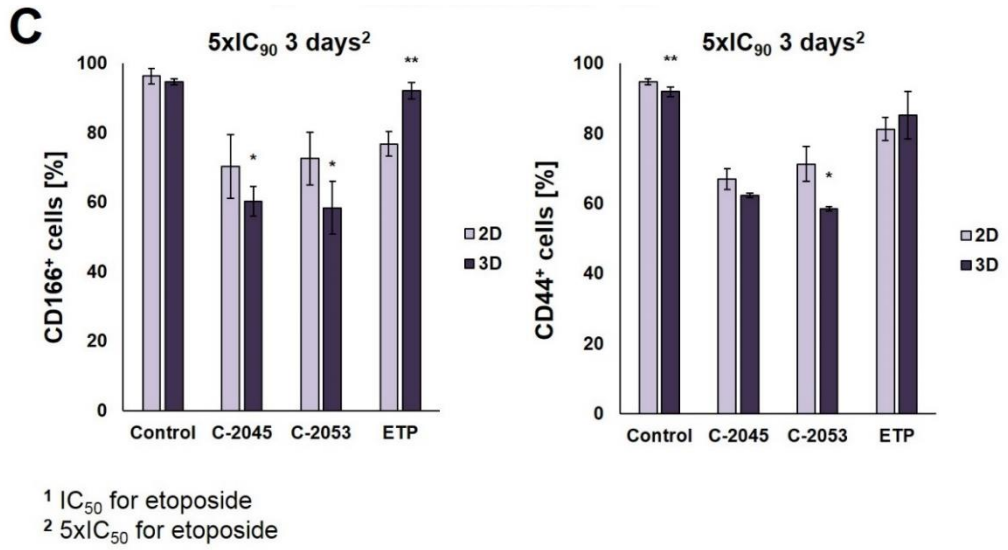

[1] IC_{50} for etoposide
[2] $5xIC_{50}$ for etoposide

Figure 5.2. Comparison of the effects of UAs and etoposide on A549 cells cultured in monolayer (2D) and spherical (3D) cultures. (**A**) The number of dead A549 cells in 2D and 3D after treatment with UAs and etoposide under the indicated conditions. (**B**) The number of early and late apoptotic cells (annexin V-positive) in both monolayer and spherical cultures after incubation with C-2045, C-2053, and etoposide at $5xIC_{90}$ doses ($5xIC_{50}$ for ETP) for 3 days. (**C**) The number of $CD166^-$ (left) and $CD44^-$ (right) cells in 2D and 3D following treatment with C-2045, C-2053, and ETP at $5xIC_{90}$ doses ($5xIC_{50}$ for ETP) for 3 days. Data are presented as the means ± SD of three to eight independent experiments. 2D vs. 3D comparisons between the controls and for each compound were performed using the Mann-Whitney U test. Significantly different from control at: * $p < 0.05$, ** $p < 0.01$, *** $p < 0.001$. (n=3-7)

The colony formation assay and the spherogenic potential assessment were performed to establish the ability of studied cells to self-renew after treatment with UAs and reference compounds. While the colony formation assay clearly demonstrated that all UAs, with the exception of C-2041, induced complete arrest of cell proliferation after only 24 h of incubation, the results from the spherogenic potential assay presented a more complex interpretation challenge. This experiment was conducted additionally, as an extension of the colony formation assay, which was performed solely with 2D cultures, in order to provide further information on the cells' capacity for self-renewal and their ability to generate spherical cultures following treatment with the studied compounds. Interestingly, although both cell lines were capable of forming spheroids, the secondary spheres after dissociation of primary A549 control spheroids did not regenerate after 3 days, suggesting, that during disaggregation into a single-cell suspension, certain changes occurred in A549 cells, which affected their spherogenic potential. The ability of cells to form spheroids is influenced by several factors, such as cell type, culture conditions, and the presence of growth factors and other signaling molecules. Since cell type and culture conditions did not change compared to spheres obtained from 2D cultures, it appears that some alterations happened in the levels of growth factors or adhesion proteins, which made it impossible for A549 cells to form secondary spheres.

Analysis of the spherogenic potential of HCT116 and A549 cells following treatment with UAs in 2D and 3D conditions, showed that generally, spherical cultures were less affected by tested compounds than their monolayer correspondents, as a greater capacity to recreate spheres was observed in secondary sphere formation compared to spheres obtained after UAs exposure in monolayer. However, it is worth noticing that C-2053 was the most potent derivative

in both culture conditions, and A549 cells did not form spheroids after incubation with this derivative in both 2D and 3D, while HCT116 spheres generated after exposure to this compound were the smallest and did not grow in time (2D) or grew to the least extent (3D). In contrast, the secondary spheres regenerated after treatment with irinotecan and etoposide grew in time and in the case of HCT116 spheres, after 14 days they reached sizes similar to the control (780 µm after treatment with IR vs 834 µm for the control). The least pronounced impact on the spherogenicity of both cell lines was observed after treatment with the C-2041 derivative, both in the case of primary and secondary spheres. This compound has repeatedly proven to be the least potent UA derivative, which may be connected to its distinct structure compared to the other three compounds (Figure 1.1) – a different aminoalkyl linker between two monoacridine units, from which UAs consist [Paluszkiewicz E. et al., 2020]. This difference in structure might influence the cellular uptake of C-2041, as well as its ability to penetrate deeper layers of spheroids.

Comparing results from different studies is very complicated due to the differences in a variety of factors, such as the type of 3D culture applied, the method used for spheroid generation and analysis, the source of the tumor cells, their passage number, the density of cells seeded, spheroid size and the incubation times [Ishiguro T.S. et al., 2017]. Regardless, most research performed on 3D cultures shows, that spheroids are a more resistant platform to therapeutic agents, and many compounds have markedly reduced efficacy in the 3D environment compared to 2D [Olejniczak-Kęder A. et al., 2019; Karlsson H., et al., 2012; Breslin S. and O'Driscoll S., 2016]. The differences in drug response between monolayer and spherical cultures may be caused by a multitude of factors, including variations in drug penetration, the presence of drug gradients, alterations in gene expression, increased survival signaling, DNA repair mechanisms, pH shifts, and the involvement of transporters associated with drug resistance. Additionally, these differences might also result from the mechanism of action of the drug itself. For instance, drugs that require active cell division for their efficacy, like 5-FU, have been proven to display higher performance in 2D cultures, as compared to 3D [Zoetmelk M. et al., 2018]. However, there are also reports that certain drugs, which are not necessarily very potent in 2D cultures, manifest their effects only in 3D. This has been observed in some cases where the molecular target is expressed only or especially in a three-dimensional environment [Friedrich J. et al., 2009].

The determination of cell viability after treatment with UAs has brought to light the very promising potential of C-2045 and C-2053 derivatives in both culture models of HCT116 and A549 cells. It is noteworthy that these compounds retained their efficacy or were even more potent in spherical cultures, as was observed when applied at a $5xIC_{90}$ dose for 3 days (Figure 5.1.A and 5.2.A). Thus, based on these findings and observations made from other experiments (morphology and size analysis, colony formation assay, and spherogenic potential assessment), in further studies, I have focused on these two UA derivatives and the reference compounds – irinotecan and etoposide.

The annexin V/PI double staining that I have performed after treatment of studied cells cultured in 2D and 3D with $5xIC_{90}$ doses of C-2045, C-2053, and $5xIC_{50}$ doses of reference

compounds confirmed the results from the cell viability assessment, showing that these two selected UA derivatives retained their activity in a 3D environment, or even proved more potent in this culture system than in a monolayer (Figure 5.1.B and 5.2.B). Most notably, both reference compounds induced apoptosis to a much smaller extent in 3D than 2D, with irinotecan losing more than half of its proapoptotic activity observed in monolayer when applied in spheroids. It is worth mentioning that, in general, in the 2D culture a predominance of late apoptotic cells was observed, while in spheroids, most cells were still in the early stages of apoptosis, which suggests that due to the compact and dense nature of the spherical cultures, along with their large volume, cell exposure to the compounds is limited and drug penetration into the deep layers of the cells is hindered. Therefore, the effect induced by the studied compounds may be delayed compared to the monolayer, where all cells are evenly exposed to an equal concentration of the drug simultaneously. Nevertheless, the fact that C-2045 and C-2053 remained potent in cell death induction in spherical cultures highlights their promising therapeutic efficacy, which was clearly evident even in the initial evaluation of UAs influence on spherical cultures through the measurement of spheroids diameter after exposure to the compound with increasing time of incubation, where in both cell lines, C-2045 and C-2053 derivatives proved to be the most potent UA derivatives and caused the most substantial reduction of spheroids diameters.

The use of spherical cultures has been found to be a more suitable method for analyzing cancer stem cells (CSCs) than monolayer. Thus, spheroids provide an appropriate model for testing new antitumor therapeutics, especially those targeting CSCs [Olejniczak A. et al., 2018]. In my work, one of my aims was to compare the levels of CSC markers in adherent and spherical cultures of HCT116 and A549 cells and assess the impact of studied compounds on this population of cells, as to determine the utility of multicellular tumor spheroids that I have obtained in research regarding CSCs. The selection of adequate CSC markers is a critical and challenging step in determining the proportion of CSC-like cells in a studied population since none of the known markers are universal and entirely reliable [Szaryńska M. et al., 2018]. Therefore in addition to the frequently used CD133 marker, which has proven to be rather controversial [Shmelkov S. et al., 2008; Lottaz C. et al., 2010, Zheng X., et al., 2007; Meng X. et al., 2009], I chose three more proteins: CD44, CD166, and EpCAM, for CSC identification in my studies. These markers have been reported to be present in lung and colon cancer cells [Walcher L., et al., 2020, Butler S. et al., 2017]. In my experiments, the levels of all selected markers observed in both HCT116 cell culture systems were relatively high and similar to those reported by other researchers [Butler S. et al., 2017; Olejniczak A. et al., 2018; Chen K.L. et al., 2011; Su Y.J. et al., 2011]. On the other hand, in A549, neither the monolayer nor the spherical model presented a significantly high fraction of $EpCAM^+$ and $CD133^+$ cells. The literature presents widely divergent data regarding EpCAM expression in A549 cells. For instance, Baharuddin et al. [Baharuddin P. et al, 2016], reported that A549 $EpCAM^+$ cells account for about 5% of all cells in monolayer culture, while Karimi-Busheri et al. [Karimi-Busheri F. et al., 2013] reported 34%. In contrast, Breuninger et al. [Breuninger S. et al., 2018] showed 96% of A549 cells to be EpCAM-positive, similar to Liao et al [Liao Z.J. et al., 2014], who stated that almost 100% of cells possess this

marker. On the other hand, although CD133 has been listed as a potential marker for CSCs in lung cancer cells, its reported level in A549 cells in most cases was very low, not exceeding 2% (Roudi R. et al., 2014; Liu J. et al., 2014; Meng X. et al., 2009; Tirino V. et al., 2009; Zhang H. et al., 2013], which was comparable with my results. Thus, determining the levels of several different markers seems to be a useful initial step for any CSC-related investigations. While in monolayer and spherical culture of A549 cells, the difference in the fraction of cells with CD166 and CD44 markers was not profound (96.2% of $CD166^+$ cells in 2D vs 94.4% in 3D and 94.6% of $CD44^+$ cells in 2D vs 91.9% in 3D), and in HCT116 these two markers were also quite similar in both culture conditions (95.8% of $CD166^+$ cells in 2D vs 90.9% in 3D and 93.2% of $CD44^+$ cells in 2D vs 96.6% in 3D), for EpCAM and CD133 there was a much more pronounced discrepancy: 92.4% of $EpCAM^+$ HCT116 cells in 2D vs 80.4% in 3D and 87.1% of $CD133^+$ cells in 2D vs 56.6% in 3D. Therefore, it is impossible to state unequivocally whether the 3D MCTS model I applied in my research differs significantly in CSCs content from the monolayer, as this clearly depends on the specific markers that are determined. Nonetheless, I can make several important observations regarding the difference in response to treatment with the studied compounds in both culture models. When analyzing two of the markers tested, CD166 and CD44, I found that in HCT116, the fraction of cells with these markers after treatment with UAs and irinotecan was lower in 2D than in 3D, indicating that the compounds lose some of their effect on CSCs when applied in spherical cultures (Figure 5.1.C). However, it is worth highlighting, that in A549 a more pronounced effect in decreasing the number of $CD166^+$ and $CD44^+$ cells was observed in spheroids (Figure 5.2.C), where the fraction of cells with these markers was about 10% lower than in the adherent model after treatment with C-2045 and C-2053. Importantly, the opposite observation was made in the case of etoposide, which already in monolayer culture had a weaker effect on CSCs than our selected UAs, and turned out to be even less potent when applied in spheroids. Thus, C-2045 and C-2053 exhibit promising effects on lung cancer cells with stem cell characteristics, especially given their enhanced efficacy in 3D.

It has been observed lately that the localization of UAs in cells is pH-dependent and an increased concentration of these compounds in organelles characterized by lower pH was detected [Pilch J. et al., 2023]. This, along with the profound influence of pH on UAs' protonation state, self-association ratio, and solubility [Kosno M. et al., 2022], may provide some insight into why some of these compounds exhibit even more promising results in 3D spheroids, which are characterized by a specific pH gradient similar to that observed *in vivo*. At physiological pH (between 6 and 8) there are two or three individual protonation forms of UAs, each of which can potentially affect the cellular processes at the molecular level differently [Kosno M. et al., 2022]. Thus, the specific form (or forms) of UA compounds that are present in spheroids may differ from that in monolayer cultures, where pH does not vary.

To sum up, my research has confirmed the potential of unsymmetrical bisacridines as promising candidates for anticancer therapy, displaying their remarkable efficacy in both 2D and 3D environments. These compounds exhibited their ability to induce apoptosis in colon and lung cancer cells, which I proved by analyzing the morphology of cell nuclei, cytometric analysis

of mitochondrial membrane potential, and cells with cleaved PARP-1 protein. Moreover, I demonstrated that UAs inhibited the growth of HCT116, H460, and A549 spheroids and influenced the viability of HCT116 and A549 cells in both culture conditions. I showed that incubation with UAs reduced the spherogenic potential of HCT116 and A549 cells, and in the case of C-2045 and C-2053 derivatives, the cells tested were either unable to form spheroids after treatment with these compounds in both 2D and 3D conditions, or the spheres generated did not grow over time. Moreover, these promising compounds also induced apoptosis in HCT116- and A549-spheres, with a similar or even higher percentage of cells being affected than in the adherent model. Most importantly, in both cell lines, C-2045 and C-2053 considerably affected the cancer stem cell-like population, with the effect being even more pronounced in A549 spheroids than in monolayer culture.

Thus, my work sheds more light on the mechanism of action of UAs in HCT116 and A549 cells cultured in 2D and 3D conditions, with additional relation to the cancer stem cells, and provides a foundation for future application of these promising compounds in anticancer therapy. Additionally, my research highlights the value of multicellular tumor spheroids and the relevance of their application in the evaluation of novel chemotherapeutic agents. This model is particularly promising, especially given that I have demonstrated its potential to provide initial insight into the effects of the studied compounds on the cancer stem cell population, which is a challenging target in the field of anticancer therapy.

6. CONCLUSIONS

The field of anticancer drug development has long sought to create effective treatments with minimal adverse effects. At the same time, the drive to establish better cellular models for drug testing, reducing reliance on animal studies, has become a priority. While traditional 2D monolayer cell cultures have been the standard for *in vitro* drug testing for decades, their limitations in replicating the complexity of tumor tissues have led researchers to focus on improving *in vitro* models that better represent clinical outcomes. This resulted in the emergence of three-dimensional (3D) cultures as invaluable tools in anticancer drug development. Multicellular tumor spheroids, the most widely employed 3D spherical cultures, bridge the gap between preclinical research and clinical trials, presenting a more accurate representation of tumors *in vivo*.

In my research, I investigated the potential of unsymmetrical bisacridines (UAs) as novel anticancer agents. Although I started with monolayer cultures, in my work I moved beyond this traditional 2D model, venturing into 3D multicellular tumor spheroids (MCTS) to evaluate the compounds' efficacy in a more *in vivo*-like setting. The transition to the 3D culture model was motivated by the desire to better replicate the tumor environment and to identify potential agents among studied UAs that perform well in this context.

My key findings presented in this doctoral thesis are listed below:

- The primary cellular response observed after treatment of HCT116 colon and H460 lung cancer cells with unsymmetrical bisacridines is apoptosis, which is notably more pronounced in H460 cells than in HCT116,
- It was possible to successfully generate functional spheroids with various morphometric features from three cancer cell lines: HCT116 colon, and H460 and A549 lung cancer cells,
- Following incubation of spheroids with UAs (C-2028, C-2041, C-2045, and C-2053), and reference compounds (irinotecan, cisplatin, and etoposide), a considerable inhibition in spheroid growth was observed. In some cases, the spheres after treatment were smaller than their initial sizes (HCT116 treated with C-2053 and irinotecan, A549 treated with C-2028, C-2045, and C-2053),
- The analysis of cell viability in 2D and 3D showed that two cell lines (HCT116 and A549) presented high fractions of alive cells in both culture models (around 90%), while H460-spheres consisted of nearly 50% dead cells. Thus, further experiments focused on HCT116 and A549 cells,
- The viability of HCT116 and A549 cells was considerably affected by UAs in both 2D and 3D, and under the same conditions, the number of dead cells was generally higher in 2D than 3D, which may be related to various factors, such as for example distinct penetration of compounds in MCTS compared to adherent cultures,

- In some cases, however, UAs retained their efficacy when applied to spheroids, or even proved more active (after a 3-day treatment with C-2045 and C-2053 compounds at 5xIC_{90} doses), which may result from the existence of specific gradients in MCTS (such as oxygen, pH), absent in monolayer cultures,
- C-2028, C-2045, and C-2053 completely blocked the proliferation of HCT116 and A549 cells already after 24h. Following treatment with C-2041, some cells underwent mitosis even after 120h of exposure,
- Incubation with UAs reduced the spherogenic potential of HCT116 and A549 cells in both culture conditions, but a greater capacity to recreate spheroids was observed after exposure of cells to the compounds in 3D than in 2D,
- The C-2053 derivative managed to stop the spherogenicity of A549 cells in both 2D and 3D conditions, while in HCT116, the spheres regenerated after treatment with this compound were the smallest and did not grow over time,
- The C-2045 and C-2053 derivatives retained their proapoptotic activity when applied in 3D, or even proved more potent than in 2D (C-2045 in HCT116 and C-2053 in A549),
- Both reference compounds (irinotecan for HCT116 and etoposide for A549 cells) induced apoptosis to a much smaller extent in spheroids than in monolayer,
- The fraction of HCT116 cells with cancer stem cell-like markers after treatment with C-2045, C-2053, and IR was lower in 2D than in 3D, indicating that UAs and IR might lose some of their effect on the CSC population when applied in spheroids compared to monolayer,
- In A549 cells, a more pronounced effect on cells with CSC-like markers after UAs treatment was observed in spheroids compared to monolayer, suggesting that these compounds might have the potential to affect CSCs *in vivo*. Etoposide had little influence on the CSC-like population in 2D and was even less effective in 3D.

Thus, the main conclusions from my thesis are as follows:

- The multicellular tumor spheroids (MCTS) derived from HCT116 and A549 cells are a good tool for the evaluation of antitumor properties of unsymmetrical bisacridines,
- Given that the 2D and 3D cell culture models of HCT116 and A549 cells differed in the intensity of observed cellular response after UAs treatment, it is important to test potential antitumor drugs in both monolayer and spherical cultures to identify the compounds with better distribution and effectiveness under conditions similar to *in vivo*,
- Among the tested unsymmetrical bisacridines, C-2045 and C-2053 derivatives demonstrate the most pronounced effect on colon and lung cancer cells, particularly evident in the context of spherical cultures. Conversely, C-2041, despite showing promise in 2D, turned out to be the least potent derivative in spheroids,

- The increased efficacy of certain UA derivatives (C-2045, C-2053) in 3D compared to 2D may be connected with specific gradients present in MCTS (pH, oxygen), which might affect the forms in which UAs are present in this culture model,
- The efficacy of UAs against cancer stem cell-like population indicates that these compounds might target cancer stem cells (CSCs) – a subset of cells implicated in drug resistance and tumor recurrence,
- The MCTS of HCT116 and A549 cells have the potential to provide preliminary insight into the influence of UAs on CSCs.

7. BIBLIOGRAPHY

Akbarzadeh, M.; Maroufi, N.F.; Tazehkand, A.P. *et al.* Current approaches in identification and isolation of cancer stem cells. *J Cell Physiol.* **2019**, *234*, 14759-14772. doi: 10.1002/jcp.28271.

Al-Hajj, M.; Wicha, M.S.; Benito-Hernandez, A.; Morrison, S.J.; Clarke, M.F. Prospective identification of tumorigenic breast cancer cells. *Proc Natl Acad Sci U S A*. **2003**, *100*, 3983-3988. doi: 10.1073/pnas.0530291100.

Amaral, R.L.F.; Miranda, M.; Marcato, P.D.; Swiech, K. Comparative analysis of 3D bladder tumor spheroids obtained by forced floating and hanging drop methods for drug screening. *Front. Physiol.* **2017**, *8*, 605. doi: 10.3389/fphys.2017.00605

American Cancer Society: Global cancer facts & figures 4th edition. Atlanta **2018**

Baharuddin, P.; Satar, N.; Fakiruddin, K.S. *et al.* Curcumin improves the efficacy of cisplatin by targeting cancer stem-like cells through p21 and cyclin D1-mediated tumour cell inhibition in non-small cell lung cancer cell lines. *Oncol Rep.* **2016**, *35***,** 13-25. doi: 10.3892/or.2015.4371.

Bielecka, Z.F.; Maliszewska-Olejniczak, K.; Safir, I.J.; Szczylik, C.; Czarnecka, A.M. Three-dimensional cell culture model utilization in cancer stem cell research. *Biol Rev Camb Philos Soc.* **2017**, *92*, 1505-1520. doi: 10.1111/brv.12293.

Borowa-Mazgaj, B. Odpowiedź komórkowa indukowana przez przeciwnowotworową pochodną akrydyny C-1748 w komórkach raka trzustki. Rola ekspresji enzymów metabolizujących w modulacji tej odpowiedzi. *Doctoral dissertation. Chemical Department PG*, **2016**

Botchkina, G.I.; Zuniga, E.S.; Das, M.; Wang, Y.; Wang, H.; Zhu, S.; Savitt, A.G.; Rowehl, R.A.; Leyfman, Y.; Ju, J.; Shroyer, K.; Ojima, I. New-generation taxoid SB-T-1214 inhibits stem cell-related gene expression in 3D cancer spheroids induced by purified colon tumor-initiating cells. *Mol Cancer*. **2010**, *9*, 192. doi: 10.1186/1476-4598-9-192.

Breslin S, O'Driscoll L. The relevance of using 3D cell cultures, in addition to 2D monolayer cultures, when evaluating breast cancer drug sensitivity and resistance. *Oncotarget.* **2016**, *7*, 45745-45756. doi: 10.18632/oncotarget.9935.

Breslin, S.; O'Driscoll, L. Three dimensional cell culture: the missing link in drug discovery. *Drug Discov. Today* **2013**, *18*, 240-249. doi: 10.1016/j.drudis.2012.10.003.

Breuninger, S.; Stangl, S.; Werner, C. *et al.* Membrane Hsp70 - a novel target for the isolation of circulating tumor cells after epithelial-to-mesenchymal transition. *Front Oncol*. **2018**, *8***,** 497. doi: 10.3389/fonc.2018.00497.

Butler, S.J.; Richardson, L.; Farias, N.; Morrison, J.; Coomber, B.L. Characterization of cancer stem cell drug resistance in the human colorectal cancer cell lines HCT116 and SW480. *Biochem Biophys Res Commun.* **2017**, *490*, 29-35. doi: 10.1016/j.bbrc.2017.05.176.

Calvet, C.Y.; André, F.M.; Mir, L.M. The culture of cancer cell lines as tumorspheres does not systematically result in cancer stem cell enrichment. *PLoS One.* **2014**, *9*, e89644. doi: 10.1371/journal.pone.0089644.

Chaicharoenaudomrung, N.; Kunhorm, P.; Noisa, P. Three-dimensional cell culture systems as an *in vitro* platform for cancer and stem cell modeling. *World J Stem Cells.* **2019**, *11*, 1065-1083. doi: 10.4252/wjsc.v11.i12.1065.

Chaitanya, G.V.; Steven, A.J.; Babu, P.P. PARP-1 cleavage fragments: signatures of cell-death proteases in neurodegeneration. *Cell Commun Signal*. **2010**, *8*, 31. doi: 10.1186/1478-811X-8-31.

Chen, K.L.; Pan, F.; Jiang, H.; Chen, J.F.; Pei, L.; Xie, F.W.; Liang, H.J. Highly enriched CD133(+)CD44(+) stem-like cells with CD133(+)CD44(high) metastatic subset in HCT116 colon cancer cells. *Clin Exp Metastasis* **2011**, *28*, 751-763. doi: 10.1007/s10585-011-9407-7.

Chen, L.S.; Wang, A.X.; Dong, B.; Pu, K.F.; Yuan, L.H.; Zhu, Y.M. A new prospect in cancer therapy: targeting cancer stem cells to eradicate cancer. *Chin J Cancer*. **2012**, *31*, 564-572. doi: 10.5732/cjc.011.10444.

Collins, A.T.; Berry, P.A.; Hyde, C.; Stower, M.J.; Maitland, N.J. Prospective identification of tumorigenic prostate cancer stem cells. *Cancer Res.* **2005**, *65*, 10946-10951. doi: 10.1158/0008-5472.

Comley, J. Spheroids rapidly becoming a preferred 3D culture format. *Drug Discov. World* **2017**, *Spring,* 31-49

Correia, C.; Weiskittel, T.M.; Ung, C.Y. *et al.* Uncovering Pharmacological Opportunities for Cancer Stem Cells-A Systems Biology View. *Front Cell Dev Biol.* **2022**, *10*, 752326. doi: 10.3389/fcell.2022.752326.

Costa, E.C.; de Melo-Diogo, D.; Moreira, A.F.; Carvalho, M.P.; Correia, I.J. Spheroids formation on non-adhesive surfaces by liquid overlay technique: Considerations and practical approaches. *Biotechnol J.* **2018**, *13*, 1700417. doi: 10.1002/biot.201700417.

Costa, E.C.; Moreira, A.F.; de Melo-Diogo, D.; Gaspar, V.M.; Cavalho, M.P.; Correia, I.J. 3D tumor spheroids: an overview on the tools and techniques used for their analysis. *Biotechnol. Adv.* **2016**, *34*, 1427-1441. doi: 10.1016/j.biotechadv.2016.11.002.

Davou, G.I.; Chuwang, N.J.; Essien, U.C.; Choji, T.P.P.; Echeonwu, B.C.; Lugos, M.D. Cytotoxicity analysis of etoposide and cisplatin on cell lines from human lung cancer and normal human lung *Int. Res. J. Med. Med. Sci.* **2019**, *7*, 40-47. doi: 10.30918/IRJMMS.72.19.022.

Dhiman, N.; Shagaghi, N.; Bhave, M.; Sumer, H.; Kingshott, P.; Rath, S.N. Selective Cytotoxicity of a Novel Trp-Rich Peptide against Lung Tumor Spheroids Encapsulated inside a 3D Microfluidic Device. *Adv Biosyst*. **2020**, *4*, e1900285. doi: 10.1002/adbi.201900285.

Edmondson, R.; Jenkins Brogile, J.; Adcock, A.F.; Yang, L. Three-dimensional cell culture systems and their applications in drug discovery and cell-based biosensors. *Assay Drug Dev. Technol.* **2014**, *12*, 207-218. doi: 10.1089/adt.2014.573.

Folkins, C.; Man, S.; Xu, P.; Shaked, Y.; Hicklin, D.J.; Kerbel, R.S. Anticancer therapies combining antiangiogenic and tumor cell cytotoxic effects reduce the tumor stem-like cell fraction in glioma xenograft tumors. *Cancer Res.* **2007**, *67*, 3560-3564. doi: 10.1158/0008-5472.

Friedrich, J.; Ebner, R.; Kunz-Schughart, L.A. Experimental anti-tumor therapy in 3-D: spheroids-old hat or new challenge? *Int J Radiat Biol*. **2007**, *83*, 849–871. doi: 10.1080/09553000701727531.

Friedrich, J.; Seidel, C.; Ebner, R.; Kunz-Schughart, L.A. Spheroid-based drug screen: considerations and practical approach. *Nat Protoc.* **2009**, *4*, 309-24. doi: 10.1038/nprot.2008.226.

Froehlich, K.; Haeger, J.D.; Heger, J. *et al.* Generation of multicellular breast cancer tumor spheroids: comparison of different protocols. *J. Mammary Gland Biol. Neoplasia.* **2016**, *21*, 89-98. doi: 10.1007/s10911-016-9359-2.

Fröhlich, E. Issues with Cancer Spheroid Models in Therapeutic Drug Screening. *Curr Pharm Des.* **2020**, *26*, 2137-2148. doi: 10.2174/1381612826666200218094200.

Gobeil, S.; Boucher, CC.; Nadeau, D.; Poirier, GG. Characterization of the necrotic cleavage of poly(ADP-ribose) polymerase (PARP-1): implication of lysosomal proteases. *Cell Death Differ.* **2001**, *8(6),* 588-594. doi: 10.1038/sj.cdd.4400851.

Ham, S.L.; Joshi, R.; Thakuri, P.S.; Tavana, H. Liquid-based three-dimensional tumor models for cancer research and drug discovery. *Exp Biol Med* **2016**, *241***,** 939-954. doi: 10.1177/1535370216643772.

He, J.; Xiong, L.; Li, Q.; Lin, L.; Miao, X.; Yan, S.; Hong, Z.; Yang, L.; Wen, Y.; Deng, X. 3D modeling of cancer stem cell niche. *Oncotarget.* **2017**, *9*, 1326-1345. doi: 10.18632/oncotarget.19847.

Hermann, P.C.; Huber, S.L.; Herrler, T. *et al*. Distinct populations of cancer stem cells determine tumor growth and metastatic activity in human pancreatic cancer. *Cell Stem Cell.* **2007**, *1*, 313-323. doi: 10.1016/j.stem.2007.06.002.

Herrmann, R.; Fayad, W.; Schwarz, S. *et al*. Screening for compounds that induce apoptosis of cancer cells grown as multicellular spheroids. *J. Biomol. Screen.* **2008**, *13*, 1-8. doi: 10.1177/1087057107310442.

Hirschhaeuser, F.; Menne, H.; Dittfeld, C.; West, J.; Mueller-Klieser, W.; Kunz-Schughart, L.A. Multicellular tumor spheroids: an underestimated tool is catching up again. *J Biotechnol*. **2010**, *148*, 3-15. doi: 10.1016/j.jbiotec.2010.01.012.

Hoarau-Vechot, J.; Rafii, A.; Touboul, C. *et al*. Halfway between 2D and animal models: Are 3D cultures the ideal tool to study cancer-microenvironment interactions? *Int J Mol Sci.* **2018**, *19*, 181. doi: 10.3390/ijms19010181.

Ho, W.Y.; Yeap, S.K.; Ho, C.L.; Rahim, R.A.; Alitheen, N.B. Development of multicellular tumor spheroid (MCTS) culture from breast cancer cell and a high throughput screening method using the MTT assay. *PLoS One*. **2012**, *7*, e44640. doi: 10.1371/journal.pone.0044640.

Ishiguro, T.S.; Ohata, H.; Sato, A.; Yamawaki, K.; Enomoto, T.; Koji, O. Tumor-derived spheroids: Relevance to cancer stem cells and clinical applications. *Cancer Sci.* **2017**, *108***,** 283-289. doi: 10.1111/cas.13155.

Jamali, T.; Kavoosi, G.; Safavi, M.; Ardestani, S.K. In-vitro evaluation of apoptotic effect of OEO and thymol in 2D and 3D cell cultures and the study of their interaction mode with DNA. *Sci Rep*. **2018**, *8*, 15787. doi: 10.1038/s41598-018-34055-w.

Kanintronkul, Y.; Worayuthakarn, R.; Thasana, N.; Winayanuwattikun, P.; Pattanapanyasat, K.; Surarit, R.; Ruchirawat, S.; Svasti, J. Overcoming multidrug resistance in human lung cancer with novel benzo[a]quinolizin-4-ones. *Anticancer Res.* **2011**, *31*, 921-928.

Karimi-Busheri, F.; Rasouli-Nia, A.; Zadorozhny, V.; Fakhrai, H. CD24+/CD38- as new prognostic marker for non-small cell lung cancer. *Multidiscip Respir Med.* **2013**, *8***,** 65. doi: 10.1186/2049-6958-8-65.

Karlsson, H.; Fryknas, M.; Larsson, R.; Nygren, P. Loss of cancer drug activity in colon cancer HCT-116 cells during spheroid formation in a new 3-D spheroid cell culture system. *Exp. Cell Res.* **2012**, *318*, 1577–1585. doi: 10.1016/j.yexcr.2012.03.026.

Katsura, Y.; Ohara, T.; Noma, K. *et al.* A novel combination cancer therapy with iron chelator targeting cancer stem cells via suppressing stemness. *Cancers* **2019**, *11,* 177. doi: 10.3390/cancers11020177.

Kim, C.F.; Jackson, E.L.; Woolfenden, A.E. *et al.* Identification of bronchioalveolar stem cells in normal lung and lung cancer. *Cell*. **2005**, *121*, 823-835. doi: 10.1016/j.cell.2005.03.032.

Kinnally, K.W.; Peixoto, P.M.; Ryu, S.Y.; Dejean, L.M. Is mPTP the gatekeeper for necrosis, apoptosis, or both? *Biochim. Biophys. Acta*. **2011**, *1813*, 616-622. doi: 10.1016/j.bbamcr.2010.09.013.

Kitel, R.; Czarnecka, J.; Rusin, A. Trójwymiarowe hodowle komórek- zastosowania w badaniach podstawowych i inżynierii tkankowej. *Post. Bioch.* **2013**, *59*, 305-314.

Konopa, J.; Horowska, B.; Paluszkiewicz, E.; Borowa-Mazgaj, B.; Augustin, E.; Skwarska, A.; Mazerska, Z. Asymmetric Bis-acridines with antitumor activity and use thereof. Gdansk University of Technology. European Patent EP 3070078, **2017**

Konopa, J.; Horowska, B.; Paluszkiewicz, E.; Borowa-Mazgaj, B.; Augustin, E.; Skwarska, A.; Mazerska, Z. Asymmetric Bis-acridines with antitumor activity and use thereof. Gdansk University of Technology. U.S. Patent US10,202,349, **2019**

Konopa, J.; Horowska, B.; Paluszkiewicz, E.; Borowa-Mazgaj, B.; Augustin, E.; Skwarska, A.; Mazerska, Z. Asymmetric Bis-acridines with antitumour activity and their uses. Gdansk University of Technology. Japanese Patent 7226918, **2023**

Kosno, M.; Laskowski, T.; Frackowiak, J.E. *et al.* Acid-base equilibrium and self-association in relation to high antitumor activity of selected unsymmetrical bisacridines established by extensive chemometric analysis. *Molecules* **2022**, *27***,** 3995. doi: 10.3390/molecules27133995.

Langhans, S.A. Three-dimensional *in vitro* cell culture models in drug discovery and drug repositioning. *Front. Pharmacol.* **2018**, *9,* 6. doi: 10.3389/fphar.2018.00006.

Lapidot, T.; Sirard, C.; Vormoor, J. *et al.* A cell initiating human acute myeloid leukaemia after transplantation into SCID mice. *Nature* **1994**, *367***,** 645–648. doi: 10.1038/367645a0.

Lee, J.; Lilly, D.; Doty, C.; Podsiadlo, P.; Kotov, N.A. *In vitro* toxicity testing of nanoparticles in 3D cell culture. *Small* **2009**, *5*, 1213-1221. doi: 10.1002/smll.200801788.

Lemasters, J.J.; Nieminen, A.L.; Qian, T. *et al.* The mitochondrial permeability transition in cell death: a common mechanism in necrosis, apoptosis and autophagy. *Biochim. Biophys. Acta* **1998**, *1366*, 177-196. doi: 10.1016/s0005-2728(98)00112-1.

Liao, Z.J.; Guo, Y.H.; Zhao, Z.; Yao, J.T.; Xu, R.; Nan, K.J. Gemcitabine inhibits the micrometastasis of non-small cell lung cancer by targeting the EpCAM-positive circulating tumor cells via the HGF/cMET pathway. *Int J Oncol.* **2014**, *45*, 651-658. doi: 10.3892/ijo.2014.2464.

Liu, J.; Mao, Z.; Huang, J.; Xie, S.; Liu, T.; Mao, Z. Blocking the NOTCH pathway can inhibit the growth of CD133-positive A549 cells and sensitize to chemotherapy. *Biochem Biophys Res Commun.* **2014**, *444*, 670-675. doi: 10.1016/j.bbrc.2014.01.164.

Lottaz, C.; Beier, D.; Meyer, K. *et al.* Transcriptional profiles of CD133+ and CD133- glioblastoma-derived cancer stem cell lines suggest different cells of origin. *Cancer Res* **2010**, *70*, 2030-2040. doi: 10.1158/0008-5472.CAN-09-1707.

Lu, H.; Stenzel, M.H. Multicellular Tumor Spheroids (MCTS) as a 3D *In vitro* Evaluation Tool of Nanoparticles. *Small* **2018**, *14*, e1702858. doi: 10.1002/smll.201702858.

Meng, X.; Li, M.; Wang, X.; Wang, Y.; Ma, D. Both CD133+ and CD133- subpopulations of A549 and H446 cells contain cancer-initiating cells. *Cancer Sci.* **2009**, *100*, 1040-1046. doi: 10.1111/j.1349-7006.2009.01144.x.

Mikhail, A.S.; Eetezadi, S.; Allen, C. Multicellular tumor spheroids for evaluation of cytotoxicity and tumor growth inhibitory effects of nanomedicines *in vitro*: a comparison of docetaxel-loaded block copolymer micelles and Taxotere®. *PLoS One* **2013**, *8*, e62630. doi: 10.1371/journal.pone.0062630.

Mittler, F.; Obeïd, P.; Rulina, A.V.; Haguet, V.; Gidrol, X.; Balakirev, M.Y. High-content monitoring of drug effects in a 3D spheroid model. *Front. Oncol.* **2017**, *7,* 293. doi: 10.3389/fonc.2017.00293

Muddineti, O.S.; Kumari, P.; Ray, E.; Ghosh, B.; Biswas, S. Curcumin-loaded chitosan-cholesterol micelles: evaluation in monolayers and 3D cancer spheroid model. *Nanomedicine* **2017**, *12*, 1435-1453. doi: 10.2217/nnm-2017-0036.

Nath, S.; Devi, G.R. Three-dimensional culture systems in cancer research: focus on tumor spheroid model. *Pharmacol. Ther.* **2016**, *163,* 94-108. doi: 10.1016/j.pharmthera.2016.03.013.

Nunes, A.S.; Barros, A.S.; Costa, E.C.; Moreira, A.F.; Correia, I.J. 3D tumor spheroids as *in vitro* models to mimic *in vivo* human solid tumors resistance to therapeutic drugs. *Biotechnol. Bioeng*. **2019**, *116*, 206-226. doi: 10.1002/bit.26845.

Olejniczak, A.; Szaryńska, M.; Kmieć, Z. *In vitro* characterization of spheres derived from colorectal cancer cell lines. *Int J Oncol*. **2018**, *52*, 599-612. doi: 10.3892/ijo.2017.4206.

Olejniczak-Kęder, A.; Szaryńska, M.; Wrońska, A.; Siedlecka-Kroplewska, K.; Kmieć, Z. Effects of 5-FU and anti-EGFR antibody in combination with ASA on the spherical culture system of HCT116 and HT29 colorectal cancer cell lines. *Int J Oncol*. **2019,** *55*, :223-242. doi: 10.3892/ijo.2019.4809.

Paluszkiewicz, E.; Horowska, B.; Borowa-Mazgaj, B. *et al.* Design, synthesis and high antitumor potential of new unsymmetrical bisacridine derivatives towards human solid tumors, specifically pancreatic cancers and their unique ability to stabilize DNA G-quadruplexes. *Eur. J. Med. Chem*. **2020**, *204*, 112599. doi: 10.1016/j.ejmech.2020.112599.

Pilch, J.; Potęga, A.; Kowalczyk, A. *et al.* pH-responsive drug delivery nanoplatforms as smart carriers of unsymmetrical bisacridines for targeted cancer therapy. *Pharmaceutics* **2023**, *15*, 201. doi: 10.3390/pharmaceutics15010201.

Pinto, B.; Henriques, A.C.; Silva, P.M.A.; Bousbaa, H. Three-dimensional spheroids as *in vitro* preclinical models for cancer research. *Pharmaceutics* **2020**, *12*, 1186. doi: 10.3390/pharmaceutics12121186.

Ricci-Vitiani, L.; Fabrizi, E.; Palio, E.; De Maria, R. Colon cancer stem cells. *J. Mol.Med* **2009**, *87*, 1097-1104. doi: 10.1007/s00109-009-0518-4.

Roudi, R.; Madjd, Z.; Ebrahimi, M.; Samani, F.S.; Samadikuchaksaraei, A. CD44 and CD24 cannot act as cancer stem cell markers in human lung adenocarcinoma cell line A549. *Cell Mol Biol Lett.* **2014**, *19***,** 23-36. doi: 10.2478/s11658-013-0112-1.

Rudnicka, K.W.; Szczęsna, E.; Miszczyk, E. *et al*. Apoptoza i autofagia – mechanizmy i metody detekcji. *Post. Biol. Kom*. **2011**, *38*, 247-265.

Selby, M.; Delosh. R.; Laudeman, J. *et al.* 3D Models of the NCI60 cell lines for screening oncology compounds*. SLAS Discov.* **2017**, *22*, 473-483. doi: 10.1177/2472555217697434.

Semov, A.; Iourtchenco, L.; Liu, L.F. *et al.* Diindolilmethane (DIM) selectively inhibits cancer stem cells. *Biochem Biophys Res Commun*. **2012**, *424***,** 45-51. doi: 10.1016/j.bbrc.2012.06.062.

Shmelkov, S.V.; Butler, J.M.; Hooper, A.T. *et al.* CD133 expression is not restricted to stem cells, and both CD133+ and CD133− metastatic colon cancer cells initiate tumors. *J Clin Invest.* **2008**, *118*, 2111–2120. doi: 10.1172/JCI34401.

Shoval, H.; Karsch-Bluman, A.; Brill-Karniely, Y. *et al*. Tumor cells and their crosstalk with endothelial cells in 3D spheroids. *Sci Rep.* **2017**, *7*, 10428. doi: 10.1038/s41598-017-10699-y.

Smyrek, I.; Mathew, B.; Fischer, S.C.; Lissek, S.M.; Becker, S.; Stelzer, E.H.K. E-cadherin, actin, microtubules and FAK dominate different spheroid formation phases and important elements of tissue integrity. *Biol Open.* **2019**, *8*, bio037051. doi: 10.1242/bio.037051.

Su, Y.J.; Lai, H.M.; Chang, Y.W.; Chen, G.Y.; Lee, J.L. Direct reprogramming of stem cell properties in colon cancer cells by CD44. *EMBO J.* **2011**, *30***,** 3186-3199. doi: 10.1038/emboj.2011.211.

Sung, H.; Ferlay, J.; Siegel, R.L.; Laversanne, M.; Soerjomataram, I.; Jemal, A.; Bray, F. Global Cancer Statistics 2020: GLOBOCAN Estimates of Incidence and Mortality Worldwide for 36 Cancers in 185 Countries. *CA Cancer J Clin*. **2021**, *71*, 209-249. doi: 10.3322/caac.21660.

Szaryńska, M.; Olejniczak, A.; Kobiela, J.; Łaski, D.; Śledziński, Z.; Kmieć, Z. Cancer stem cells as targets for DC-based immunotherapy of colorectal cancer. *Sci Rep.* **2018**, *8*, 12042. doi: 10.1038/s41598-018-30525-3.

Tirino, V.; Camerlingo, R.; Franco, R. *et al.* The role of CD133 in the identification and characterisation of tumour-initiating cells in non-small-cell lung cancer. *Eur J Cardiothorac Surg.* **2009**, *36*, 446-453. doi: 10.1016/j.ejcts.2009.03.063.

Vinci, M.; Gowan, S.; Boxall, F. *et al*. Advances in establishment and analysis of three-dimensional tumor spheroid-based functional assays for target validation and drug evaluation. *BMC Biol*. **2012**, *22,* 10-29. doi: 10.1186/1741-7007-10-29.

Walcher, L.; Kistenmacher, A.K.; Suo, H. *et al*. Cancer stem cells-origins and biomarkers: perspectives for targeted personalized therapies. *Front Immunol.* **2020**, *11*, 1280. doi: 10.3389/fimmu.2020.01280.

Waltz, A.; Unger, C.; Kramer, N.; Unterleuthner, D.; Scherzer, M.; Hengstschläger, M.; Schwanzer-Pfeiffer, D.; Dolznig, H. The resazurin reduction assay can distinguish cytotoxic from cytostatic compounds in spheroid screening assays. *J. Biomol. Screen.* **2014**, *19*, 1047–1059. doi: 10.1177/1087057114532352.

Weiswald, L.B.; Bellet, D.; Dangles-Marie, V. Spherical cancer models in tumor biology. *Neoplasia* **2015**, *17***,** 1-15. doi: 10.1016/j.neo.2014.12.004.

Wernitznig, D.; Kiakos, K.; Del Favero, G.; Harrer, N.; Machat, H.; Osswald, A.; Jakupec, M.A.; Wernitznig, A.; Sommergruber, W.; Keppler, B.K. First-in-class ruthenium anticancer drug (KP1339/IT-139) induces an immunogenic cell death signature in colorectal spheroids *in vitro*. *Metallomics* **2019**, *11*, 1044–1048. doi: 10.1039/c9mt00051h.

Yong Ho, W.; Keong Yeap, S.; Ling Ho, C. *et al*. Development of multicellular tumor spheroids (MCTS) culture from breast cancer cell and high throughput screening method using MTT assay. *PLoS One* **2012**, *7*, e44640. doi: 10.1371/journal.pone.0044640.

Zanoni, M.; Piccinini, F.; Arienti, C. *et al.* 3D tumor spheroid models for *in vitro* therapeutic screening: a systematic approach to enhance the biological relevance of data obtained. *Sci Rep* **2016***, 6***,** 19103. doi: 10.1038/srep19103.

Zhang, C.; Yang, Z.; Dong, D.L. *et al.* 3D culture technologies of cancer stem cells: promising ex vivo tumor models. *J Tissue Eng.* **2020**, *11*, 2041731420933407. doi: 10.1177/2041731420933407.

Zhang, H.; Yang, N.; Sun, B. *et al.* CD133 positive cells isolated from A549 cell line exhibited high liver metastatic potential. *Neoplasma* **2014**, *61***,** 153-160. doi: 10.4149/neo_2014_021.

Zheng, X.; Shen, G.; Yang, X.; Liu, W. Most C6 cells are cancer stem cells: evidence from clonal and population analyses. *Cancer Res* **2007**, *67*, 3691–3697. doi: 10.1158/0008-5472.CAN-06-3912.

LIST OF FIGURES

LIST OF TABLES

PROFESSIONAL EXPERIENCE

December 2020 – August 2023	Department of Pharmaceutical Technology and Biochemistry Gdańsk University of Technology **Research investigator -** Laboratory work as part of the National Science Center OPUS grant UMO-2019/33/B/NZ7/02534, Principal Investigator: Prof. Zofia Mazerska PhD, DSc I was responsible for the evaluation of the impact of unsymmetrical bisacridines on cell cycle progression and cytoplasmic membrane alterations of HepG2 liver, LS174T colon, and DU145 prostate cancer cells, and for establishing the relationship between the expression of nuclear receptors and proteins involved in the cell cycle progression and apoptosis in these cells after UAs exposure.
May 2019 – July 2020	Department of Pharmaceutical Technology and Biochemistry Gdańsk University of Technology **Research investigator -** Laboratory work as part of the National Science Center OPUS grant UMO-2016/23/B/NZ7/03324. Principal Investigator: Ewa Augustin, PhD, DSc, Assoc. Prof. I was responsible for the analysis of the cellular response induced by unsymmetrical bisacridines in HCT116 colon and H460 lung cancer cells and normal CCD 841 CoN and MRC-5 cells. I performed the observations of the morphology of the cell nuclei after UAs treatment and the cytometric analysis of changes in the mitochondrial membrane potential and cleaved PARP protein level after incubation with the studied compounds.

SCIENTIFIC ACHIEVEMENTS

Publications

- **Kulesza J**., Paluszkiewicz E., Augustin E. (2023). Anticancer potential of unsymmetrical bisacridines in multicellular tumor spheroids of colon and lung cancer cells: relevance for cancer stem cells. *Cancers* IF 5.2; Ministry Points: 200; Q1. ***SUBMITTED***
- Mania S., Banach-Kopeć A., Staszczyk K., **Kulesza J**., Augustin E., Tylingo R. (2023). An influence of molecular weight, deacetylation degree and method of obtaining chitosan xerogels on their antimicrobial activity and cytotoxicity. *Carbohydrate Research* IF 3.1; Ministry Points: 100; Q1. ***AFTER REVIEW, MINOR REVISION***
- Pawłowska M., **Kulesza J**., Augustin E. (2022). c-Myc protein level affected by unsymmetrical bisacridines influences apoptosis and senescence induced in HCT116 colorectal and H460 lung cancer cells. *International Journal of Molecular Sciences* 23, 3061. https://doi.org/10.3390 IF 5.6; Ministry Points: 140; Q1.
- **Kulesza J**., Pawłowska M., Augustin E. (2021). The influence of antitumor unsymmetrical bisacridines on 3D cancer spheroids growth and viability. *Molecules* 26, 6262. https://doi.org/10.3390/molecules26206262 IF 4.927; Ministry Points: 140; Q1.

Conference presentations

Oral communications

- XXV Gliwice Scientific Meetings, Maria Skłodowska-Curie National Research Institute of Oncology and Silesian University of Technology, Gliwice, Poland, 19-20.11.2021, **Kulesza J.**, Pawłowska M., Augustin E.: “c-Myc protein level affected by unsymmetrical bisacridines plays a role in apoptosis induced by these compounds in HCT116 colorectal and H460 cancer cells.”

Poster communications

- The 47th FEBS Congress and the 22nd Young Scientists’ Forum 2023, Federation of European Biochemical Societies, Tours, 6-12.07.2023, **Kulesza J.**, Augustin E.: ”Study of the influence of unsymmetrical bisacridines on the cellular response and cancer stem cell population in HCT116 colon and A549 lung cancer cells cultured in 2D and 3D.” *FEBS Open Bio* 13(S2) s.68 https://doi.org/10.1002/2211-5463.13646
- The 28th Euroconference on Apoptosis, Inflammation, Cancer and Neurodegeneration, European Cell Death Organization, Bonn, Germany, 26-29.09.2022, Kurdyn A., **Kulesza J.**, Pawłowska M., Paluszkiewicz E., Augustin E.: ”Unsymmetrical bisacridine derivatives show anticancer potential by inducing apoptosis in human prostate, colon, and pancreatic cancer cells.” abstract book, p. 59
- The Biochemistry Global Summit, IUBMB-FEBS-PABMB Congress, Federation of European Biochemical Societies, Lisbon, Portugal, 9-14.07.2022, **Kulesza J.**,

Pawłowska M., Augustin E.: ”3D spheroid culture system of HCT116 colon and A549 lung cancer cells in the study of the cellular response induced by antitumor unsymmetrical bisacridines in these cells.” *FEBS Open Bio* 12(S1) s.88 https://doi.org/10.1002/2211-5463.13440

- The Biochemistry Global Summit, IUBMB-FEBS-PABMB Congress, Federation of European Biochemical Societies, Lisbon, Portugal, 9-14.07.2022, Pawłowska M., Frąckowiak J., **Kulesza J.**, Augustin E., Mazerska Z.: ”Interactions of antitumor unsymmetrical bisacridines with ABC transporters: MDR1, MRP1 and MRP2.” *FEBS Open Bio* 12(S1) s.111 https://doi.org/10.1002/2211-5463.13440

- XXV Gliwice Scientific Meetings, Maria Skłodowska-Curie National Research Institute of Oncology and Silesian University of Technology, Gliwice, Poland, 19-20.11.2021, **Kulesza J.**, Pawłowska M., Augustin E.: “c-Myc protein level affected by unsymmetrical bisacridines plays a role in apoptosis induced by these compounds in HCT116 colorectal and H460 cancer cells.”

- The 45th FEBS Congress, Federation of European Biochemical Societies, Ljubljana, Slovenia, 3-8.07.2021, **Kulesza J.**, Pawłowska M., Augustin E.: “Effects of unsymmetrical bisacridines on the spherical culture system of HCT116 colon and H460 lung cancer cell lines.” *FEBS Open Bio* 11(S1) s.422 https://doi.org/10.1002/2211-5463.13205

- The 45th FEBS Congress, Federation of European Biochemical Societies, Ljubljana, Slovenia, 3-8.07.2021, Pawłowska M., **Kulesza J.**, Mazerska Z., Augustin E.: “New antitumor unsymmetrical bisacridines derivatives affect c‑myc and K‑Ras level leading to cell death or accelerated senescence in lung and colon cancer cells.” *FEBS Open Bio* 11(S1) s.413 https://doi.org/10.1002/2211-5463.13205

Awards and scholarships

- The FEBS Grant for the 22nd Young Scientists’ Forum 2023 and 47th FEBS Congress (6-12.07.2023, Tours, France)

- The FEBS Bursary for the IUBMB–FEBS–PABMB Congress (9-14.07.2022, Lisbon, Portugal)

- Francium Supporting Outstanding Doctoral Candidates – scholarship of the IDUB program (10.2022 – 09.2023)

- Award for co-authorship of a publication in a journal listed in the Scopus database and having 140 points in accordance with the latest current Polish Minister of Education and Science List (02.2022) for the publication:
  Kulesza J.; Pawłowska M.; Augustin E. The Influence of Antitumor Unsymmetrical Bisacridines on 3D Cancer Spheroids Growth and Viability.